Response of DNA molecules to external fields

Electric and hydrodynamic

Sachdev, Shaurya

DOI
10.4233/uuid:d343d5af-8f40-4328-8969-39d8f4b7f939

Publication date
2020

Document Version
Final published version

Citation (APA)
Sachdev, S. (2020). *Response of DNA molecules to external fields: Electric and hydrodynamic*. [Dissertation (TU Delft), Delft University of Technology]. https://doi.org/10.4233/uuid:d343d5af-8f40-4328-8969-39d8f4b7f939

ISBN 978-90-8593-430-1
Casimir PhD Series: 2020-03

RESPONSE OF DNA MOLECULES TO EXTERNAL FIELDS ELECTRIC AND HYDRODYNAMIC

SHAURYA SACHDEV

RESPONSE OF DNA MOLECULES TO EXTERNAL FIELDS

ELECTRIC AND HYDRODYNAMIC

SHAURYA SACHDEV

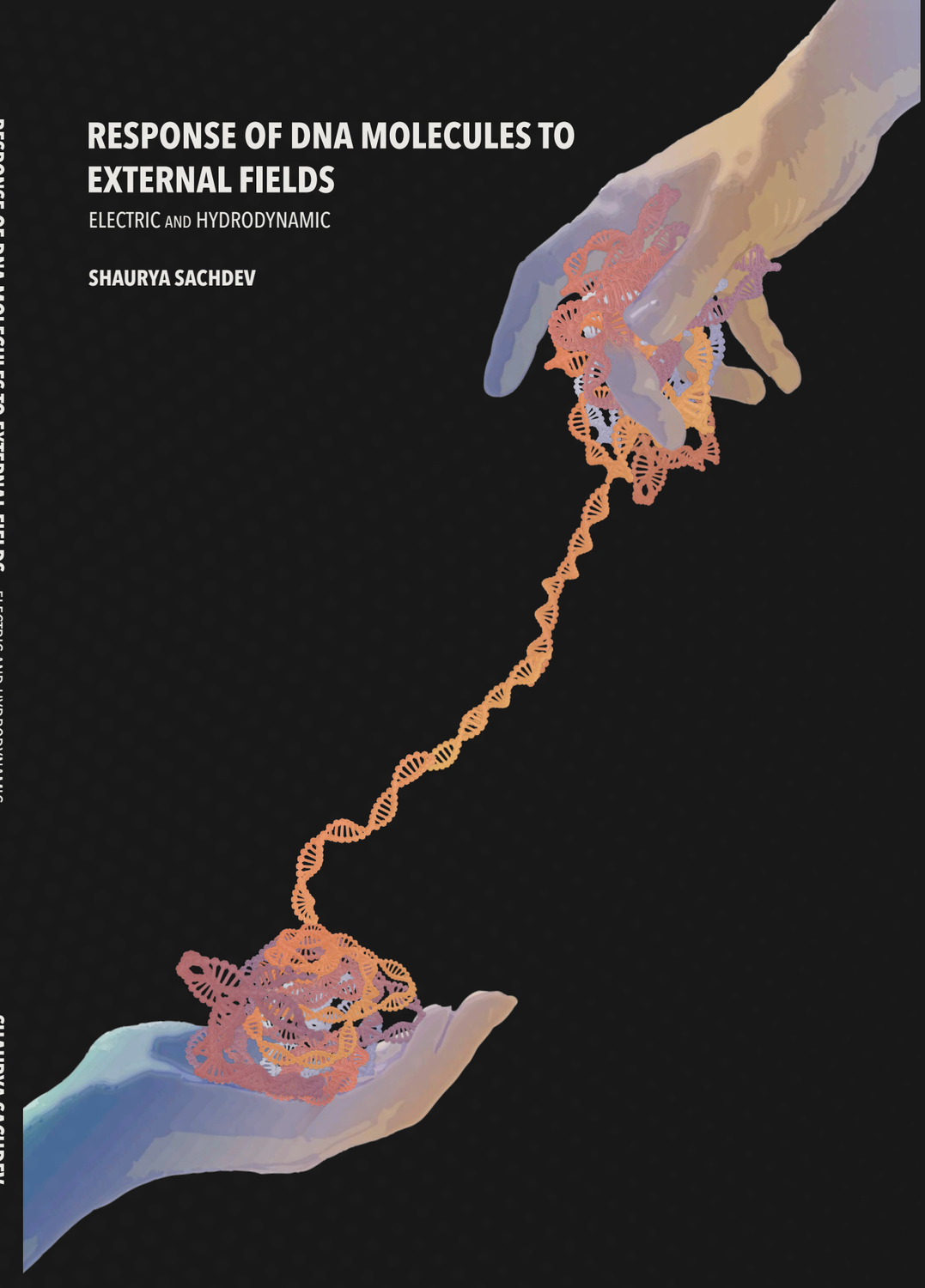

INVITATION

To the public defence of my doctoral thesis:

RESPONSE OF DNA MOLECULES TO EXTERNAL FIELDS
ELECTRIC AND HYDRODYNAMIC

The defence ceremony is to be held on Monday the 20th of January 2020 at 1500 hours in the Senaatszaal of the Aula, Delft University of Technology, Mekelweg 5, Delft.

Prior to the defence, at 1430 hours, I will give a brief introduction to my PhD research.

Following the defence there will be a reception to which you are warmly invited.

Shaurya Sachdev
shauryasachdev@gmail.com

Propositions

accompanying the dissertation

RESPONSE OF DNA MOLECULES TO EXTERNAL FIELDS

ELECTRIC AND HYDRODYNAMIC

by

Shaurya SACHDEV

1. DNA-membrane complex formation occurs even for small DNA molecules, such as 25 bp to 100 bp, during electro-permeabilization *(this thesis, Chapter 2)*.
2. Condensation based on Onsager's criterion explains DNA-membrane complex formation during electro-permeabilization *(this thesis, Chapter 2)*.
3. Bulk electrophoretic mobility, not stochastic threading, determines translocation efficiency of DNA molecules into GUVs during electro-permeabilization *(this thesis, Chapter 3)*.
4. Probing molecular processes during polymer filament thinning in an extensional flow, requires a stagnation point lacking in co-flow and cross-flow microfluidic geometries *(this thesis, Chapter 4)*.
5. Increasing the complexity of the GUVs by adding cell membrane entities will lead to mechanistic insights on DNA uptake, while adding the cytoskeleton will only increase the complexity.
6. Seeing is not believing; visualization of a phenomenon need not reveal mechanistic insights.

   a. Golzio M., Teissié J. and Rols M. P., ***Direct visualization at the single-cell level*** *of electrically mediated gene delivery*, Proceedings of the National Academy of Sciences 99(3), 1292-7 (2002).

   b. Paganin-Gioanni A., Bellard E., Escoffre J. M., Rols M. P., Teissié J. and Golzio M., ***Direct visualization at the single-cell level*** *of siRNA electrotransfer into cancer cells*, Proceedings of the National Academy of Sciences 108(26), 10443-7 (2011).
7. Inconveniently large errors in biological experiments are conveniently blamed on inherent variability and complexity of biological specimens.
8. Over emphasis on exam results steers young scientists away from questioning.
9. A good question is the best answer to the prayers of a PhD student.
10. Large windows and small doors is more than an architectural feature, it reflects Dutch attitude towards the outsider.

These propositions are regarded as opposable and defendable, and have been approved as such by the promotors prof. dr. ir. M. T. Kreutzer and dr. P. E. Boukany.

RESPONSE OF DNA MOLECULES TO EXTERNAL FIELDS

ELECTRIC AND HYDRODYNAMIC

RESPONSE OF DNA MOLECULES TO EXTERNAL FIELDS

ELECTRIC AND HYDRODYNAMIC

Dissertation

for the purpose of obtaining the degree of doctor
at Delft University of Technology,
by the authority of the Rector Magnificus prof. dr. ir. T. H. J. J. van der Hagen,
chair of the board of Doctorates,
to be defended publicly on Monday 20 January 2020 at 1500 hours

by

Shaurya SACHDEV

Master of Science in Chemical Engineering,
Delft University of Technology, Delft, The Netherlands,
born in New Delhi, India.

This dissertation has been approved by the

promotor: prof. dr. ir. M. T. Kreutzer
promotor: dr. P. E. Boukany

Composition of the doctoral committee:

Rector Magnificus,	chairperson
Prof. dr. ir. M. T. Kreutzer,	Delft University of Technology
Dr. P. E. Boukany,	Delft University of Technology

Independent members:

Dr. V. Garbin,	Delft University of Technology
Dr. M. Tarek,	CNRS, University of Lorraine
Prof. dr. D. Miklavčič,	University of Ljubljana
Prof. dr. ir. J. T. Padding,	Delft University of Technology
Prof. dr. S. J. Picken,	Delft University of Technology

Reserve member:

Prof. dr. E. J. R. Sudhölter,	Delft University of Technology

Keywords: electroporation, electropermeabilization, gene electrotransfer, DNA aggregation, giant unilamellar vesicles, GUVs, DNA translocation, microfluidics, polymer rheology, extensional rheology, filament thinning, droplet breakup

Printed by: Ipskamp Printing

Front & Back: Beautiful cover art by Turkuaz Nacafi that captures the entire content of this thesis in a single illustration.

Casimir PhD Series: 2020-03

ISBN 978-90-8593-430-1

An electronic version of this dissertation is available at
http://repository.tudelft.nl/.

CONTENTS

1

INTRODUCTION

1

This thesis is about DNA molecules in electric and hydrodynamic fields with a focus on electric field mediated DNA delivery and extensional flow of polymer solutions. The specific research objectives explored within these broader domains, are explored individually in the subsequent chapters as follows:-

1. Effect of DNA size on DNA-membrane interaction and complex formation during electropermeabilization - explored in Chapter 2.

2. Effect of DNA size on translocation efficiency during electropermeabilization of Giant Unilamellar Vesicles (GUVs) - explored in Chapter 3.

3. The conformation of DNA (polymer) molecules during break-up of polymer droplets at a microfluidic T-junction - explored in Chapter 4.

These chapters are either published or are under-review, and are self-sufficient in explaining in detail the research objectives and the outcome obtained as a result of pursuing the objective. However, before delving into them, the motivation behind choosing these objectives is provided by introducing electric field mediated DNA delivery and extensional flow of polymer solutions in Section 1.1 and Section 1.2, respectively.

The main findings and conclusions of this thesis are summarized in Chapter 5, along with an outlook and suggestions for future directions.

1.1. ELECTRIC FIELD MEDIATED DNA DELIVERY

Delivering nucleic acids (DNA and RNA) into cells is required for therapeutic purposes of treatment and vaccination of cancer and other infectious diseases [1–6]. For such cases, it is necessary for the nucleic acid to be delivered into the cell's nucleus (DNA) or the cytoplasm (RNA). The journey of the nucleic acid to its target destinations is hindered by several extra- and intra-cellular impediments which severely limits their delivery preventing the therapeutic action reaching clinically acceptable level [7–9]. Different strategies have been developed that can overcome these physical barriers and can be broadly classified into carrier and membrane disruption based methods [10].

A membrane disruption technique that has been the subject of rigorous investigation is the application of electric field to transiently permeabilize the cell membrane, a process known as electropermeabilization or electroporation. Due to its simplicity, ease of application, independence on cell type and high throuhput, electropermeabilization is one of the most popular method amongst various membrane disruption based techniques [10–13]. After successful pre-clinical studies [14–16], electropermeabilization progressed into clinical studies to exploit the therapeutic potential of nucleic acid delivery [17, 18], commonly known as gene electro-transfer (GET). There are now approximately 90 clinical trials [19], testing the efficacy of electric field mediated nucleic acid delivery for DNA [20–22] and RNA based therapeutics [6, 22, 23].

Despite the surge in the number of clinical trials employing GET since 2004 [20], the efficiency of GET using trial and error approach is below the efficiency achieved by viral methods [19]. Furthermore, the current approach based on trial and error is proving to be time consuming and expensive. In order to overcome these limitations, an approach

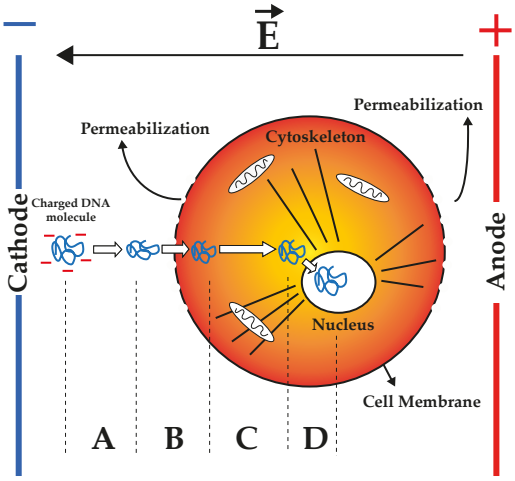

Figure 1.1.1: Schematic overview of DNA delivery using electric pulses and the barrier it encounters in its journey. (A) DNA molecules migrate towards the cell membrane due to electrophoresis under the application of electric field. The extra-cellular matrix (or medium) is the first barrier DNA molecules encounter. (B) Electric field simultaneously induces transient permeabilization of the cell membrane. (C) The electrophoretically migrated DNA molecules then interact with the permeabilized cell membrane and are subsequently internalized or translocated. The cell membrane constitutes the second barrier in the journey. (C) The internalized DNA molecules then travel through the cytoskeleton towards the nucleus, which acts as the third barrier. (D) Upon, reaching the nucleus, they translocate across the nuclear envelope where they express their gene. The nuclear barrier represents the final barrier for DNA molecules. Adapted from [24].

based on targeting the rate limiting steps has the potential to further significantly enhance the efficiency of GET. So far little is known about the mechanism of DNA delivery using electric field pulses and as a result, the major limiting steps for DNA uptake remain unknown.

One of the main aims of this research is to improve the understanding of bio-physical mechanisms behind electric field mediated DNA delivery at the membrane level (Processes B figure 1.1.1). By understanding these mechanisms we would be able to identify the limiting steps involved in these processes and hence would be able to devise completely new strategies to overcome them and significantly improving the efficiency of electric field mediated DNA delivery [19].

In the subsequent sections, first the phenomenon of electropermeabilization or the how electric field induced permeabilization of the cell membrane is explained. This is followed by a description of our (lack of-) understanding about the bio-physical mechanism of DNA translocation across the cell membrane in the presence of an electric field. Finally, the research goals pursued in this research are explained.

1.1.1. ELECTROPERMEABILIZATION

Electropermeabilization is a process in which the cell membrane is transiently permeabilised by the action of high intensity electric field pulses which enables exchange of molecules in and out of the cell (schematically shown in Figure 1.1.2). Conventionally,

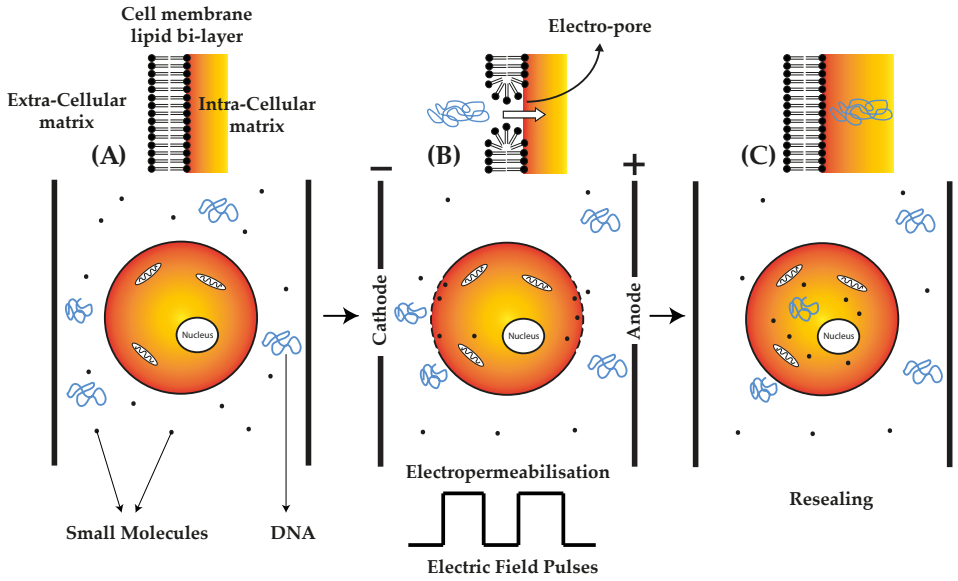

Figure 1.1.2: Delivery of molecules (small and large) using electropermeabilisation. On application of electric field pulses, the cell membrane gets transiently permeabilised allowing both, small and large molecules to enter and leave the cell. The structural re-arrangements at the molecular level in the cell membrane are zoomed in and shown in the top part of the figure. (a) Before the application of electric field pulses. Lipid membrane acts as a barrier to the molecules. (b) During the application of electric field pulses, hydrophilic pores are formed allowing molecules to enter the cell. (c) After the application of electric field pulses, the cell membrane is resealed. Adapted from [24].

electropermeabilisation is inferred by an abrupt increase in the conductivity of lipid bilayers [25–30] or via the uptake of molecules which otherwise cannot penetrate through the cell membrane [31–35].

One way to explain permeabilization in terms of events taking place at the molecular level is through the formation of transient hydrophilic pores in the cell membrane as shown in Figure 1.1.2 (a-c, top panel). These hydrophilic pores are formed when lipid molecules of the cell membrane re-arrange in the presence of electric field, increasing the membrane's electrical conductivity and allowing the passage of molecules through them. Molecular dynamics (MD) simulations [36–38] and theories [39] have provided the evidence for the existence of these pores under an electric field. Thus, formation of electro-pores, or electroporation, provides an explanation for electropermeabilisation at the molecular level. A direct experimental evidence for the existence of these pores has been limited due to their transient nature and small size (O(nm)), however recent experiments [28, 29] have been able to provide support for the electro-pore theory.

Alternate theories suggesting lipid peroxidation as the molecular explanation for permeabilization is also gaining traction [40].

The breakdown of the cell membrane leading to permeabilisation occurs due to the generation of trans-membrane potential (TMP) by the applied electric field. It has been observed that only when the TMP exceeds a critical threshold value, that cell membrane

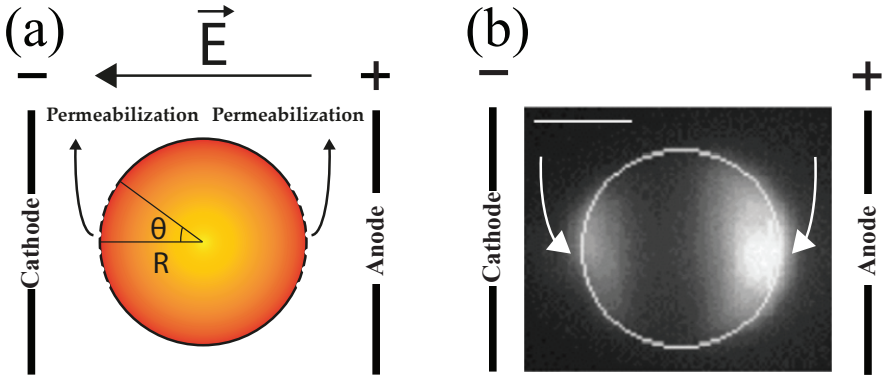

Figure 1.1.3: Extent of permeabilization in the presence of electric field pulses. (a) Schematic showing the extent and the part of the cell that would be permeabilized in the presence of electric field pulses according the Schwan equation. (b) Delivery of Propium Iodide (PI) molecules using electropermeabilization [12, 34]. On application of electric field pulses, the cell membrane gets transiently permeabilised along the poles of the cell, as predicted by Schwan [42, 43], and PI molecules can be seen entering from cathode and the anode facing sides of the cell membrane, as indicated by white arrows. Scale Bar = 10 μm. Adapted from [12].

is permeabilized. This TMP value is around 0.25 to 1.5 V for cells and it is known as the critical or threshold TMP [41]. Therefore, only those parts of the cell membrane would be permeabilised or porated where the TMP is greater than the threshold TMP. If the cell membrane can be considered as shperical dielectric shell, then the induced TMP due to the electric field that is applied varies as $\triangle\psi_{induced} = 1.5ERcos(\theta)$, as predicted by Schwan [42, 43]. Here, E is the magnitude of the electric field that is applied, R is the radius of the cell, θ is the angle with respect to the direction of applied electric field and 1.5 comes from the geometric factor related to spheres [24]. Thus, the parts of the cell membrane that will be permeabilised first are the ones corresponding to values of $|cos(\theta)| \approx 1$ or $\theta \approx 0°$ and $180°$ i.e. the sides of the cell facing the cathode and the anode (Figure 1.1.3 (a)). This was confirmed experimentally and is shown in Figure 1.1.3 (b) [34, 44]. Here the molecules to be delivered were fluorescent Propium Iodide (PI) dye molecules and upon the application of electric field they could be seen entering from the sides of the cell facing the cathode and the anode [34]. This helps to understand which parts of the cell membrane become permeabilised upon application of electric field pulses and from where, the molecules to be administered, can enter the cell.

Transfer of ions and small molecules into the cell during electroporation is a relatively simple process which can be explained via diffusion through the electro-pores created in the membrane [32, 45, 46]. Since permeabilization occurs on either side of the cell facing the cathode and the anode, ions and small molecules can diffuse through both the sides. This also implies, as long as the pore remains open, small molecules and ions will be able to diffuse freely inside the cell, and this takes place both during and after the application of pulses, till the pores reseal [32]. Transfer of DNA molecules via electric field pulses, however, is a complicated process which involves the interaction of the DNA molecules with the cell membrane. This is explained in the next sub-section (Section 1.1.2).

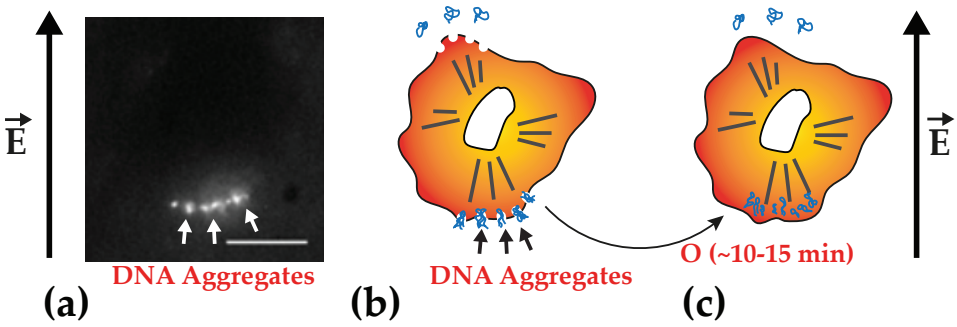

Figure 1.1.4: (a) DNA membrane interaction visualized in terms of formation of DNA aggregates or spots on the cathode facing of side of the cell membrane for Chinese Hamster Ovary (CHO) cells [47]. Scale bar=5 µm. (b) Schematic showing how the DNA is aggregated at the membrane level. These DNA aggregates are then internalized on a time scale of 10-15 mins (b to c)

.

1.1.2. DNA MEMBRANE INTERACTION

This interaction of DNA molecules with the cell membrane can be visualized in terms of the DNA aggregates or DNA complexes (Figure 1.1.4 (a) and (b)) that are formed on the cathode facing side of the cell membrane when the electric field is applied [34, 47]. Therefore, DNA molecules do not enter the cell directly and are rather *"trapped"* near the cell membrane [48]. They appear inside the cytoskeleton in the minutes following following electric field pulse application [34] (Figure 1.1.4 (c)). The threshold value of electric field intensity leading to DNA membrane interaction and internalization is the same as that for cell membrane permeabilization [34].

It is important to address this interaction since it forms the precursor to DNA internalization. Thus, in order to understand how the DNA in translocated across the membrane or internalized it first important to understand how it interacts with the membrane. Despite this fact, the mechanism of DNA membrane interaction still remains unknown. However, several possible mechanisms of DNA membrane interaction have been proposed and are explained below.

It is believed that the cationic lipids present in the cell membrane can facilitate the adsorption of DNA to the cell membrane. Sphingosine, a mono-alkyl cationic lipid is likely to provide the counter-ionic interaction of the lipid bi-layer with the anionic DNA molecules [49]. The binding of DNA to liposomes containing sphingosine has been systematically investigated previously and is likely to be facilitated by the protonated amino group in sphingosine with the negatively charged phosphates of the DNA [49, 50]. Divalent cations such as Mg^{2+} or Ca^{2+} can also facilitate the adsorption of DNA molecules on cell membrane [51–53].

It is also possible that the formation of DNA aggregates is due to the reduced mobility of DNA molecules inside the cytoplasm leading to a crowding or jamming like phenomena [47, 48, 54]. This is consistent with the fact that the cytoplasmic mobility of DNA molecules with size > 250 bp is significantly reduced [55]. The actin cytoskeleton was responsible for this DNA size dependent mobility [56]. Rosazza *et al.* 2011, labelled the

actin cytoskeleton and found that actin patches were formed when the cells were pulsed in the presence of electric field and DNA molecules. Moreover, actin patches were co-localized in space, time and number with these DNA aggregates, suggesting that actin in the cytoskeleton could be involved in the formation of DNA aggregates [57].

While all these mechanisms provide possible routes to adsorption of DNA on the membrane and DNA aggregation at the membrane, they also indicate an influence of DNA size on this interaction. Recently, it was shown that siRNA molecules had direct and rapid access to the cytoskeleton during electric field pulses [35]. This access took place without the formation of aggregates at the cell membrane. siRNA molecules are small nucleic acids consisting of around 25 nucleotides (~ 25 bp). Large nucleic acids such as pDNA (4700 bp)form DNA aggregates at the membrane during electric field pulses [34]. Both pDNA and siRNA have similar bio-chemical structure and the same negative charge density, however, differ in size. Therefore a possible route to understanding the bio-physical mechanism of DNA aggregation during electric field pulses could be to investigate the effect of DNA size on DNA aggregation.

1.1.3. DNA TRANSLOCATION

The next crucial step in electro-transformation involves the translocation of the DNA across the lipid bi-layer or internalization. DNA is a charged macromolecule (polyanion) which can be electrophoretically driven to the cathode facing side of the cell under the influence of electric field. Once it reaches the membrane surface, it has to translocate and enter the cell. However, the main *"motive"* force behind the translocation is still unknown.

Chernomordik *et al.* 1990 proposed that uptake of DNA into cell sized vesicles was facilitated via endocytosis (Figure 1.1.5 (a)) [51]. In case of cells, experimental evidences are also suggesting electric field induced endocytosis as the dominant mechanism of DNA internalization [53, 58–66]. On the other hand, Lurquin and Athanasiou 2000 in fact showed free DNA molecules could be found inside the vesicles when pulsed with an electric field [67]. This was recently confirmed when plasmid DNA molecules were internalized into EggPC vesicles without the formation of these endocytic vesicles [54].

Although a direct translocation mechanism does not seem intuitive because of the inherent difference between the size of the pore which is estimated to be around O(1-10) nm [28, 38, 68, 69] and of the radius of the statistical coil of the pDNA, which is in the range of O(100) nm [66, 70]. However, both the DNA and the membrane are flexible structres and the DNA can expand the pore while it is translocating across it [71]. This process is represented in Figure 1.1.5 (b) and (c). The assumption of pore expansion, as a result of DNA being forced through, is based on the observation that high molecular weight dextrans were able to enter the cell in the presence of Calf Thymus DNA (20 kbp) and λ-DNA (48.5 kbp) which were otherwise impermeable even in the presence of electric field leading to electroporation [71].

For a mechanism of direct entry as opposed to electric field induced endocytosis, the translocation efficiency should only depend on the cross-pore eletrophoretic mobility of the DNA molecule. Under the above mentioned assumption, the cross-pore electrophoretic mobility is equal to the bulk electrophoretic mobility. It is known that the bulk electrophoretic mobility does not scale with DNA size (bp) [72], therefore, for such

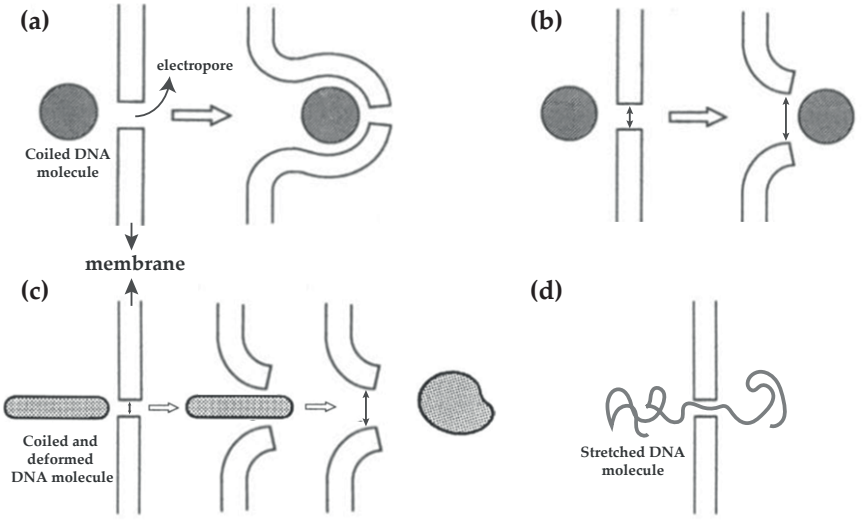

Figure 1.1.5: Possible mechanisms for DNA translocation across a pore in the membrane. (a) Membrane invagination leading to endocytosis. (b) Direct entry via pore expansion as a result of small DNA molecules being forced through the pore. (c) Direct entry of large DNA molecules which could be stretched due to the electric field and being forced into the pore also leading to pore expansion. (d) The electro-pores are small such that the DNA molecules cannot translocate as coiled molecules. They have to unravel as they translocate through the pores. Schematic adapted from [71, 74, 75].

a mechanism, the transfection efficiency should be the same for different sized DNA molecules. However, if the pore is not large enough for the DNA to translocate freely then the mechanism of translocation would be different and would as depicted in Figure 1.1.5(d). In this case, cross-pore mobility should be different than that of the bulk electrophoretic mobility and the transfection efficiency should depend on the size of the DNA molecule [73]. For such a scenario as depicted in Figure 1.1.5(d), the entire DNA molecule does not enter as one blob and the diffusion could not be ignored if the pulse duration is short.

Thus, by varying the size of the DNA molecule, the mechanism of DNA translocation under electric field pulses can be inferred. This mechanism is necessary to identify since different mechanisms of translocation lead to different pathways of internal trafficking inside the cytoskeleton, and thus require different strategies in order to enhance electric field mediated DNA delivery.

1.2. EXTENSIONAL FLOW OF POLYMER SOLUTIONS

Interaction of flexible macromolecules, such as polymers and DNA, with extensional flow fields gives rise to rich and pronounced effects in fluid motion. Pure extensional flows are irrotational with only stream-wise velocity gradients, and can unravel flexible polymer molecules in the direction of flow [76, 77]. The rich phenomena of polymer solutions is thus due to elastic stresses arising as a result of stretching polymer molecules

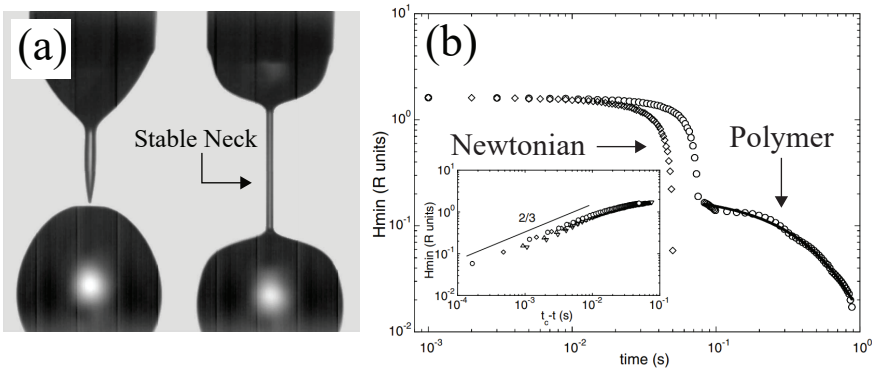

Figure 1.2.1: (a) Droplet pinch-off and filament thinning for a pure water drop (left) and a 100 ppm polyethylene oxide (PEO, 4 $\times 10^6$ amu) polymer solution (right). The stable neck during filament thinning for polymer solutions is marked by an arrow. (b) Evolution of minimum filament thickness ($h_{\min}$) as a function of time for a pure water drop (Newtonian) and a 250 ppm PEO solution (polymer). Inset shows the power-law scaling of the minimum thickness for Newtonian drops and for polymer solutions prior to neck formation; $h_{\min} \propto (t_c - t)^{2/3}$, where t_c is the time to break-up. $R = 2$ mm, and is the radius of the capillary. Figure adapted from [79].

in response to extensional flow fields.

Within the class of extensional flows, filament stretching and thinning during jet break-up or droplet pinch-off has been the subject of rigorous investigation. The remarkable delay observed in the eventual break-up of a thinning filament, due to the formation of a stable neck, is a striking feature of polymer solutions exploited in various commercial processes such as ink-jet printing, spraying and jetting of fertilizers and pesticides, fibre spinning, extrusion of polymer *etc.* [76, 78]

An example of polymer filament stretching and thinning during droplet pinch-off is shown in Figure 1.2.1 [79]. For Newtonian fluids (Figure 1.2.1 (a) left), the droplet snaps off and breaks due to gravitational force and capillary pressure. Polymeric fluids behave strikingly different in this regard. The addition of even dilute amounts of polymers leads to the formation of a stable neck as shown in Figure 1.2.1 (a) on the right. The delay in polymer droplet pinch-off as a consequence of stable neck formation is evident from the evolution of the minimum filament thickness ($h_{\min}$) plotted as a function of time and shown in Figure 1.2.1 (b). The Newtonian filament exhibits a sudden pinch off, and follows a power-law scaling till breakup (inset of Figure 1.2.1 (b)). Polymer filament, on the other hand inhibits the sudden pinch-off by forming a stable neck that thins down slowly (and exponentially) in time. The present study focuses on experimentally exploring the molecular picture behind this stable neck formation.

For Newtonian fluids, the filament stretching and pinch-off is described by scaling laws, where the exponent is determined by the balance between inertial, viscous and capillary forces [80]. In case of polymer fluids, filament thinning prior to stable neck formation is also determined by the same scaling laws (see Figure 1.2.1 (b) inset). This indicates an absence of elastic stresses, and depending on the solvent viscosity, inertial and/or viscous forces balance the capillary forces pinching the filament. The resulting

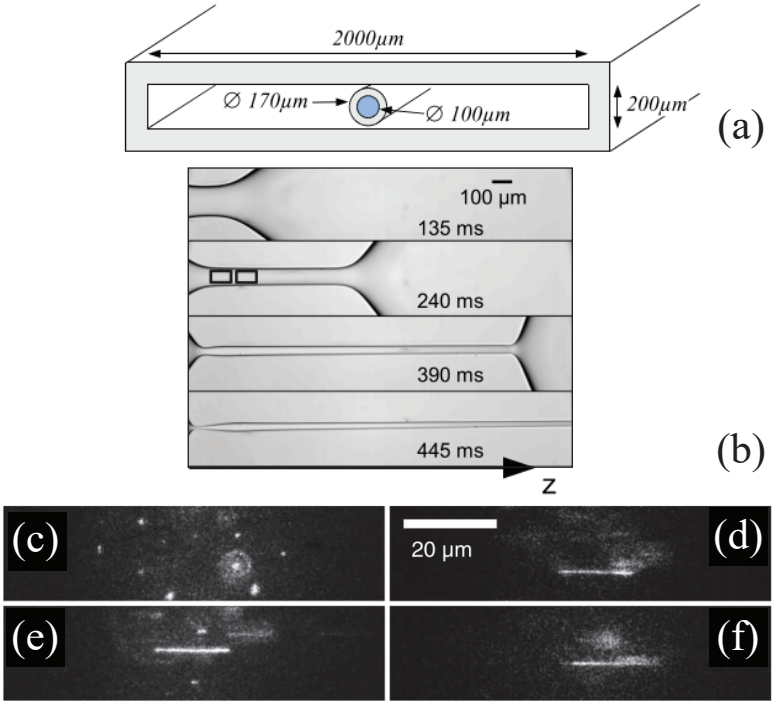

Figure 1.2.2: Images from [83].(a) A co-flowing microfluidic device used to investigate droplet pinch-off. (b) Droplet pinch-off for poly-acrylamide dissolved in 30% aqueous sucrose solution with fluorescently labelled T4-DNA molecules. A stable neck formation can be seen for t>135 ms. (c)-(f) Snapshots of an individual DNA molecule at different stages of the neck formation. The snapshots are from the location of the neck as marked by black boxes in (b). (c) Conformations of DNA molecules before the formation of stable neck. Majority of DNA molecules are coiled. (d) Conformation of DNA molecules in the stable neck. DNA molecules can be found both in stretched and coiled configuration. (e) Another snapshot showing a stretched DNA molecule in the stable neck. (f) The same stretched DNA molecule after a time of 130 ms.

extensional flow within the filament eventually leads to the unravelling of the polymer molecules. Due to uncoiling and stretching of polymer molecules, the elastic stresses become dominant and are able to resist the capillary forces, leading to an elasto-capillary balance. The cylindrical shape acquired by the thinning filament, which is referred to as stable neck formation, is due to the increasing dominance of the elastic stresses over the viscous stresses in this elasto-capillary balance, and also results in an an exponential decay of the filament [81, 82].

From a molecular perspective, several constitutive equations that incorporate the stresses generated as a result of stretching polymer molecules have been utilized in explaining and even reproducing the experimental profiles of polymer filament thinning [81, 82, 84–89]. Another approach to linking the macroscopic properties to the microscopic behaviour at the molecular level is by direct observation of single polymer molecules [90]. Such an approach was followed recently by Ingremeau *et al.* 2013 in droplet pinch-off experiments [83]. They observed that the conformational distribution of DNA molecules

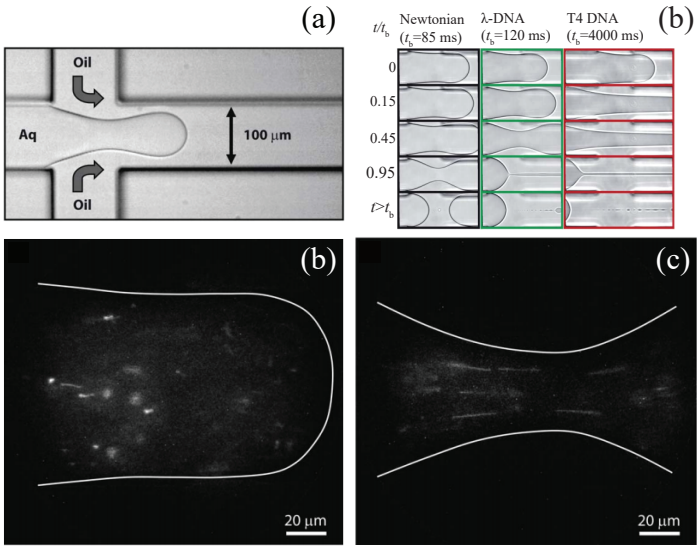

Figure 1.2.3: Images from [91](a) Cross-flow microfluidic geometry used for droplet pinch-off. (b) Droplet pinch-off for Newtonian system (black), λ-DNA (green) and T4-DNA (red). Stable neck formation is only observed for polymeric systems λ-DNA and T4-DNA. t_b is the breakup time of droplets. (c) Conformations of DNA molecules before droplet pinch-off (t/t_b=0) for a suspension of λ-DNA molecules. Majority of the DNA molecules are coiled. (d) Conformation of DNA molecules at (t/t_b=0.5) where majority of the DNA molecules are in their stretched conformation.

in the stable neck remains constant with time, and related it to a constant extensional viscosity during polymer droplet pinch-off. However, full extension of DNA molecules inside the stable neck was not observed in the co-flow microfluidic geometry adopted by them (Figure 1.2.2). As mentioned by the authors, for the Weissenberg's number in the extensional flow, the accumulated Hencky's strain was enough to observe full extension of the DNA molecules. On the other hand, Juarez *et al.* 2011, used a microfluidic cross-slot geometry (Figure 1.2.3) and observed that DNA molecules suddenly stretch just before the onset of a stable neck formation, and a fraction of DNA molecules also reach full extension [91]. This is also consistent with explanation that at the onset of the stable neck formation, extensional strain rates increase dramatically reaching values much higher than the inverse relaxation time of the polymer molecules, allowing a fraction of DNA molecules to reach full extension [79]. However, observations of DNA molecules could not be made during the stable neck formation due to high velocities and lack of a stagnation point in the cross-slot geometry (Figure 1.2.3) [91].

The inconsistencies in these findings could be traced to lack of a stagnation point in the cross-flow and co-flow microfluidic geometries. To this end, droplet break-up at microfluidic T-junction has been employed in order to investigate polymer conformation during the entire duration of stable neck formation and thinning. Due to the inherent stagnation point in the middle of the droplet, a detailed molecular picture can be obtained giving local information about the polymer conformations during polymeric filament thinning.

1

REFERENCES

[1] S. L. Ginn, A. K. Amaya, I. E. Alexander, M. Edelstein, and M. R. Abedi, *Gene therapy clinical trials worldwide to 2017: An update,* The journal of gene medicine **20**, e3015 (2018).

[2] C. E. Dunbar, K. A. High, J. K. Joung, D. B. Kohn, K. Ozawa, and M. Sadelain, *Gene therapy comes of age,* Science **359**, eaan4672 (2018).

[3] K. Sridharan and N. J. Gogtay, *Therapeutic nucleic acids: current clinical status,* British journal of clinical pharmacology **82**, 659 (2016).

[4] R. L. Juliano, *The delivery of therapeutic oligonucleotides,* Nucleic acids research **44**, 6518 (2016).

[5] N. Pardi, M. J. Hogan, F. W. Porter, and D. Weissman, *mrna vaccines—a new era in vaccinology,* Nature Reviews Drug Discovery **17**, 261 (2018).

[6] B. A. Sullenger and S. Nair, *From the rna world to the clinic,* Science **352**, 1417 (2016).

[7] Z. Zhou, X. Liu, D. Zhu, Y. Wang, Z. Zhang, X. Zhou, N. Qiu, X. Chen, and Y. Shen, *Nonviral cancer gene therapy: Delivery cascade and vector nanoproperty integration,* Advanced drug delivery reviews **115**, 115 (2017).

[8] S. F. Dowdy, *Overcoming cellular barriers for rna therapeutics,* Nature biotechnology **35**, 222 (2017).

[9] M. Elsabahy, A. Nazarali, and M. Foldvari, *Non-viral nucleic acid delivery: key challenges and future directions,* Current drug delivery **8**, 235 (2011).

[10] M. P. Stewart, A. Sharei, X. Ding, G. Sahay, R. Langer, and K. F. Jensen, *In vitro and ex vivo strategies for intracellular delivery,* Nature **538**, 183 (2016).

[11] C. Favard, D. S. Dean, and M.-P. Rols, *Electrotransfer as a non viral method of gene delivery.* Current gene therapy **7**, 67 (2007).

[12] J. M. Escoffre, T. Portet, L. Wasungu, J. Teissié, D. Dean, and M. P. Rols, *What is (Still not) known of the mechanism by which electroporation mediates gene transfer and expression in cells and tissues,* Molecular Biotechnology **41**, 286 (2009).

[13] J. Teissie, *Electrically mediated gene delivery: basic and translational concepts,* in *Novel Gene Therapy Approaches* (IntechOpen, 2013).

[14] L. Heller, K. Merkler, J. Westover, Y. Cruz, D. Coppola, K. Benson, A. Daud, and R. Heller, *Evaluation of toxicity following electrically mediated interleukin-12 gene delivery in a b16 mouse melanoma model,* Clinical Cancer Research **12**, 3177 (2006).

[15] M. L. Lucas, L. Heller, D. Coppola, and R. Heller, *Il-12 plasmid delivery by in vivo electroporation for the successful treatment of established subcutaneous b16. f10 melanoma,* Molecular Therapy **5**, 668 (2002).

[16] M. L. Lucas and R. Heller, *Il-12 gene therapy using an electrically mediated nonviral approach reduces metastatic growth of melanoma,* DNA and cell biology **22**, 755 (2003).

[17] A. I. Daud, R. C. DeConti, S. Andrews, P. Urbas, A. I. Riker, V. K. Sondak, P. N. Munster, D. M. Sullivan, K. E. Ugen, J. L. Messina, *et al.*, *Phase i trial of interleukin-12 plasmid electroporation in patients with metastatic melanoma,* Journal of clinical oncology **26**, 5896 (2008).

[18] L. C Heller and R. Heller, *Electroporation gene therapy preclinical and clinical trials for melanoma,* Current gene therapy **10**, 312 (2010).

[19] L. D. Cervia and F. Yuan, *Current progress in electrotransfection as a nonviral method for gene delivery,* Molecular pharmaceutics **15**, 3617 (2018).

[20] R. Heller and L. C. Heller, *Gene electrotransfer clinical trials,* in *Advances in genetics*, Vol. 89 (Elsevier, 2015) pp. 235–262.

[21] L. Lambricht, A. Lopes, S. Kos, G. Sersa, V. Préat, and G. Vandermeulen, *Clinical potential of electroporation for gene therapy and dna vaccine delivery,* Expert opinion on drug delivery **13**, 295 (2016).

[22] C. J. Melief, T. van Hall, R. Arens, F. Ossendorp, and S. H. van der Burg, *Therapeutic cancer vaccines,* The Journal of Clinical Investigation **125**, 3401 (2015).

[23] S. Wilgenhof, J. Corthals, A. M. Van Nuffel, D. Benteyn, C. Heirman, A. Bonehill, K. Thielemans, and B. Neyns, *Long-term clinical outcome of melanoma patients treated with messenger rna-electroporated dendritic cell therapy following complete resection of metastases,* Cancer Immunology, Immunotherapy **64**, 381 (2015).

[24] S. Šatkauskas, P. Ruzgys, and M. S. Venslauskas, *Towards the mechanisms for efficient gene transfer into cells and tissues by means of cell electroporation,* Expert opinion on biological therapy **12**, 275 (2012).

[25] I. Abidor, V. Arakelyan, L. Chernomordik, Y. A. Chizmadzhev, V. Pastushenko, and M. Tarasevich, *Electric breakdown of bilayer lipid membranes: I. the main experimental facts and their qualitative discussion,* Journal of electroanalytical chemistry and interfacial electrochemistry **104**, 37 (1979).

[26] K. Kinosita Jr and T. Y. Tsong, *Voltage-induced conductance in human erythrocyte membranes,* Biochimica et Biophysica Acta (BBA)-Biomembranes **554**, 479 (1979).

[27] K. C. Melikov, V. A. Frolov, A. Shcherbakov, A. V. Samsonov, Y. A. Chizmadzhev, and L. V. Chernomordik, *Voltage-induced nonconductive pre-pores and metastable single pores in unmodified planar lipid bilayer,* Biophysical journal **80**, 1829 (2001).

[28] J. T. Sengel and M. I. Wallace, *Imaging the dynamics of individual electropores,* Proceedings of the National Academy of Sciences **113**, 5281 (2016).

[29] J. T. Sengel and M. I. Wallace, *Measuring the potential energy barrier to lipid bilayer electroporation,* Philosophical Transactions of the Royal Society B: Biological Sciences **372**, 20160227 (2017).

[30] R. Benz, F. Beckers, and U. Zimmermann, *Reversible electrical breakdown of lipid bilayer membranes: a charge-pulse relaxation study,* The Journal of membrane biology **48**, 181 (1979).

[31] E. Neumann, M. Schaefer-Ridder, Y. Wang, and P. Hofschneider, *Gene transfer into mouse lyoma cells by electroporation in high electric fields.* The EMBO journal **1**, 841 (1982).

[32] G. Pucihar, T. Kotnik, D. Miklavčič, and J. Teissié, *Kinetics of transmembrane transport of small molecules into electropermeabilized cells,* Biophysical journal **95**, 2837 (2008).

[33] B. Gabriel and J. Teissie, *Time courses of mammalian cell electropermeabilization observed by millisecond imaging of membrane property changes during the pulse,* Biophysical journal **76**, 2158 (1999).

[34] M. Golzio, J. Teissié, and M.-P. Rols, *Direct visualization at the single-cell level of electrically mediated gene delivery,* Proceedings of the National Academy of Sciences **99**, 1292 (2002).

[35] A. Paganin-Gioanni, E. Bellard, J. Escoffre, M. Rols, J. Teissie, and M. Golzio, *Direct visualization at the single-cell level of sirna electrotransfer into cancer cells,* Proceedings of the National Academy of Sciences **108**, 10443 (2011).

[36] D. P. Tieleman, *The molecular basis of electroporation,* BMC biochemistry **5**, 10 (2004).

[37] D. P. Tieleman, H. Leontiadou, A. E. Mark, and S.-J. Marrink, *Simulation of pore formation in lipid bilayers by mechanical stress and electric fields,* Journal of the American Chemical Society **125**, 6382 (2003).

[38] M. Tarek, *Membrane electroporation: a molecular dynamics simulation,* Biophysical journal **88**, 4045 (2005).

[39] J. C. Weaver and Y. A. Chizmadzhev, *Theory of electroporation: a review,* Bioelectrochemistry and bioenergetics **41**, 135 (1996).

[40] T. Kotnik, L. Rems, M. Tarek, and D. Miklavčič, *Membrane electroporation and electropermeabilization: mechanisms and models,* Annual review of biophysics **48**, 63 (2019).

[41] B. E. Henslee, A. Morss, X. Hu, G. P. Lafyatis, and L. J. Lee, *Electroporation dependence on cell size: optical tweezers study,* Analytical chemistry **83**, 3998 (2011).

[42] H. Schwan, *Dielectrophoresis and rotation of cells,* in *Electroporation and electrofusion in cell biology* (Springer, 1989) pp. 3–21.

[43] T. Kotnik, G. Pucihar, and D. Miklavčič, *Induced transmembrane voltage and its correlation with electroporation-mediated molecular transport,* The Journal of membrane biology **236**, 3 (2010).

[44] M. Hibino, H. Itoh, and K. Kinosita Jr, *Time courses of cell electroporation as revealed by submicrosecond imaging of transmembrane potential.* Biophysical journal **64**, 1789 (1993).

[45] M. M. Sadik, J. Li, J. W. Shan, D. I. Shreiber, and H. Lin, *Quantification of propidium iodide delivery using millisecond electric pulses: experiments,* Biochimica et Biophysica Acta (BBA)-Biomembranes **1828**, 1322 (2013).

[46] M. Yu and H. Lin, *Quantification of propidium iodide delivery with millisecond electric pulses: a model study,* arXiv preprint arXiv:1401.6954 (2014).

[47] J.-M. Escoffre, T. Portet, C. Favard, J. Teissié, D. S. Dean, and M.-P. Rols, *Electromediated formation of dna complexes with cell membranes and its consequences for gene delivery,* Biochimica et Biophysica Acta (BBA)-Biomembranes **1808**, 1538 (2011).

[48] C. Faurie, M. Rebersek, M. Golzio, M. Kanduser, J.-M. Escoffre, M. Pavlin, J. Teissie, D. Miklavcic, and M.-P. Rols, *Electro-mediated gene transfer and expression are controlled by the life-time of dna/membrane complex formation,* The journal of gene medicine **12**, 117 (2010).

[49] N. I. Hristova, I. Tsoneva, and E. Neumann, *Sphingosine-mediated electroporative dna transfer through lipid bilayers,* FEBS letters **415**, 81 (1997).

[50] M. I. Angelova and I. Tsoneva, *Interactions of dna with giant liposomes,* Chemistry and physics of lipids **101**, 123 (1999).

[51] L. V. Chernomordik, A. V. Sokolov, and V. G. Budker, *Electrostimulated uptake of dna by liposomes,* Biochimica et Biophysica Acta (BBA)-Biomembranes **1024**, 179 (1990).

[52] S. Haberl, D. Miklavčič, and M. Pavlin, *Effect of mg ions on efficiency of gene electrotransfer and on cell electropermeabilization,* Bioelectrochemistry **79**, 265 (2010).

[53] M. Wu and F. Yuan, *Membrane binding of plasmid dna and endocytic pathways are involved in electrotransfection of mammalian cells,* PloS one **6**, e20923 (2011).

[54] T. Portet, C. Favard, J. Teissié, D. S. Dean, and M.-P. Rols, *Insights into the mechanisms of electromediated gene delivery and application to the loading of giant vesicles with negatively charged macromolecules,* Soft Matter **7**, 3872 (2011).

[55] G. L. Lukacs, P. Haggie, O. Seksek, D. Lechardeur, N. Freedman, and A. Verkman, *Size-dependent dna mobility in cytoplasm and nucleus,* Journal of biological chemistry **275**, 1625 (2000).

[56] E. Dauty and A. Verkman, *Actin cytoskeleton as the principal determinant of size-dependent dna mobility in cytoplasm a new barrier for non-viral gene delivery,* Journal of Biological Chemistry **280**, 7823 (2005).

[57] C. Rosazza, J.-M. Escoffre, A. Zumbusch, and M.-P. Rols, *The actin cytoskeleton has an active role in the electrotransfer of plasmid dna in mammalian cells,* Molecular Therapy **19**, 913 (2011).

[58] C. Rosazza, S. Haberl Meglic, A. Zumbusch, M.-P. Rols, and D. Miklavcic, *Gene electrotransfer: a mechanistic perspective,* Current Gene Therapy **16**, 98 (2016).

[59] C. Rosazza, E. Phez, J.-M. Escoffre, L. Cézanne, A. Zumbusch, and M.-P. Rols, *Cholesterol implications in plasmid dna electrotransfer: Evidence for the involvement of endocytotic pathways,* International Journal of Pharmaceutics **423**, 134 (2012).

[60] C. Rosazza, H. Deschout, A. Buntz, K. Braeckmans, M.-P. Rols, and A. Zumbusch, *Endocytosis and endosomal trafficking of dna after gene electrotransfer in vitro,* Molecular Therapy-Nucleic Acids **5**, e286 (2016).

[61] B. Markelc, E. Skvarca, T. Dolinsek, V. P. Kloboves, A. Coer, G. Sersa, and M. Cemazar, *Inhibitor of endocytosis impairs gene electrotransfer to mouse muscle in vivo,* Bioelectrochemistry **103**, 111 (2015).

[62] C.-C. Chang, M. Wu, F. Yuan, *et al.*, *Role of specific endocytic pathways in electrotransfection of cells,* Molecular Therapy-Methods & Clinical Development **1**, 14058 (2014).

[63] L. D. Cervia, C.-C. Chang, L. Wang, and F. Yuan, *Distinct effects of endosomal escape and inhibition of endosomal trafficking on gene delivery via electrotransfection,* PloS one **12**, e0171699 (2017).

[64] M. Mao, L. Wang, C. C. Chang, K. E. Rothenberg, J. Huang, Y. Wang, B. D. Hoffman, P. B. Liton, and F. Yuan, *Involvement of a Rac1-Dependent Macropinocytosis Pathway in Plasmid DNA Delivery by Electrotransfection,* Molecular Therapy **25**, 803 (2017).

[65] L. Wang, S. E. Miller, and F. Yuan, *Ultrastructural analysis of vesicular transport in electrotransfection,* Microscopy and Microanalysis **24**, 553 (2018).

[66] M. Pavlin and M. Kandušer, *New insights into the mechanisms of gene electrotransfer–experimental and theoretical analysis,* Scientific reports **5**, 9132 (2015).

[67] P. F. Lurquin and K. Athanasiou, *Electric field-mediated dna encapsulation into large liposomes,* Biochemical and biophysical research communications **267**, 838 (2000).

[68] G. Saulis and R. Saulė, *Size of the pores created by an electric pulse: Microsecond vs millisecond pulses,* Biochimica et Biophysica Acta (BBA)-Biomembranes **1818**, 3032 (2012).

[69] W. Krassowska and P. D. Filev, *Modeling electroporation in a single cell,* Biophysical journal **92**, 404 (2007).

[70] D. A. Zaharoff and F. Yuan, *Effects of pulse strength and pulse duration on in vitro dna electromobility,* Bioelectrochemistry **62**, 37 (2004).

[71] S. Sukharev, V. Klenchin, S. Serov, L. Chernomordik, and C. YuA, *Electroporation and electrophoretic dna transfer into cells. the effect of dna interaction with electropores,* Biophysical journal **63**, 1320 (1992).

[72] N. C. Stellwagen, C. Gelfi, and P. G. Righetti, *The free solution mobility of dna,* Biopolymers: Original Research on Biomolecules **42**, 687 (1997).

[73] M. Yu, W. Tan, and H. Lin, *A stochastic model for dna translocation through an electropore,* Biochimica et Biophysica Acta (BBA)-Biomembranes **1818**, 2494 (2012).

[74] V. Klenchin, S. Sukharev, S. Serov, L. Chernomordik, and C. YuA, *Electrically induced dna uptake by cells is a fast process involving dna electrophoresis,* Biophysical journal **60**, 804 (1991).

[75] M. Muthukumar, *Polymer translocation through a hole,* The Journal of Chemical Physics **111**, 10371 (1999).

[76] G. H. McKinley and T. Sridhar, *Filament-stretching rheometry of complex fluids,* Annual Review of Fluid Mechanics **34**, 375 (2002).

[77] J. Dinic, Y. Zhang, L. N. Jimenez, and V. Sharma, *Extensional relaxation times of dilute, aqueous polymer solutions,* ACS Macro Letters **4**, 804 (2015).

[78] G. H. McKinley, *Visco-elasto-capillary thinning and break-up of complex fluids,* in Rheology Reviews, edited by D. M. Binding and K. Walters (British Society of Rheology, Aberystwyth, UK , 1 (2005).

[79] Y. Amarouchene, D. Bonn, J. Meunier, and H. Kellay, *Inhibition of the finite-time singularity during droplet fission of a polymeric fluid,* Physical Review Letters **86**, 3558 (2001).

[80] J. Eggers, *Nonlinear dynamics and breakup of free-surface flows,* Reviews of modern physics **69**, 865 (1997).

[81] C. Clasen, J. Plog, W.-M. Kulicke, M. Owens, C. Macosko, L. Scriven, M. Verani, and G. H. McKinley, *How dilute are dilute solutions in extensional flows?* Journal of Rheology **50**, 849 (2006).

[82] V. Entov and E. Hinch, *Effect of a spectrum of relaxation times on the capillary thinning of a filament of elastic liquid,* Journal of Non-Newtonian Fluid Mechanics **72**, 31 (1997).

[83] F. Ingremeau and H. Kellay, *Stretching polymers in droplet-pinch-off experiments,* Physical Review X **3**, 041002 (2013).

[84] D. Bousfield, R. Keunings, G. Marrucci, and M. Denn, *Nonlinear analysis of the surface tension driven breakup of viscoelastic filaments,* Journal of non-newtonian fluid mechanics **21**, 79 (1986).

[85] H.-C. Chang, E. A. Demekhin, and E. Kalaidin, *Iterated stretching of viscoelastic jets,* Physics of Fluids **11**, 1717 (1999).

[86] S. L. Anna and G. H. McKinley, *Elasto-capillary thinning and breakup of model elastic liquids,* Journal of Rheology (1978-present) **45**, 115 (2001).

[87] C. Clasen, J. Eggers, M. A. Fontelos, J. Li, and G. H. McKinley, *The beads-on-string structure of viscoelastic threads,* Journal of Fluid Mechanics **556**, 283 (2006).

[88] E. Turkoz, J. M. Lopez-Herrera, J. Eggers, C. B. Arnold, and L. Deike, *Axisymmetric simulation of viscoelastic filament thinning with the oldroyd-b model,* Journal of Fluid Mechanics **851** (2018).

[89] J. Eggers, M. Herrada, and J. Snoeijer, *Self-similar breakup of polymeric threads as described by the oldroyd-b model,* arXiv preprint arXiv:1905.12343 (2019).

[90] C. M. Schroeder, *Single polymer dynamics for molecular rheology,* Journal of Rheology **62**, 371 (2018).

[91] G. Juarez and P. E. Arratia, *Extensional rheology of dna suspensions in microfluidic devices,* Soft Matter **7**, 9444 (2011).

2

DNA-Membrane Interaction

DNA-membrane complex formation during electroporation is DNA size dependent

Size of DNA molecules governs their interaction with the cell membrane during electroporation and their subsequent transport inside the cell. In order to investigate the effect of DNA size on DNA-membrane interaction during electroporation, cells are electro-pulsed with DNA molecules; 15 bp, 25 bp, 50 bp, 100 bp and 1000 bp (bp = base pairs). Within the experimental parameter space, DNA-membrane complexes or DNA aggregates are observed at the cell membrane for DNA molecules containing 25 or more base pairs. No aggregates are observed for DNA molecules containing 15 bp. For all DNA sizes, direct access to the cytoplasm is observed, however the amount translocated decays with the size. The observed dependency of DNA aggregate formation on the size of the DNA molecules is consistent with the Onsager's theory of condensation of anisotropic rod-like molecules.

This chapter is published in Biochimica et Biophysica Acta (BBA)-Biomembranes **1862**, 183089 (2019) [1].

2.1. INTRODUCTION

The physical and chemical nature of the bio-molecule plays a huge role in electric field mediated molecular delivery [2]. Depending upon the pulse parameters, large nucleic acids such as plasmid DNA (pDNA), enter the cells pre-dominantly via endocytosis after electropermeabilization [3–12]. The endosomal (or endocytotic) cargo is recognized by the cell and handed-off to the intra-cellular pathways after uptake. Their trafficking through the cytoskeleton is mediated by the microtubule network and its associated machinery (dyenin motor) [13–15]. Small nucleic acids, such as small interfering RNA (siRNA), on the contrary enter the cell passively [16–18] and undergo fast, but hindered diffusion through the actin network [19, 20]. The different pathways after uptake have very different outcomes in cargo degradation, chance of reaching their assigned target and, ultimately, therapeutic effect. Electric field mediated DNA delivery has enjoyed success in clinical trials which can be mainly attributed to a trial-and-error based approach of optimization [21, 22]. Further increase in therapeutic efficiency is needed, and can be achieved by understanding the biophysical mechanism of transport [23]. Hence, key to optimization relies on identifying and targeting the rate limiting factors such as mechanisms of cellular uptake and intra-cellular pathways which are highly sensitive to the size of nucleic acids. The influence of size of the nucleic acids on their uptake during electroporation thus plays a crucial role in enhancing the efficiency of electric field mediated gene delivery.

When we focus on the role of nucleic acid size in electroporation (or electropermeabilization), the following experimental and theoretical picture emerges. For lipid vesicles, experiments and theoretical models suggest electrophoresis of DNA molecules through large(-enough) pores formed in the vesicle membrane during electroporation [24, 25]. The influence of size is thus contained in the bulk electrophoretic mobility which in-turn is independent of the size of the DNA molecule [26]. On restricting the pore size to the thickness of a base-pair, the transport is determined by cross-pore electrophoretic mobility and entropic effects from the DNA molecule become dominant. A different theoretical model taking these effects into account suggests that the translocation efficiency follows a power law decay with the size of the DNA molecule [27]. The models and experiments provide the basis for the influence of size of nucleic acids for vesicles where active mechanisms are *de-facto* absent. In case of living cells, plasmid DNA (pDNA) molecules interact with the cell membrane during electric field pulses forming DNA-membrane complexes (referred to as DNA aggregates) at the cell membrane [28, 29]. In a time scale of 10-15 min after pulses, these aggregates are internalized via the active machinery of endocytosis [4–11]. Smaller nucleic acids, such as small interfering RNA (siRNA) [16] and antisene DNA molecules containing Locked Nucleic Acids (LNA/DNA chimeras) [17, 18], have direct access to the cytoplasm during electric field pulses. The influence of size of nucleic acids is manifested distinctly in the form of interaction of these molecules with the cell membrane by forming DNA aggregates. This aggregation of nucleic acids thus provides a signature for identifying the mechanism of nucleic acids uptake and subsequent intra-cellular pathways.

A basis for size dependent aggregation or condensation of DNA molecules can be understood from entropic arguments provided by Onsager's criterion [30]. According to this criterion, rod-like molecules with sufficient anisotropy can condense into a ne-

matic state beyond a critical concentration. In the nematic phase, rod-like molecules gain enough (translational) entropy compared to a randomly oriented isotropic state, sufficient to drive this transition [31]. Such a theory takes into account the size of the molecules, length L and thickness d, predicting the isotropic to nematic transition for L ≥ 4d [30]. Nucleic acids of size 25 bp are close to this transition [32].

The experiments and observations are only available for large nucleic acids such as pDNA (4700 bp) and small nucleic acids such as siRNA and LNA/DNA oligomers (20-25 bp). Although the difference in their uptake mechanism during electroporation is widely recognized and acknowledged, there is a huge gap of intermediate sizes for which the uptake mechanism is not identified. This prevents us from obtaining a precise and complete understanding of the influence of the size of nucleic acid on their uptake during electropermeabilization. Very few studies have been performed so far that have systematically investigated the effect of size of the DNA molecules on electroporation mediated nucleic acid delivery. However, they have primarily focussed on either the translocation (cross-membrane transport) [33] or transfection (ultimate gene expression) efficiency as a function of the size of the nucleic acid [33, 34]. Till date no study has focussed on influence of size of the DNA molecule directly on DNA aggregation at the membrane level that could generate much needed insights into the mechanism of uptake and intra-cellular trafficking.

In this paper, we varied the size of the DNA molecules from 15 bp to 1000 bp, in order to investigate its effect on DNA membrane interaction and cross-membrane transport due to (or during) application of pulsed electric field. This study shows that DNA aggregation at the membrane level is sensitive to the size of the DNA molecules. DNA molecules of size 15 bp had direct access to the cytoplasm and their transport took place without the formation DNA aggregates for the electric pulsing conditions used. DNA molecules of size 25 bp did form DNA aggregates; however, this was a function of electric pulse amplitude. DNA molecules of size 50 bp, 100 bp and 1000 bp showed distinct DNA aggregate formation; however, direct access to the cytoplasm during electric field pulses was also observed for these sizes. This suggests multiple modes of transport for the same size of DNA molecule. Moreover, these results demonstrate that DNA aggregate formation is an onset phenomenon and happens for even small DNA molecules such as 25 bp to 100 bp and is consistent with Onsager's criterion for condensation of rod-like molecules.

2.2. MATERIALS AND METHODS

2.2.1. CELL LINES AND SUB-CULTURING

The Chinese Hamster Ovary cells, CHO-K1 (or CHO), were grown in Nutrient Mixture Ham F-12 (Sigma Aldrich®) supplemented with ≈ 10% Fetal Bovine Serum (Sigma Aldrich®) and ≈ 1% Antibiotic-Antimycotic solution (Gibco®). The cells were incubated at 37°C with 5% CO_2 and the subculture was performed three times a week. For electropulsation experiments, 0.25×10^5 cells were plated (per well) on a µ-slide chambered coverslip of 4 wells (Ibidi®), with 500 µl of culture medium 24 h before the application of the electric pulses.

Human lung carcinoma cells, A549, were grown in a medium consisting of Dulbecco's

Modified Eagle's Medium (Sigma Aldrich®) supplemented with ≈ 10% Fetal Bovine Serum (FBS) (Sigma Aldrich®) and ≈ 1% Antibiotic-Antimycotic solution (Gibco®). The cells were incubated at 37°C with 5% CO_2 and the subculture was performed three times a week. For electropulsation of A549 cells, 0.30×10^5 cells were plated (per well) on a µ-slide chambered coverslip of 4 wells (Ibidi®) with 500 µl of culture medium 24 h before the application of the electric pulses.

2.2.2. DNA FRAGMENTS AND STAINING

DNA fragments of different sizes (1000 bp, 100 bp, 50 bp, 25 bp and 15 bp) were purchased from ThermoFisher® under the brand of NoLimits™ DNA. Each DNA fragment stock vial consisted of 10 µg of DNA at a concentration of 0.5 µg/µl in 10 mM Tris-HCl (pH 7.6) and 1 mM EDTA. The DNA molecules were stained in the stock vials using YOYO-1 dye (1 mM in DMSO from ThermoFisher®). This dye has been commonly used to visualize DNA molecules under physical forces [35]. The bp:YOYO-1 dye molecule staining ratio was kept constant at 10:1 for all the experiments and staining was performed on ice for 1 hour. Such a staining ratio is known to cause a 15% reduction in electrophoretic mobility of DNA molecule which is predominantly attributed to a reduction in the net effective charge of the YOYO-1-DNA complex [36, 37].

2.2.3. ELECTROPULSATION OF CELLS

Just before the electropulsation experiments, the cells were taken out of the incubator and the culture medium was removed from the µ-slide and the cells were washed twice with Dulbecco's Phosphate Buffered Saline from Sigma Aldrich®. The chambers were then filled with 500 µl of pulsing buffer (10 mM KH_2PO_4/Na_2HPO_4, 1 mM $MgCl_2$ and 250 mM sucrose at a pH of 7.4) containing 10 μg/ml of stained DNA solution. Stainless steel electrodes of 3 mm gap were immersed in the chamber and fixed to the walls to ensure a uniform electric field distribution. To apply the electric field, these electrodes were connected to a cell electropulsator (BetaTech Electro cell B10 HV-LV, France), which can deliver unipolar and bipolar square-wave pulses. All experiments were conducted at room temperature and atmospheric pressure. The maximum time allowed for the cells to be out of the incubator during all the experiments was 30 min.

2.2.4. CONFOCAL IMAGING OF DNA UPTAKE

To image the localization and dynamics of DNA molecules, experiments were performed on a confocal microscope (ZEISS LSM 710, Germany). 488 nm Argon laser was used to excite the YOYO-1 labelled DNA molecules and the images were acquired using a 40X (1.3 NA oil immersion) objective. The scanning speed of the laser was adjusted to obtain a pixel dwell of 7.04 µs. The field of view consisted of 1836 × 1836 pixels spanning 212.55 × 212.55 μm^2. All the images were acquired at an 8-bit pixel depth.

2.3. RESULTS

In order to observe the effect of DNA size on electric field mediated DNA delivery, linear DNA fragments of size 15 bp, 25 bp, 50 bp, 100 bp and 1000 bp were chosen. All DNA fragments were fluorescently labelled with YOYO-1 dye. The effect of DNA size was then

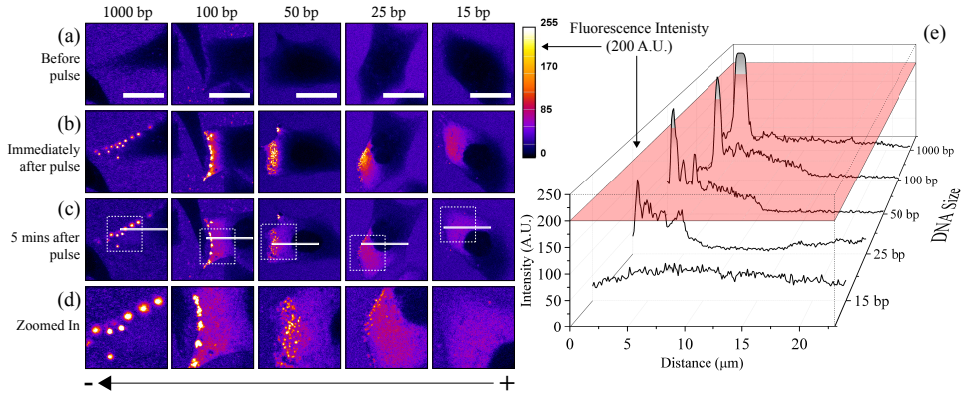

Figure 2.3.1: Figure showing representative CHO cells before and after the application of electric pulses. The images are color coded according to the intensity of fluorescently labelled DNA molecules. The color bar represents the corresponding fluorescence intensity values. (a) Represents the state of the cell before the application of electric pulses. Scale bar = 20 μm. (b) Represents the state of the cell immediately (within ≈ 1 min) after the application of electric pulses. The electric pulse amplitude was 0.4 kV/cm with a pulse duration of 5 ms. 10 pulses were applied at a frequency of 1 Hz. (c) Represents the state of the cell 5 min after the application of electric pulses. (d) Shows a zoomed in view of the cells 5 min after the electric pulses were applied. The field of view in (d) is defined by the dotted white box drawn in (c). In each experiment the size of the DNA molecules was varied as indicated above each column. The direction of applied electric field is indicated by the arrow shown below (d). (e) Shows the fluorescence intensity profiles along the solid white box drawn in (c).

observed in terms of fluorescence intensity of DNA molecules interacting with the cell membrane (as DNA aggregates) after the application of electric pulses. The results are shown in Figure 2.3.1.

Figure 2.3.1 (a) shows CHO cells before application of electric pulses for all DNA sizes. Fluorescently labelled DNA molecules were found to be homogeneously distributed around the cells and no DNA membrane interaction or penetration of DNA molecules into the cells was observed. After applying a train of 10 electric field pulses at an amplitude of 0.4 kV/cm with a pulse duration of 5 ms and at a frequency of 1 Hz, DNA molecules were found to both interact with the membrane, and also be delivered into the cells. This is shown in Figure 2.3.1 (b) (Immediately after pulse) for each size of DNA studied. DNA membrane interaction or DNA aggregation at the membrane was observed for 1000 bp, 100 bp, 50 bp and 25 bp as local bright spots of high fluorescence intensity. Direct access of DNA molecules to the cytoplasm was observed for all DNA sizes as seen by a homogeneous fluorescence intensity inside the cells. The cells were allowed to relax, and observations were made again after 5 min of applying the electric pulses. This was done in order to distinguish the locally accumulated but free DNA from aggregated DNA at the membrane, as the primary contributor towards local bright spots. From Figure 2.3.1 (c) (5 min after pulse), it can be seen that the bright spots remain similar in number and area (to the corresponding images in Figure 2.3.1 (b)) for DNA sizes of 1000 bp, 100 bp and 50 bp. However, a lot of bright spots that were seen for 25 bp (Figure 2.3.1 (b)) were no longer present 5 min after pulse (Figure 2.3.1 (c)), rendering them as mainly accumulated but free DNA rather than aggregated DNA. Figure 2.3.1 (d) shows zoomed in view

of cells 5 min after the application of electric pulses for the dotted white boundaries depicted in Figure 2.3.1 (c), to clearly indicate the DNA aggregates as local bright spots, as observed for DNA size of 1000 bp, 100 bp and 50 bp. Experiments using bipolar electric pulses were also done to confirm that these bright spots are stable DNA aggregates for both CHO and A549 cells (see Supplementary Information - Section 2.A).

Figure 2.3.1 (e) shows fluorescence intensity profiles along the region marked by solid white box in Figure 2.3.1 (c) for each DNA size. The profiles correspond to the fluorescence intensity along the penetration distance into the cell and are averaged along the width of the box. It can be seen that the fluorescence intensity peaks near the cell membrane for the DNA sizes that form aggregates (1000 bp, 100 bp, 50 bp). The peaks in the profile correspond to fluorescence from DNA aggregates that are located on the edge of the cell membrane. On penetrating further into the cell the fluorescence intensity drops but is still greater than zero. This fluorescence was not present before the application of electric pulses and hence correspond to free DNA that has been translocated into the cell in non aggregated form.

The fluorescence intensity profiles in Figure 2.3.1 (e) suggest that aggregated DNA can be distinguished from free DNA by choosing an appropriate fluorescence intensity threshold. Since the peaks along the profile reach a minimum value of 200 A.U. (Arbitrary Units) when DNA aggregates are formed, as can be seen by the pink cutting-plane in Figure 2.3.1 (e), it can be argued that DNA aggregates have at least a fluorescence intensity of 200 A.U. On the contrary the free DNA inside the cytoplasm correspond to a fluorescence intensity < 200 A.U. Therefore, we chose the fluorescence intensity of 200 A.U. as the threshold to distinguish between aggregated DNA at the membrane and free DNA inside the cytoplasm.

The distinction between fluorescence intensity of aggregated DNA and free DNA, based on a threshold described in Figure 2.3.1 (e), is used to analyse their cellular uptake separately and independently, as a function of DNA size. Figure 2.3.2 (a) shows a representative CHO cell (5 min after the application of electric pulses) for a DNA size of 50 bp. Segmenting the image with a threshold intensity of 200 A.U., divides the image into two parts: a region with aggregated DNA (> 200 A.U.) and region with free DNA (< 200 A.U.). The boundaries dividing these two regions are shown in Figure 2.3.2 (b) marked in red. The regions depicting aggregated DNA are shown in Figure 2.3.2 (c), filled in green. In order to get more insights into the effect of DNA size on aggregation of DNA molecules, the apparent area of these regions (fluorescence intensity > 200 A.U.) was calculated for a number of cells, 5 min after the application of electric pulses, for each DNA size. The resulting net aggregated area was summed up for each DNA size and normalized by the number of cells analysed. This is shown in Figure 2.3.2 (e) and (f) for CHO and A549 cells respectively, and for two different electric pulse amplitudes. Experiments were done on two different cell lines (CHO and A549) to check the consistency of the trend. To further confirm the trend observed, a second independent set of experiments was performed for DNA size of 25-100 bp, and the data is shown in Section 2.D of Supplementary Information. Since 15 bp DNA did not show any aggregate formation, the aggregated area per cell is almost 0. The aggregated area per cell for DNA molecules of size 25 bp is only slightly higher than for 15 bp and is consistent with the observations in Figure 2.3.1 (c-e) for 25 bp. On increasing the size of DNA further, the apparent area per cell of aggregated

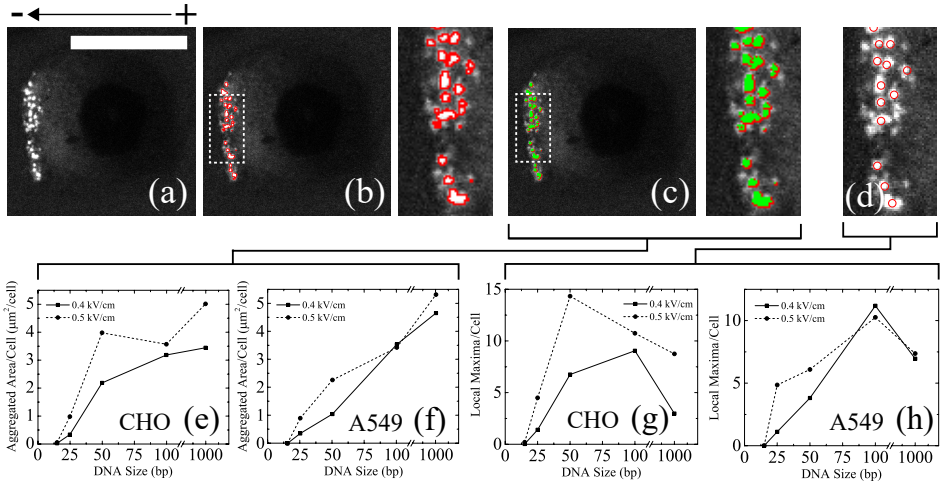

Figure 2.3.2: Characterization of DNA aggregates. (a) Image of a representative CHO cells 5 min after the application of electric pulses with DNA molecules of size 50 bp. Scale bar = 20 μm. The electric pulse amplitude was 0.4 kV/cm with a pulse duration of 5 ms. 10 pulses were applied at a frequency of 1 Hz. (b) The image in (a) was segmented applying a fluorescence intensity threshold of 200 A.U. resulting in two regions of high (> 200 A.U.) and low (< 200 A.U.) fluorescence intensities demarcated by a red outline. (c) High fluorescence intensity region (> 200 A.U.) is depicted coloured in green. (d) Local maxima or DNA aggregates detected by applying Gaussian filters (see Supplementary Information - Section 2.B for detailed algorithm of local maxima detection). Aggregated area per cell as a function of size of the DNA molecule for (e) CHO and (f) A549 cell lines. Number of local maxima detected as a function of size of the DNA molecule for (g) CHO and (h) A549 cell lines. For each data point in (e)-(h), 45 cells on average were analysed with a minimum of 25 cells and maximum of 81 cells.

DNA molecules increases further for both the cell lines (CHO and A549). It should also be noted that a higher electric field intensity led to an increase in the aggregated DNA area per cell. This is especially pronounced for a DNA size of 25 bp, where a considerably higher amount of DNA molecules was found to interact with the membrane forming DNA aggregates.

Apart from aggregated area per cell, the number of aggregates per cell was calculated by applying Gaussian filters to the images and identifying the DNA aggregates (or bright spots) as local maxima. These local maxima of fluorescence intensity are identified in red circles in figure 2.3.2 (d) on DNA aggregates for the same representative CHO cell as in Figure 2.3.2 (a)-(c). The detailed algorithm for detecting the number of DNA aggregates as local maxima is given in Supplementary Information - Section 2.B. The total number of local maxima was calculated for a number of cells, for each DNA size, and then normalized by the number of cells analysed. The same cells were analysed to calculate local maxima as in Figure 2.3.2 (e) and (f). Figure 2.3.2 (g) and (h) shows the number of local maxima per cell as a function of DNA size for CHO and A549 cells, respectively, and for two different electric pulse amplitudes. The number of local maxima per cell follows a similar behaviour as the net aggregated DNA area/cell shown in figure 2.3.2 (f). However, there is a dip in the number of aggregates for a 1000 bp. This dip could possibly be explained by the fact that the experiments were done by keeping the DNA concentra-

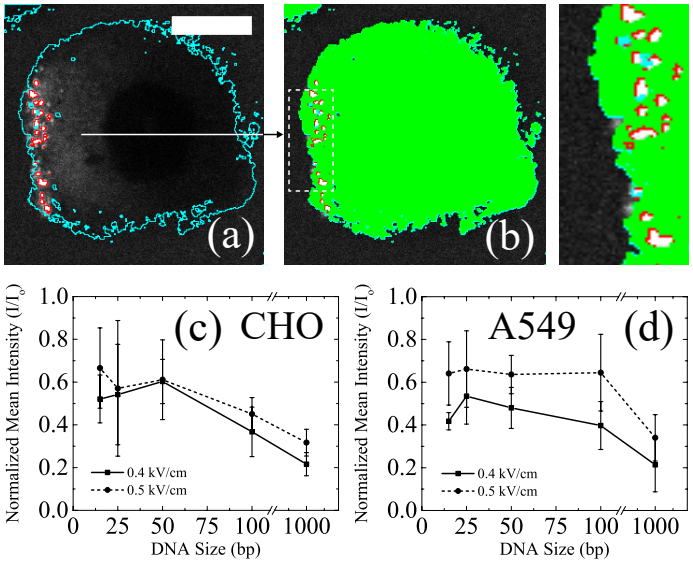

Figure 2.3.3: Characterization of free DNA that has direct access to the cytoplasm. (a) Image of a representative CHO cells 5 mins after the application of electric pulses with DNA molecules of size 50 bp. Scale bar = 10 µm. The electric pulse amplitude was 0.4 kV/cm with a pulse duration of 5 ms. 10 pulses were applied at a frequency of 1 Hz. The image was segmented by applying a fluorescence intensity threshold of 200 A.U. resulting in two regions of high (> 200 A.U.) and low (< 200 A.U.) fluorescence intensities demarcated by a red outline. The cell contour is demarcated by a cyan outline. (b) Low fluorescence intensity region (< 200 A.U.) is depicted in green. (c) Mean fluorescence intensity of free DNA (green region) as a function of the size of DNA molecule is shown in (c) and (d) for CHO and A549 cell lines, respectively. The error bar represents standard deviation around the average of the mean fluorescence intensity of free DNA depicted by the region coloured in green in each cell. For each data point in (c) and (d), 11 cells were analysed on average with a minimum of 5 cells and a maximum of 22 cells.

tion constant at 10 µg/ml . Thus the cells were always exposed to the same number of base-pairs but the number of DNA molecules was decreasing with increasing DNA size.

Increasing DNA size increases the contribution towards aggregated DNA as seen by the aggregated DNA area per cell and number of local maxima per cell in figure 2.3.2 (e-h). By segmenting the image and considering fluorescence intensity < 200 A.U., a similar analysis can be done for free DNA. This is shown in Figure 2.3.3. A representative CHO cell is shown in Figure 2.3.3 (a) 5 mins after the application of electric pulses for a DNA size of 50 bp. The image is segmented with a threshold fluorescence intensity of 200 A.U. and the segmentation result is demarcated by red outlines. The cell contour is shown in cyan. The algorithm for determining the cell contour is shown in Supplementary Information - Section 2.C. The region corresponding to a fluorescence intensity < 200 A.U., filled in green is shown in figure 2.3.3 (b). The mean fluorescence intensity within this region is calculated for each individual cell after 5 min of electric pulse application (I_{after}). The mean fluorescence intensity before the application of electric pulses (I_{before}), within the same region (shown in green), is subtracted from this value in order to estimate the fluorescence intensity of free DNA translocated inside the cytoplasm as $I = I_{\text{after}} - I_{\text{before}}$.

After normalizing with the mean fluorescence intensity of DNA molecules outside the cells (I_o), the corresponding result (I/I_o) is plotted in figure 2.3.3 (c) and (d) as a function of DNA size and for CHO and A549 cell lines, respectively, and for two different electric pulse amplitudes. Contrary to aggregated DNA, the fluorescence intensity of free DNA decreases with increasing DNA size.

2.4. DISCUSSION

Our results indicate that DNA aggregation at the cell membrane is not only observed for large DNA sizes such as 1000 bp, as previously reported in literature, but also for small DNA sizes of 25 bp, 50 bp and 100 bp. With an increasing size there is an increasing tendency for the DNA molecules to aggregate at the cell membrane. At the same time, the amount of DNA that has direct access to the cytoplasm (free DNA) tend to decreases with the size of the DNA molecule. Such a dependency of amount of aggregated and free DNA on the size of the DNA molecule is discussed below with possible suggestions for the mechanism of DNA aggregation.

Aggregated DNA can be considered to be in a different physical state compared to bulk DNA. Due to localized high fluorescence intensity of DNA aggregates, this state can be referred to as a condensed state of DNA molecules. Persistence length of DNA under physiological conditions is around 50 nm or 150 bp [38, 39]. Therefore, DNA molecules of size 15 bp, 25 bp, 50 bp and 100 bp are essentially rod-like molecules, whereas DNA molecules of size 1000 bp are coiled. Condensation of rod-like molecules, by increasing the concentration, was first described by Onsager in 1949 [30]. According to his theory, rod-like molecules can condense into liquid crystal (nematic) phases if they posses sufficient anisotropy; L ≥ 4d, where L is the length of the molecule and d is the thickness (or diameter) of the molecule. If we consider the thickness of DNA molecules to be around 2 nm and the inter-base-pair distance to be 0.34 nm [40], DNA molecules of size ~ 25 bp and higher possess sufficient anisotropy as required by the Onsager's criterion to be condensed into a nematic phase. On the other hand, DNA molecules of size 15 bp are sufficiently isotropic and hence will not condense into a nematic phase. We observed aggregates for DNA molecules of size 25 bp and higher, and no aggregates were observed for a DNA size of 15 bp consistent with Onsager's criterion.

Isotropic to nematic phase transition of hard rods was proposed for a 3-dimensional system [30]. In case of electroporation, it is believed that DNA molecules are adsorbed on the cell membrane by the divalent cations, which enhance DNA aggregation [4]. Moreover, even after applying bipolar pulses, the aggregates remained anchored to the membrane (see Supplementary Information - Section 2.A). During electroporation, we are primarily dealing with a 2-dimensional system. Onsager's criteria for the isotropic-nematic phase transition (L ≥ 4d) was also shown to be valid for a 2-dimensional system of adsorbed short DNA strands confined between lipid bilayers [41]. In another study, it was shown that DNA origami nano-needles with sufficient anisotropy adsorbed on a lipid bilayer of a GUV, underwent an isotropic to nematic phase transition beyond a critical surface charge density [42]. These DNA nano-needles formed locally ordered domains in the nematic phase that were below 1 μm in size, consistent with the size of DNA aggregates that we observed (around 200-500 nm).

Based on entropic arguments by Onsager, an extremely high concentration is re-

quired to condense DNA into a nematic phase [30, 32]. It is possible that such high concentrations are never achieved by a non-permeabilizing electric field. However, upon permeabilization, electric field lines concentrate and penetrate the permeable sites on the cell membrane [43, 44]. Due to local enhancement of electric field at these permeable sites, the DNA molecules should also get concentrated, possibly reaching high enough concentrations required for the isotropic to nematic phase transition to kick in. Experiments were done for 2 different values of electric field intensities above the permeabilizing threshold. A general trend observed was that with higher electric field intensity, more DNA aggregates were observed. With an increasing field intensity, the permeabilized area is increased [45, 46], which could in principle account for higher number DNA aggregates per cell.

In addition, such a phenomenon also explains why DNA molecules are not only found in the aggregated state, but also have direct access to the cytoplasm. With a permeable electric field, the adsorbed DNA molecules can get locally accumulated at the permeable sites. As the size of the DNA molecules increases, its tendency, owing to its increasing anisotropy, to condense or aggregate increases (Figure 2.3.2). At the same time its tendency to translocate through the permeable structures and gain direct access to the cytoplasm decreases (Figure 2.3.3). During electroporation, it is also believed that there is a heterogenous population of the size of these permeable sites or defects [47, 48],, with longer pulses tending to favour a population of larger pores [49, 50]. It is possible that DNA molecules that gain direct access to the cytoplasm, enter the cells primarily through these permeable sites [3, 51, 52]. With a larger pore size there is an increasing probability that DNA molecules can translocate without getting stuck at the membrane. These observations are consistent with 2 classes of DNA molecules we observed, DNA molecules in the aggregated state at the membrane, and DNA molecules that have direct access to the cytoplasm.

For DNA molecules that have direct access to the cytoskeleton, relative contributions of electrophoretic drift and diffusion can be understood using the Péclet number (Pe). The Péclet number is defined by $Pe = t_{\text{diffusion}}/t_{\text{drift}}$, which compares the time-scale of diffusion $t_{\text{diffusion}}$, to the time-scale of drift t_{drift} [53]. The diffusive time scale can be defined by $t_{\text{diffusion}} = L^2/D$, where L is an appropriate length scale and D is the diffusion coefficient. The drift time can be defined by $t_{\text{drift}} = L/v$. Thus the Péclet number is defined as $Pe = vL/D$. For transport of DNA molecules through bulk, $v = \mu E$, where μ is the electrophoretic mobility of the DNA molecule and E is the applied electric field. Therefore, the bulk Péclet number is $Pe = (\mu E R_o)/D$, where radius of cells R_o is considered as an appropriate length scale. For permeabilizing electric field, $ER_o \sim 1$ V, according to Schwan equation [54], and as also considered in Ref. [24]. Therefore, the Péclet number for bulk transport of DNA molecules is $Pe \sim \mu/D(1\text{ V})$. The electrophoretic mobility of DNA molecules of size 15 bp-100 bp, can be considered as $\mu \sim 3.2 \times 10^{-4}$ cm^2 V^{-1} s^{-1} [55, 56], and the diffusion coefficient can be considered as $D \sim 6.5 \times 10^{-6}$ cm^2 s^{-1}bp$^{-0.68}$ [19]. With these values the Péclet number is $Pe \sim 50(\text{bp})^{0.68}$. Thus, for DNA sizes between 15 bp and 100 bp, Pe varies between 300 and 1200, implying that electrophoretic drift dominates diffusion for transport of DNA molecules in bulk during the electric field pulse. These estimates also support the hypothesis that DNA becomes highly concentrated next to the membrane during the pulse.

For transport through the pore, the Péclet number can be considered as $Pe_{\text{pore}} = v_{\text{pore}} L / D_{\text{pore}}$, where v_{pore} is the velocity and D_{pore} is the diffusivity, of the translocating DNA molecule through the pore. Contour length of the DNA molecule (L_c) can be considered as an appropriate length scale (L). Precise determination of v_{pore} and D_{pore} is beyond the scope of this work, however some estimates can be provided considering the framework followed in Ref. [55]. As shown in Ref. [55], $v_{\text{pore}}/D_{\text{pore}}$ was independent of the applied potential difference, for a DNA size of 500 bp. $v_{\text{pore}}/D_{\text{pore}} = 0.15 \pm 0.1$ nm^{-1}, for DNA translocating through pores of diameter 2.6-6 nm, similar to electro-pore diameters. Thus, Péclet number can be considered as $Pe_{\text{pore}} \sim 0.15 L_c$. For DNA sizes of 15-100 bp $L_c = 0.34 \times$bp nm and hence Pe_{pore} ranges between ~ 0.7 and 5. This indicates similar contributions of electrophoretic drift and diffusion for DNA molecules translocating through a pore. It should be noted that the applied potential difference ($\sim$ 0.20-0.35 V) and the aqueous solution across each side of the pore was different in Ref. [55]. In our experiments, DNA molecules encounter the cytoskeleton while translocating through the electro-pore. In this case, the diffusion coefficient is be lower [20], and might make electrophoretic drift as the dominant mode of transport of DNA molecules through the membrane.

Onsager's theory seems to describe the dependency of the size of the DNA molecule on DNA aggregate formation at the cell membrane during electroporation. However, it must be noted that high concentrations ($\approx$ 500 mg/ml) are required for the isotropic to nematic phase transition (based on entropic arguments) [30, 32]. There are also other mechanisms which can lead to DNA condensation and do not require such high concentrations. A common method to condense and precipitate DNA molecules is to use multivalent cations [57, 58]. For instance multivalent poly-amine cations (tri-valent and tetra-valent) caused condensation of 25 bp DNA molecules [59]. In this case, counter-ion induced attraction of the DNA molecules was most likely the reason for DNA condensation, and the condensed DNA molecules could be found in liquid crystal phases. Divalent cations have also been shown to condense DNA molecules in 2-dimensions [60]. DNA molecules adsorbed on a GUV through cationic lipids collapsed into a condensed phase through curvature mediated interactions [61, 62]. Thus, the origin of condensation or aggregation of DNA molecules is different in these cases (divalent cations or curvature mediated) compared to Onsager's criterion (high concentration), however their dependency on the size of the DNA molecule, to the best of our knowledge, is not explored. Thus, there is a possibility that the DNA molecules are condensing and aggregating at the cell membrane through different pathways during electroporation and further research is necessary to completely elucidate the origins and the nature of these DNA aggregates.

2.5. CONCLUSION

DNA aggregate formation was not only observed for large DNA molecules of size of 1000 bp but also for short DNA molecules of size 25 bp, 50 bp and 100 bp, whose persistence length is larger than the contour length, and hence behave as rod-like molecules. No DNA aggregates were observed for a DNA size of 15 bp. With increasing DNA size the tendency of the DNA molecules to aggregate increased, while the tendency to translocate freely into the cytoplasm decreased. In doing so, we probed the effects of size and

anisotropy of the DNA molecules on the DNA-membrane complex formation. These observations are consistent with the Onsager's theory of condensation of rod-like molecules.

APPENDIX

2.A. BI-POLAR ELECTRO-PULSATION RESULTS

It was previously observed that around 1 s was required for the DNA-membrane complex to form a stable aggregate [63]. Hence, applying bi-polar pulses can confirm the presence of stable DNA aggregates and bi-polar electric pulses with an interval of at least 2 s between the reversal of polarity should lead to the formation of DNA aggregates on both sides of the cell membrane facing the electrode.

In order to test this, the following pulsing conditions were used for various DNA sizes: bi-polar electric field amplitude ±0.4 kV/cm or ±0.5 kV/cm with a duration of 5 ms, and a 2 s time interval between the reversal of polarity. 10 such pulses were applied with a period of 4.01 s. All bi-polar experiments were performed using the same experimental procedure mentioned in the "Materials and Methods" section of the main text.

As can be seen from Figure 2.A.1 and Figure 2.A.2 for CHO cells and A549 cells respectively, bright spots or DNA aggregates were formed on both sides of the cell membrane facing the electrode for DNA sizes of 1000 bp, 100 bp and 50 bp (bp = base pairs). For a DNA size of 25 bp, only few DNA aggregates were observed depending on the electric pulse amplitude, whereas for a DNA size of 15 bp, no DNA aggregates were observed.

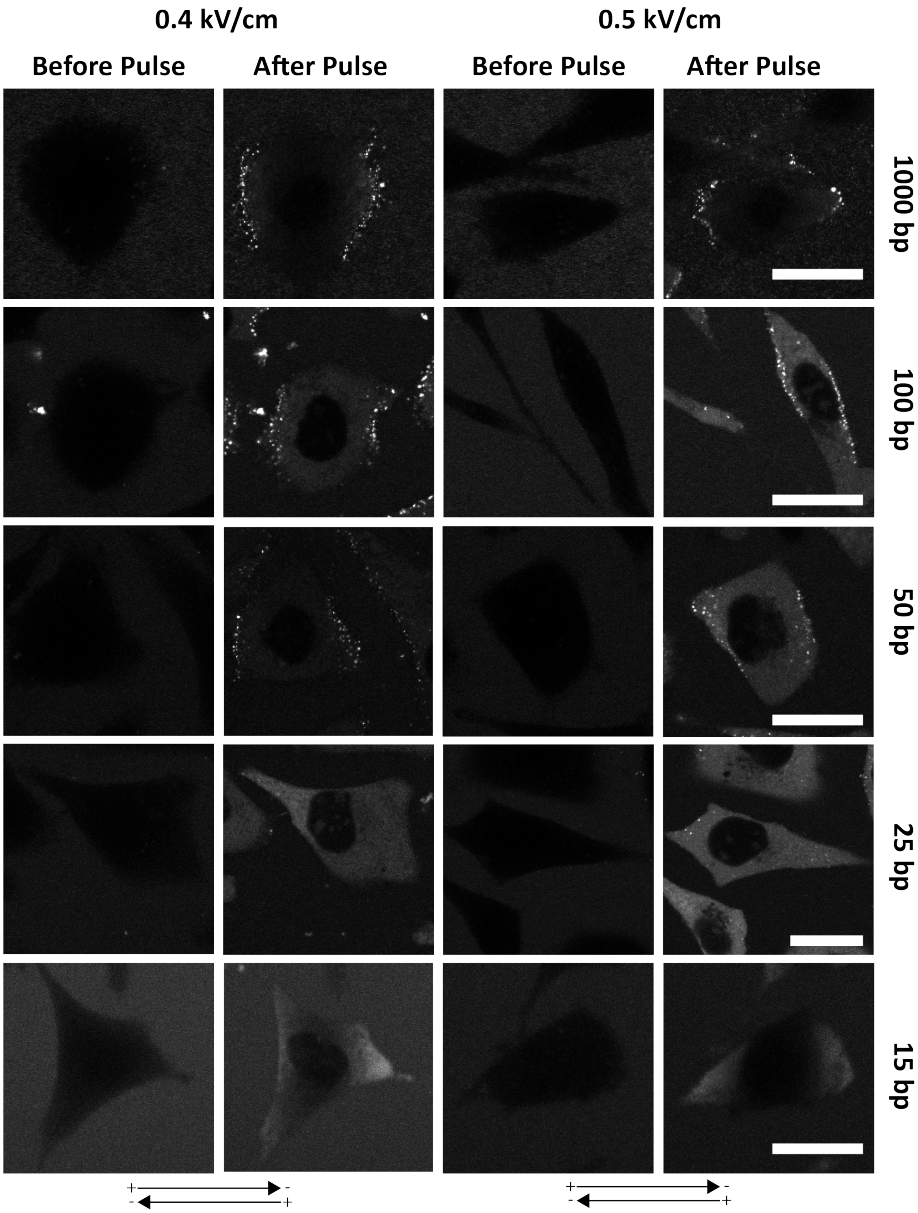

Figure 2.A.1: Representative CHO cells before and after the application of bi-polar electric pulses. Electric field amplitude applied was 0.4 kV/cm and 0.5 kV/cm as mentioned at the top of the image. Pulse duration was 5 ms with a time interval of 2 s before the reversal of polarity. 10 pulses were applied with a time period of 4.01 s. DNA size was varied as shown for each row. Scale bar = 20 μm.

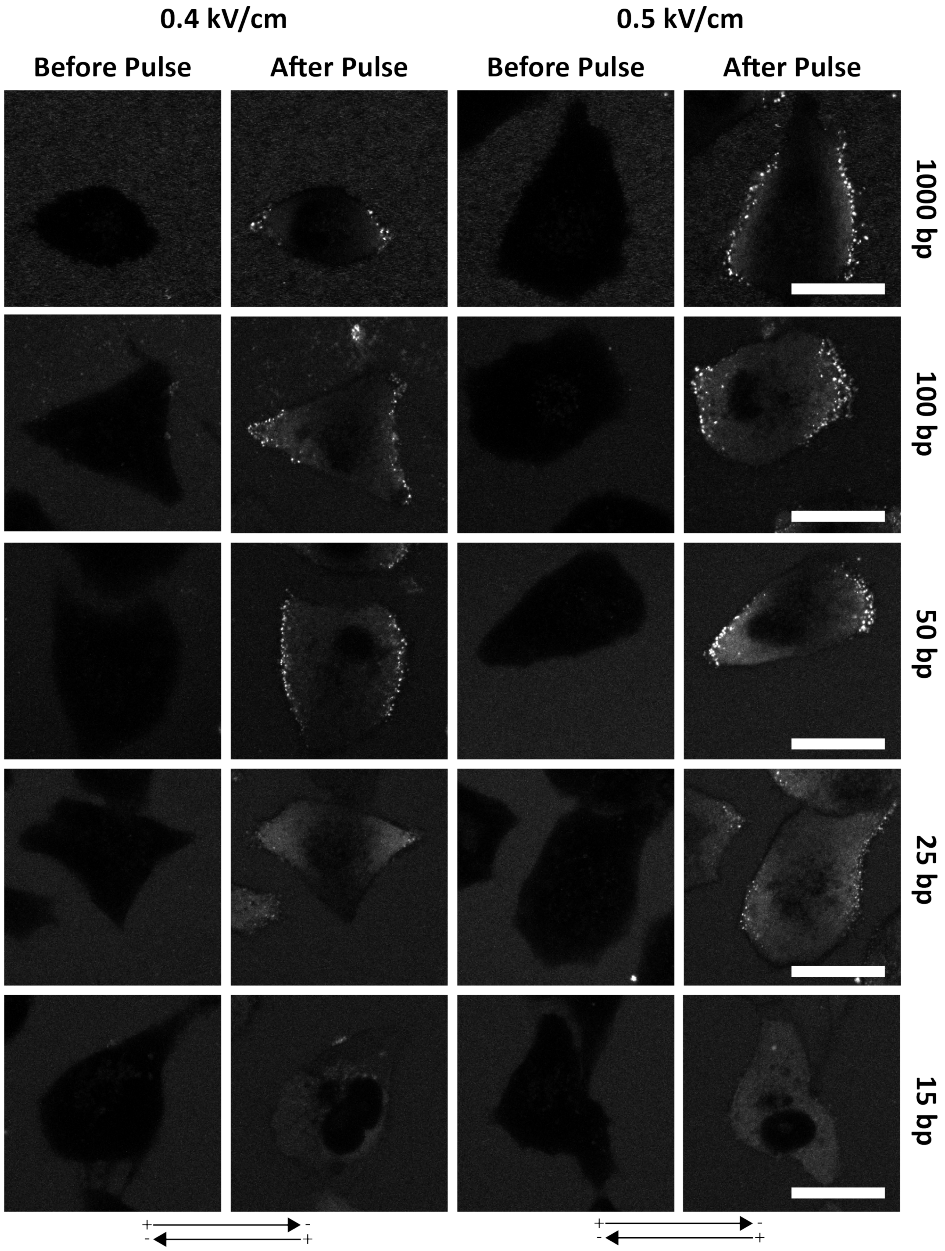

Figure 2.A.2: Representative A549 cells before and after the application of bi-polar electric pulses. Electric field amplitude applied was 0.4 kV/cm and 0.5 kV/cm as mentioned at the top of the image. Pulse duration was 5 ms with a time interval of 2 s before the reversal of polarity. 10 pulses were applied with a time period of 4.01 s. DNA size was varied as shown for each row. Scale bar = 20 µm.

2.B. LOCAL MAXIMA PROCESSING ALGORITHM

The algorithm to detect DNA aggregates as local maxima was adapted from [64] and is explained here. For our purpose, 4 Gaussian filters were chosen (Table 2.B.1) in order to capture DNA aggregates of different sizes.

Each of the filters in Table 2.B.1 were applied individually to the image being processed. A sample process is shown in Figure 2.B.1 for a single filter of standard deviation of 1 pixel and size of 3 x 3 pixel^2. Figure 2.B.1 (a) shows a color-coded image (according to fluorescence intensity) of a CHO cell 5 mins after the application of electric pulses for a DNA size of 50 bp (bp = base pairs). A zoomed in view of the aggregated area as demarcated by the dotted white box in Figure 2.B.1 (a), is shown in Figure 2.B.1 (b).

To detect the DNA aggregates as local maxima, first a median filter of size 3 x 3 pixel^2 was applied to the original image and the result is shown in Figure 2.B.1 (c). Then a fluorescence intensity threshold of 200 A.U. was applied to the image such that all pixels with a fluorescence intensity $\geq$ 200 A.U. retained their intensity values, and fluorescence intensity of all the other pixels was set to zero. This is shown in Figure 2.B.1 (d). Then the image was convolved with a Gaussian filter of standard deviation of 1 pixel and a size of 3 x 3 pixel^2 and the result is shown in Figure 2.B.1 (e). This converted the DNA aggregates into local maxima. Then a fluorescence intensity threshold of 200 A.U. was re-applied to the image as shown in Figure 2.B.1 (f). Then the DNA aggregates were detected as local maxima. A pixel was considered as a local maximum if it had a fluorescence intensity value which was higher than all its 8 neighboring pixels. The local maxima detected using this method is shown demarcated by red circles in Figure 2.B.1 (g). These local maxima detected are superimposed on the original raw gray-scale image as shown in Figure 2.B.1 (h). The same process was repeated for the remaining Gaussian filters in Table 2.B.1.

After applying the Gaussian filters on the particular image, the coordinates of the local maxima corresponding to each filter size were obtained. This is shown in Figure 2.B.2 (a) for the same cell as in Figure S3. Another representative CHO cell 5 mins after the application of electric pulses for a DNA size of 100 bp is shown Figure 2.B.2 (b), with DNA aggregates detected as local maxima. Figure 2.B.2 (a.1) and (b.1) show a zoomed in view of the aggregated area of the cell, where the field of view is defined by the dotted white box in Figure 2.B.2 (a) and (b) respectively. Figure 2.B.2 (a.2) and (b.2) show a further zoomed in view of the aggregated area, where the field of view is defined by the dotted red box in Figure 2.B.2 (a.1) and (b.1) respectively. A few DNA aggregates were detected as a local maxima multiple times, by the same and as well as different Gaussian filters, as

Table 2.B.1: List of Gaussian filters used. Pixel scaling: 1836 pixels = 212.55 µm.

Standard Deviation (Pixels)	Size of the filter (pixel^2)
1	3 × 3
2	7 × 7
3	9 × 9
5	15 × 15

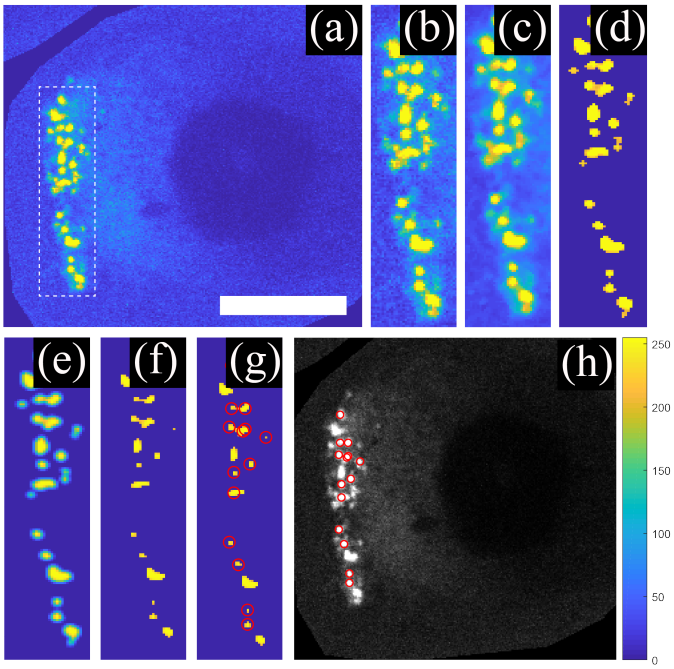

Figure 2.B.1: Imaging processing algorithm for detecting DNA aggregates as local maxima. (a) Color-coded image of a CHO cell 5 mins after the application of electric pulses for a DNA size of 50 bp (bp = base pairs). Scale bar = 10 μm (or approx. 86 pixels). Electric field amplitude was 0.4 kV/cm and 10 pulses of 5 ms duration were applied at a frequency of 1 Hz. (b) Zoomed in view of the aggregated area. The field of view corresponds to the dotted white box drawn in (a). (c) Image after the application of a 3 x 3 pixel^2 median filter. (d) Image after applying a fluorescence intensity threshold of 200 A.U. (e) Image after being convolved with a Gaussian filter of standard deviation of 1 pixel and a size of 3 x 3 pixel^2. (f) Image after applying a fluorescence intensity threshold of 200 A.U. (g) Detected local maxima as shown by red circles. (h) Super-imposed local maxima on the original gray-scale image. Color bar corresponds to fluorescence intensity for images in (a)-(g).

shown in Figure 2.B.2 (a.2) and (b.2), marked by red arrows. To prevent this over counting of the local maxima, the overlapping local maxima were cleared as follows:-

- For each filter of standard deviation n (where n=1,2,3,5) all the coordinates were checked individually as follows:-
  - For each local maximum coordinate if there was another local maximum within a circle of $radius \leq \sqrt{2}n$, where n is the standard deviation of that filter, then that coordinate was removed.

  [This would remove overlapping local maxima corresponding to Gaussian filters of the same standard deviations.]

- Then all the local maxima coordinate from the filter of standard deviation of n=1 were retained.

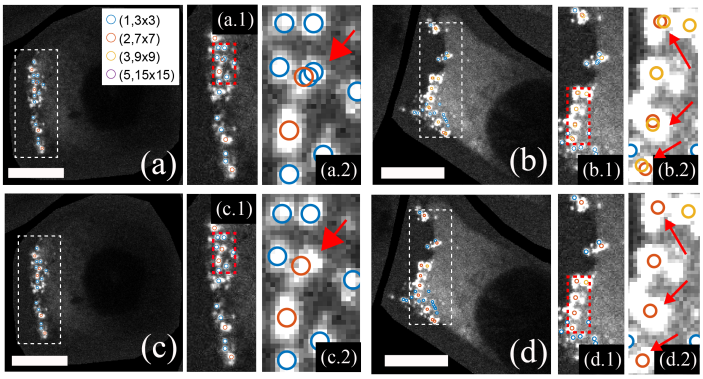

Figure 2.B.2: Representative CHO cell 5 mins after the application of electric pulses. Scale bar = 10 μm (or approx. 86 pixels). Legend = (p, q x q) where p represents the standard deviation of the filter in pixels and q represents the size of the filter in pixels. DNA aggregates detected as local maxima from multiple filters in Table 2.B.1 marked by circles is shown in (a) and (b) before clearing the results, and in (c) and (d) after clearing the results, respectively. DNA size used in (a) and (c) was 50 bp and the DNA size used in (b) and (d) was 100 bp. Electric field amplitude was 0.4 kV/cm for (a) and (c) and 0.5 kV/cm for (b) and (d). For both the cases, 10 pulses of 5 ms duration were applied at a frequency of 1 Hz. (a.1), (b.1), (c.1) and (d.1) show a zoomed in view of the aggregated area of the cell, where the field of view is defined by the dotted white box in (a), (b), (c) and (d). (a.2), (b.2), (c.2) and (d.2) show a further zoomed in view of the aggregated area defined by the dotted red box in (a.1), (b.1), (c.1) and (d.1) respectively.

- For local maxima coordinate corresponding to filter of standard deviation (n=2,3,5) the following methodology was followed:-
  - For each filter with standard deviation of n, all coordinates were checked individually. For a particular coordinate, if there were any other local maxima detected with a circle of $radius \leq n\sqrt{2}$, from any other local maxima coordinate corresponding to filters of standard deviation $< n$, then this particular coordinate was removed. Else it was retained.

[This would remove overlapping local maxima corresponding to Gaussian filters of different standard deviations.]

Figure 2.B.2 (c) and (d) shows the DNA aggregates detected as local maxima after removing the overlaps for cells shown in Figure 2.B.2 (a) and (b) respectively. Figure 2.B.2 (c.1) and (d.1) show a zoomed in view of the aggregated area of the cell, where the field of view is defined by the dotted white box in Figure 2.B.2 (c) and (d) respectively and Figure 2.B.2 (c.2) and (d.2) show a further zoomed in view of the aggregated area, where the field of view is defined by the dotted red box in Figure 2.B.2 (c.1) and (d.1) respectively. As can be seen by the red arrows in Figure 2.B.2 (c.2) and (d.2), each DNA aggregate was now detected by a single local maximum. All the local maxima from each filter were then summed up in order to obtain total number of local maxima.

2.C. CELL CONTOUR DETECTION

To identify the cell contour, the images of the cell before the application of electric pulses were selected. This is shown for a representative CHO cell in Figure 2.C.1 (a) for a DNA size of 50 bp. Then a median 4 x 4 pixel^2 was applied to this image and the resulting image is shown in Figure 2.C.1 (b). A threshold intensity was chosen using the *"graythresh()"* built-in function in MATLAB® using the image in Figure 2.C.1 (b) as an argument, which determines an automatic threshold using the Otsu's method [65]. The image in (b) was then segmented using this threshold intensity. The segmentation result is shown in Figure 2.C.1 (c) with the cell contour as the boundary separating the white and the black regions.

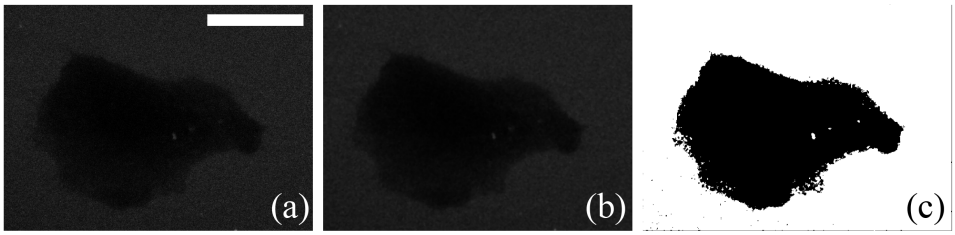

Figure 2.C.1: Detection of cell contour using image segmentation. (a) Representative CHO cell before the application of electric pulses. Scale bar = 20 μm. (b) Image after applying a 4 x 4 pixel^2 median filter. (c) Image after segmenting the image in (b) using a threshold intensity determined from the *"graythresh()"* built-in function in MATLAB®.

2.D. MULTIPLE RUNS FOR AGGREGATED AREA/CELL AND LOCAL MAXIMA/CELL

In order to confirm the trend in Figure 2 (e)-(h) of the main manuscript, a second independent set of experiments was performed for the critical sizes of DNA molecule and the results are shown below by dotted black and red lines. Solid black and red lines represent the same data as shown in Figure 2 (e)-(h).

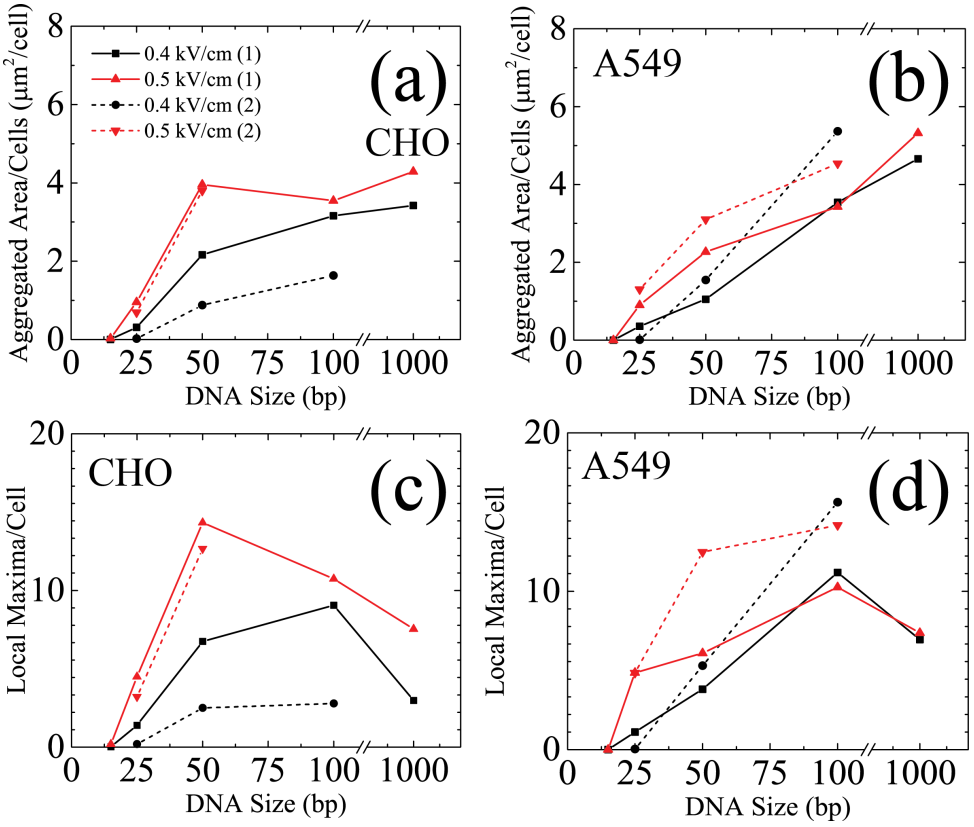

Figure 2.D.1: Aggregated area/cell for CHO cells (a), and A549 cells (b). Number of local maxima/cells for CHO cells (c) and A549 cells (d). Solid black and red lines represent the same data as shown in Figure 2 (e)-(h) of the main text. Dotted black and red lines represent the data from experiments on another batch of cells.

REFERENCES

[1] S. Sachdev, S. F. Moreira, Y. Keehnen, L. Rems, M. T. Kreutzer, and P. E. Boukany, *Dna-membrane complex formation during electroporation is dna size-dependent,* Biochimica et Biophysica Acta (BBA) - Biomembranes **1862**, 183089 (2020).

[2] M. P. Stewart, R. Langer, and K. F. Jensen, *Intracellular delivery by membrane disruption: mechanisms, strategies, and concepts,* Chemical reviews **118**, 7409 (2018).

[3] C. Rosazza, S. Haberl Meglic, A. Zumbusch, M.-P. Rols, and D. Miklavcic, *Gene electrotransfer: a mechanistic perspective,* Current Gene Therapy **16**, 98 (2016).

[4] M. Wu and F. Yuan, *Membrane binding of plasmid dna and endocytic pathways are involved in electrotransfection of mammalian cells,* PloS one **6**, e20923 (2011).

[5] C. Rosazza, E. Phez, J.-M. Escoffre, L. Cézanne, A. Zumbusch, and M.-P. Rols, *Cholesterol implications in plasmid dna electrotransfer: Evidence for the involvement of endocytotic pathways,* International Journal of Pharmaceutics **423**, 134 (2012).

[6] C. Rosazza, H. Deschout, A. Buntz, K. Braeckmans, M.-P. Rols, and A. Zumbusch, *Endocytosis and endosomal trafficking of dna after gene electrotransfer in vitro,* Molecular Therapy-Nucleic Acids **5**, e286 (2016).

[7] B. Markelc, E. Skvarca, T. Dolinsek, V. P. Kloboves, A. Coer, G. Sersa, and M. Cemazar, *Inhibitor of endocytosis impairs gene electrotransfer to mouse muscle in vivo,* Bioelectrochemistry **103**, 111 (2015).

[8] C.-C. Chang, M. Wu, F. Yuan, *et al.*, *Role of specific endocytic pathways in electrotransfection of cells,* Molecular Therapy-Methods & Clinical Development **1**, 14058 (2014).

[9] L. D. Cervia, C.-C. Chang, L. Wang, and F. Yuan, *Distinct effects of endosomal escape and inhibition of endosomal trafficking on gene delivery via electrotransfection,* PloS one **12**, e0171699 (2017).

[10] M. Mao, L. Wang, C. C. Chang, K. E. Rothenberg, J. Huang, Y. Wang, B. D. Hoffman, P. B. Liton, and F. Yuan, *Involvement of a Rac1-Dependent Macropinocytosis Pathway in Plasmid DNA Delivery by Electrotransfection,* Molecular Therapy **25**, 803 (2017).

[11] L. Wang, S. E. Miller, and F. Yuan, *Ultrastructural analysis of vesicular transport in electrotransfection,* Microscopy and Microanalysis **24**, 553 (2018).

[12] M. Pavlin and M. Kandušer, *New insights into the mechanisms of gene electrotransfer–experimental and theoretical analysis,* Scientific reports **5**, 9132 (2015).

[13] E. E. Vaughan and D. A. Dean, *Intracellular trafficking of plasmids during transfection is mediated by microtubules,* Molecular Therapy **13**, 422 (2006).

[14] E. E. Vaughan, R. C. Geiger, A. M. Miller, P. L. Loh-Marley, T. Suzuki, N. Miyata, and D. A. Dean, *Microtubule acetylation through hdac6 inhibition results in increased transfection efficiency,* Molecular Therapy **16**, 1841 (2008).

[15] C. Rosazza, A. Buntz, T. Rieß, D. Wöll, A. Zumbusch, and M.-P. Rols, *Intracellular tracking of single-plasmid dna particles after delivery by electroporation,* Molecular Therapy **21**, 2217 (2013).

[16] A. Paganin-Gioanni, E. Bellard, J. Escoffre, M. Rols, J. Teissie, and M. Golzio, *Direct visualization at the single-cell level of sirna electrotransfer into cancer cells,* Proceedings of the National Academy of Sciences **108**, 10443 (2011).

[17] S. Chabot, J. Orio, R. Castanier, E. Bellard, S. J. Nielsen, M. Golzio, and J. Teissié, *Lna-based oligonucleotide electrotransfer for mirna inhibition,* Molecular Therapy **20**, 1590 (2012).

[18] S. Chabot, J. Teissié, and M. Golzio, *Targeted electro-delivery of oligonucleotides for rna interference: sirna and antimir,* Advanced Drug Delivery Reviews **81**, 161 (2015).

[19] G. L. Lukacs, P. Haggie, O. Seksek, D. Lechardeur, N. Freedman, and A. Verkman, *Size-dependent dna mobility in cytoplasm and nucleus,* Journal of biological chemistry **275**, 1625 (2000).

[20] E. Dauty and A. Verkman, *Actin cytoskeleton as the principal determinant of size-dependent dna mobility in cytoplasm a new barrier for non-viral gene delivery,* Journal of Biological Chemistry **280**, 7823 (2005).

[21] L. Lambricht, A. Lopes, S. Kos, G. Sersa, V. Préat, and G. Vandermeulen, *Clinical potential of electroporation for gene therapy and dna vaccine delivery,* Expert opinion on drug delivery **13**, 295 (2016).

[22] R. Heller and L. C. Heller, *Gene electrotransfer clinical trials,* in *Advances in genetics*, Vol. 89 (Elsevier, 2015) pp. 235–262.

[23] L. D. Cervia and F. Yuan, *Current progress in electrotransfection as a nonviral method for gene delivery,* Molecular pharmaceutics **15**, 3617 (2018).

[24] T. Portet, C. Favard, J. Teissié, D. S. Dean, and M.-P. Rols, *Insights into the mechanisms of electromediated gene delivery and application to the loading of giant vesicles with negatively charged macromolecules,* Soft Matter **7**, 3872 (2011).

[25] D. L. Perrier, L. Rems, and P. E. Boukany, *Lipid vesicles in pulsed electric fields: fundamental principles of the membrane response and its biomedical applications,* Advances in colloid and interface science **249**, 248 (2017).

[26] N. C. Stellwagen, C. Gelfi, and P. G. Righetti, *The free solution mobility of dna,* Biopolymers: Original Research on Biomolecules **42**, 687 (1997).

[27] M. Yu, W. Tan, and H. Lin, *A stochastic model for dna translocation through an electropore,* Biochimica et Biophysica Acta (BBA)-Biomembranes **1818**, 2494 (2012).

[28] M. Golzio, J. Teissié, and M.-P. Rols, *Direct visualization at the single-cell level of electrically mediated gene delivery,* Proceedings of the National Academy of Sciences **99**, 1292 (2002).

[29] E. Neumann, *Membrane electroporation and direct gene transfer,* Bioelectrochemistry and Bioenergetics **28**, 247 (1992).

[30] L. Onsager, *The effects of shape on the interaction of colloidal particles,* Annals of the New York Academy of Sciences **51**, 627 (1949).

[31] D. Frenkel, *Perspective on "the effect of shape on the interaction of colloidal particles",* in *Theoretical Chemistry Accounts* (Springer, 2000) pp. 212–213.

[32] M. Nakata, G. Zanchetta, B. D. Chapman, C. D. Jones, J. O. Cross, R. Pindak, T. Bellini, and N. A. Clark, *End-to-end stacking and liquid crystal condensation of 6–to 20–base pair dna duplexes,* Science **318**, 1276 (2007).

[33] B. D. Hornstein, D. Roman, L. M. Arévalo-Soliz, M. A. Engevik, and L. Zechiedrich, *Effects of circular dna length on transfection efficiency by electroporation into hela cells,* PloS one **11**, e0167537 (2016).

[34] T. Xie and T. Y. Tsong, *Study of mechanisms of electric field-induced dna transfection. iii. electric parameters and other conditions for effective transfection,* Biophysical Journal **63**, 28 (1992).

[35] L. Rems, D. Kawale, L. J. Lee, and P. E. Boukany, *Flow of dna in micro/nanofluidics: From fundamentals to applications,* Biomicrofluidics **10**, 043403 (2016).

[36] C. Carlsson, A. Larsson, and M. Jonsson, *Influence of optical probing with yoyo on the electrophoretic behavior of the dna molecule,* Electrophoresis **17**, 642 (1996).

[37] H. R. Reese, *Effects of dna charge and length on the electrophoretic mobility of intercalated dna,* Biopolymers: Original Research on Biomolecules **34**, 1349 (1994).

[38] S. Pan, D. At Nguyen, T. Sridhar, P. Sunthar, and J. Ravi Prakash, *Universal solvent quality crossover of the zero shear rate viscosity of semidilute dna solutions,* Journal of Rheology **58**, 339 (2014).

[39] A. Brunet, C. Tardin, L. Salome, P. Rousseau, N. Destainville, and M. Manghi, *Dependence of dna persistence length on ionic strength of solutions with monovalent and divalent salts: a joint theory–experiment study,* Macromolecules **48**, 3641 (2015).

[40] M. Mandelkern, J. G. Elias, D. Eden, and D. M. Crothers, *The dimensions of dna in solution,* Journal of Molecular Biology **152**, 153 (1981).

[41] N. F. Bouxsein, C. Leal, C. S. McAllister, K. K. Ewert, Y. Li, C. E. Samuel, and C. R. Safinya, *Two-dimensional packing of short dna with nonpairing overhangs in cationic liposome–dna complexes: from onsager nematics to columnar nematics with finite-length columns,* Journal of the American Chemical Society **133**, 7585 (2011).

[42] A. Czogalla, D. J. Kauert, R. Seidel, P. Schwille, and E. P. Petrov, *Dna origami nanoneedles on freestanding lipid membranes as a tool to observe isotropic–nematic transition in two dimensions,* Nano letters **15**, 649 (2014).

[43] J. C. Neu, K. C. Smith, and W. Krassowska, *Electrical energy required to form large conducting pores,* Bioelectrochemistry **60**, 107 (2003).

[44] J. Li and H. Lin, *The current-voltage relation for electropores with conductivity gradients,* Biomicrofluidics **4**, 013206 (2010).

[45] B. Gabriel and J. Teissié, *Direct observation in the millisecond time range of fluorescent molecule asymmetrical interaction with the electropermeabilized cell membrane,* Biophysical journal **73**, 2630 (1997).

[46] J.-M. Escoffre, E. Bellard, E. Phez, M.-P. Rols, and C. Favard, *Effect of electric field intensity on plasmid dna/membrane interaction during in-vitro gene electrotransfer,* Drug Delivery Letters **2**, 22 (2012).

[47] D. Chang and T. S. Reese, *Changes in membrane structure induced by electroporation as revealed by rapid-freezing electron microscopy,* Biophysical journal **58**, 1 (1990).

[48] J. T. Sengel and M. I. Wallace, *Imaging the dynamics of individual electropores,* Proceedings of the National Academy of Sciences **113**, 5281 (2016).

[49] J. Teissie, M. Golzio, and M. Rols, *Mechanisms of cell membrane electropermeabilization: a minireview of our present (lack of?) knowledge,* Biochimica et Biophysica Acta (BBA)-General Subjects **1724**, 270 (2005).

[50] R. S. Son, K. C. Smith, T. R. Gowrishankar, P. T. Vernier, and J. C. Weaver, *Basic features of a cell electroporation model: illustrative behavior for two very different pulses,* The Journal of Membrane Biology **247**, 1209 (2014).

[51] J.-M. Escoffre, T. Portet, C. Favard, J. Teissié, D. S. Dean, and M.-P. Rols, *Electromediated formation of dna complexes with cell membranes and its consequences for gene delivery,* Biochimica et Biophysica Acta (BBA)-Biomembranes **1808**, 1538 (2011).

[52] J. Teissie, *Electrically mediated gene delivery: basic and translational concepts,* in *Novel Gene Therapy Approaches* (IntechOpen, 2013).

[53] T. M. Squires and S. R. Quake, *Microfluidics: Fluid physics at the nanoliter scale,* Reviews of modern physics **77**, 977 (2005).

[54] T. Kotnik, G. Pucihar, and D. Miklavčič, *Induced transmembrane voltage and its correlation with electroporation-mediated molecular transport,* The Journal of membrane biology **236**, 3 (2010).

[55] S. Carson, J. Wilson, A. Aksimentiev, and M. Wanunu, *Smooth dna transport through a narrowed pore geometry,* Biophysical journal **107**, 2381 (2014).

[56] E. Stellwagen, Y. Lu, and N. C. Stellwagen, *Unified description of electrophoresis and diffusion for dna and other polyions,* Biochemistry **42**, 11745 (2003).

[57] G. C. Wong and L. Pollack, *Electrostatics of strongly charged biological polymers: ion-mediated interactions and self-organization in nucleic acids and proteins,* Annual Review of Physical Chemistry **61**, 171 (2010).

[58] A. Cherstvy, *Electrostatic interactions in biological dna-related systems,* Physical Chemistry Chemical Physics **13**, 9942 (2011).

[59] X. Qiu, K. Andresen, J. S. Lamb, L. W. Kwok, and L. Pollack, *Abrupt transition from a free, repulsive to a condensed, attractive dna phase, induced by multivalent polyamine cations,* Physical Review Letters **101**, 228101 (2008).

[60] I. Koltover, K. Wagner, and C. R. Safinya, *Dna condensation in two dimensions,* Proceedings of the National Academy of Sciences **97**, 14046 (2000).

[61] C. Herold, P. Schwille, and E. P. Petrov, *Dna condensation at freestanding cationic lipid bilayers,* Physical Review Letters **104**, 148102 (2010).

[62] A. G. Cherstvy and E. P. Petrov, *Modeling dna condensation on freestanding cationic lipid membranes,* Physical Chemistry Chemical Physics **16**, 2020 (2014).

[63] C. Faurie, M. Rebersek, M. Golzio, M. Kanduser, J.-M. Escoffre, M. Pavlin, J. Teissie, D. Miklavcic, and M.-P. Rols, *Electro-mediated gene transfer and expression are controlled by the life-time of dna/membrane complex formation,* The journal of gene medicine **12**, 117 (2010).

[64] N. (2013), *Fast 2d peak finder,* MATLAB Central File Exchange (2018 (Retrieved June 1, 2018)), (https://nl.mathworks.com/matlabcentral/fileexchange/37388-fast-2d-peak-finder.

[65] N. Otsu, *A threshold selection method from gray-level histograms,* IEEE transactions on systems, man, and cybernetics **9**, 62 (1979).

3

DNA TRANSLOCATION

DNA translocation to giant unilamellar vesicles during electroporation is independent of DNA size

Delivery of naked DNA molecules into living cells via physical disruption of membrane under electric pulses have potential biomedical applications ranging from gene electrotransfer, electro-chemotherapy, to gene therapy, yet the mechanisms involved in DNA transport remain vague. To investigate the mechanism of DNA translocation across the cell membrane, giant unilamellar vesicles (GUVs) were electroporated in the presence of DNA molecules keeping the size of the DNA molecules as a variable parameter. We experimentally determined the translocation efficiency for each size of the DNA molecule, to compare the results with the existing and conflicting theories of the translocation mechanism i.e. stochastic threading and bulk electrophoresis. We observed that the translocation efficiency is independent of DNA size (ranging from 25 bp - 20000 bp, bp = base pairs), implying that DNA molecules translocate freely across the electro-pores in the lipid membrane in their native polymer conformation, as opposed to unravelling and threading through the electro-pore. Bulk electrophoretic mobility determines the relationship between translocation efficiency and the size of the DNA molecule. This research provides experimental evidence of the mechanistic understanding of DNA translocation across lipid membranes which is essential for devising efficient and predictable protocols for electric field mediated naked DNA delivery.

This chapter is published in Soft Matter **15**, 9187 (2019) [1].

3.1. INTRODUCTION

Physical disruption of cell membrane and DNA transport are of fundamental interest in cell biology, biophysics and soft materials. Application of electric pulses to disrupt the cell membrane (electroporation) is a simple, easy and popular technique to deliver nucleic acids such as DNA (Deoxyribonucleic Acid) and RNA (Ribonucleic Acid) into living cells. The transport mechanism of these nucleic acids, especially DNA molecules, across the cell membrane during electroporation, is however, poorly understood. [2–4] The cell membrane is a complex entity comprising not only phospholipids and various lipid domains, but also containing inclusions such as membrane proteins and cholestrol [5]. A dense cytoskeleton network known as actin cortex is also present underneath the cell membrane [6]. Therefore, inferring the mechanism of DNA translocation across the cell membrane by conducting experiments on cells is inherently a complex and a challenging task due to simultaneous involvement of several cell membrane and cytoskeleton entities. An important step towards understanding the transport mechanism of DNA across the cell membrane is to decouple several cell membrane and cytoskeleton entities and obtain rudimentary knowledge about the transport process by using lipid vesicles as cell membrane models [4].

Experiments on lipid vesicles have revealed much needed insights into the mechanism of DNA electro-transfer across the cell membrane. For instance, Chernomordik *et al.* suggested that large native T7 DNA (~ 40000 bp) and plasmid DNA (or pDNA ~ 4700 bp) followed an endocytosis-like mechanism of translocation into large unilamellar vesicles (LUVs, mean diameter ~ 500 nm) during electroporation [7]. On the other hand, Lurquin *et al.* observed no endocytosis of DNA molecules (~ 7600 bp) into giant unilamellar vesicles (GUVs, mean size ~ 2.5 μm -20 μm) during electroporation, suggesting a mechanism of direct entry (or transport) through the electro-pores formed during electroporation [8]. To resolve this discrepancy, recently Portet *et al.* (2011) conducted experiments using GUVs (mean diameter ~ 20 μm) and pDNA (~ 4700 bp) [9]. Combining experiments with a proposed theoretical framework, they concluded direct entry of DNA molecules through electro-pores via electrophoresis as the mode of transport instead of electro-induced endocytosis. A similar mechanism of direct translocation of small interfering RNA through electro-pores was also observed during nano-second electroporation of GUVs [10]. Investigating electroporation of GUVs in the presence of DNA molecules has thus been conducive in revealing how DNA molecules are transported across the cell membrane during electroporation. This was otherwise often challenging to unveil with experiments on living cells due to complexities associated with the coupling of the cell membrane and cytoskeleton entities.

GUVs provide the opportunity to obtain precise and mechanistic understanding of DNA electro-transfer. For instance, in the experiments and the theoretical framework of Portet *et al.* (2011) it was assumed that the pores were large enough such that DNA molecules can translocate across the electro-pore in their native polymer conformation [9]. In this scenario, the transport of DNA molecules should depend on the bulk electophoretic mobility of DNA molecules. However, only one size (pDNA ~ 4700 bp) was tested for the theoretical framework established. If pores are not large enough compared to the size of the DNA molecule (radius of gyration), Yu and Lin [11] proposed a different theoretical model for DNA transport by considering that the pore is small enough

to allow only a single base pair (bp) to pass through it at a time. In this scenario, the DNA molecules are not transported across the cell membrane in their native polymer conformation but rather translocate through the electro-pore one base pair at a time. This is equivalent to a single-file translocation or stochastic threading of DNA molecules across artificial nano-pores [12]. According to this model, the DNA transport or translocation efficiency (*TE*) scales with the size of the DNA as $TE \sim N^{-1.5}$, where N represents the number of base pairs. Thus, by conducting systematic experiments on model cell membranes such as GUVs and varying the size of the DNA molecules, the diverse and conflicting theories can be tested in order to obtain a more accurate understanding of DNA transport across the cell membrane during electroporation.

In this research, GUVs are electroporated in the presence of DNA molecules of different sizes (25 bp, 100 bp, 500 bp, 1000 bp, 10000 bp, 15000 bp and 20000 bp) individually, in order to the test the different mechanisms of DNA translocation *i.e.* the theoretical framework of Portet *et al.* (2011) [9] that claims direct entry of the DNA molecules and the theoretical framework of Yu and Lin [11] that claims single-file translocation of DNA molecules across the electropore. By comparing the experimental translocation efficiencies with the predictions from the theoretical frameworks, it was inferred that DNA molecules directly enter the GUVs during electroporation in their native configuration as proposed by Portet *et al.* (2011) [9]. The results of this study provide a mechanistic understanding of DNA translocation across an electro-pore which is not only necessary for understanding DNA translocation across real cell membranes, but also for predictable loading and dosage control of nucleic acids into vesicles using electroporation. Moreover, with such a diverse range of DNA sizes tested that span three orders of magnitude, these results can also be utilized to optimize loading of vesicles with small nucleic acids (such as siRNA, ~ 20 bp) for gene silencing applications, and large nucleic acids (such as pDNA, ~ 5000 bp) for gene therapeutic applications, using liposome mediated transfection.

3.2. MATERIALS AND METHODS

3.2.1. GUV PREPARATION

The lipids used to prepare GUVs were 1,2-dioleoyl-sn-glycero-3-phosphocholine (DOPC) and 1,2-dioleoyl-sn-glycero-3-phosphoethanolamine-N-(lissamine rhodamine B sulfonyl) (ammonium salt) (Rhodamine-PE) and were purchased from Avanti Polar Lipids, Inc. The lipids were dissolved in chloroform (Sigma-Aldrich) at a mass concentration of 1 mg/ml and were stored at -20°C. The lipid solutions were mixed, at room temperature, in order to achieve a concentration of 99.5 mol% DOPC and 0.5 mol% Rhodamine-PE. 20 µl of this lipid solution was deposited on the conducting side of two Indium Tin Oxide (ITO) slides (Sigma-Aldrich), separately. The ITO slides were then placed inside the cavity of a custom made Teflon chamber with the conducting sides facing each other and separated by a distance of 1.5 mm. The cavity of the Teflon chamber was filled with 1 ml of 240 mM aqueous sucrose solution. The electroformation procedure was followed to prepare the GUVs [13]. A sinusoidal potential of 1.5 V_{pp} was applied to the ITO slides at a frequency of 10 Hz and for a period of 2 hrs. Subsequently, a square-wave potential of 1.225 V was applied for a period of 1 hr and at a frequency of 5 Hz. An arbitrary-waveform

generator (Agilent 33220A 20MHz) was used for electroformation. After the electroformation procedure, the solution was diluted 20 times with 260 mM aqueous glucose solution to a final volume of 5 ml. With this procedure, GUVs were prepared having 240 mM aqueous sucrose solution on the inside and 260 mM aqueous glucose solution on the outside.

3.2.2. DNA SAMPLES AND STAINING PROCEDURE

To investigate the effect of biomolecule size, individual DNA fragments with 25 bp, 100 bp, 500 bp, 1000 bp, 10000 bp, 15000 bp and 20000 bp were purchased from Thermo Fisher Scientific Inc. under the brand of NoLimits™ DNA. For each DNA size, the stock vial consisted of 10 µg of DNA at a concentration of 0.5 µg/µl in 10 mM Tris-HCl (pH 7.6) and 1 mM EDTA. To visualize and quantify the DNA uptake, DNA molecules were stained in the stock vials using YOYO-1 dye (1 mM in DMSO from Thermo Fisher Scientific Inc). The bp:YOYO-1 dye molecule staining ratio was 10:1 to achieve a sufficient fluorescent signal-to-noise ratio, without significantly influencing the contour length of the DNA molecules [14, 15]. Staining was carried out on ice for a period 1 hour.

3.2.3. ELECTROPULSATION OF GUVS

Electropulsation was carried out in µ-Slide 4 Well Ibidi® chambers (Cat. No: 80426), to monitor the process of DNA uptake using an inverted confocal microscope. Custom made stainless steel electrodes with a 3 mm gap were placed inside 1 of the 4 chambers. 475 µl of 260 mM aqueous glucose solution was added to the chamber along with with 2.5 µl of the stained DNA stock solution. 22.5 µl of solution from the Teflon chamber containing the GUVs was added into the µ-Slide 4 Well chamber. Care was taken to pipette the solution in between the electrodes. The final volume inside the µ-Slide 4 Well containing the electrodes was 500 µl and the DNA concentration was 2.5 µg/ml. The electrodes were connected to the electropulsator (BetaTech Electro cell S20, France) to apply the electric field pulses. A voltage of 135 V was applied between the electrodes for a period of 5 ms. 10 such pulses were applied at a frequency of 0.33 Hz. This created an electric field (E_o) of 0.45 kV/cm. All experiments were done on GUVs having an initial diameter (D_i) of ~ 30 µm.

3.2.4. CONFOCAL IMAGE ACQUISITION OF DNA UPTAKE

All the experiments were performed on a confocal microscope (ZEISS LSM 710, Germany) and the images were acquired using a 40× (1.3 NA oil immersion) objective. YOYO-1-labelled DNA molecules were excited by a 488 nm Argon laser and the rhodamine-labelled GUVs were excited by a 543 nm Helium-Neon (He-Ne) laser. Both the lasers were used simultaneously for excitation. The emission filter for the YOYO-1 labelled DNA acquisition was set to 491 nm - 538 nm, while the emission filter for the rhodamine labelled GUVs was set to 569 nm - 797 nm. The resulting image was a combination of two separate channels *i.e.* the channel corresponding to the fluorescence from rhodamine-labelled GUVs (referred to as *red* channel) and the channel corresponding to YOYO-1-labelled DNA molecules (referred to as *green* channel). The scanning speed of the laser was adjusted to obtain a pixel dwell of 1.27 µs. The field of view consisted of 512 × 512 pixels spanning 212.55 × 212.55 μm^2. The pixel depth was set to 16-bit and a line aver-

aging of 2 was applied in order to improve the signal-to-noise ratio.

3.2.5. IMAGE PROCESSING

The diameter of the GUV was determined using the *red* channel and the mean fluorescence intensity of DNA molecules inside and outside the GUV was determined using the *green* channel. Both the channels were from the same frame or the image acquired by the confocal microscope. Multiple frames were captured and analysed to obtain transient information of the DNA uptake process. The *red* channel image was enhanced using the '*imadjust()*' function in MATLAB® to optimize the detection of GUV as a circle and determine the corresponding diameter. The GUV was detected as a circle using the in-built function '*imfindcircles()*' in MATLAB® that uses the Circular Hough Transform algorithm [16]. The arguments used for the '*imfindcircles()*' function were as follows; the enhanced *red* channel image on which the circle was to be detected, 20 and 50 pixels as the minimum and maximum radius respectively, for the circle to be detected, and 0.94-0.96 as the '*Sensitivity*' for optimal detection. Default values and settings were used for all other arguments. The radius and the center coordinates of the detected circle (GUV) returned by this function were superimposed on the *green* channel images to calculate the mean fluorescence intensity of the DNA molecules inside and outside of the GUVs. Inside of the GUVs corresponded to an area of a circle with 0.9 times the radius of the detected circle. Outside of the GUVs correspond to an area that lied outside a circle of radius 1.2 times the detected circle. The *green* channel images were not adjusted or enhanced for calculating the mean fluorescence intensity of DNA molecules.

3.3. RESULTS

In order to test the different models of DNA translocation across lipid bi-layers (DNA translocation in their native polymer conformation through the electro-pore [9] or DNA unravelling and threading through the electro-pore [11]), the experiments were performed on DNA molecules of the following sizes; 25 bp, 100 bp, 500 bp, 1000 bp, 10000 bp, 15000 bp and 20000 bp. The wide range of DNA sizes provided an opportunity to test these two different theories over three orders of DNA size. The DNA molecules were fluorescently labeled with YOYO-1 dye (1:10 dye:bp staining ratio) in order to obtain the translocation efficiency as a ratio of the mean fluorescence intensity of DNA molecules inside and outside the GUV. GUVs were made of 99.5 mol% DOPC and 0.5 mol% Rhodamine-PE. Rhodamine-PE lipids were added as tracer lipids in order to detect the GUV during and after the application of electric field pulses, under the confocal microscope. The initial GUV diameter (D_i) was chosen to be 30 μm for all the experiments and the electric field applied was 0.45 kV/cm (E_o). This led to the generation of a trans-membrane potential (*TMP*) of ~ 1 V, at the poles facing the electrodes, according to the simplified Schwan equation; $TMP = 1.5 E_o D_i/2$ [17]. 10 such electric field pulses were applied, each of 5 ms duration and at a frequency of 0.33 Hz. The concentration of DNA molecules was kept constant at 2.5 μg/ml, for all experiments with different DNA sizes. These values are typically used in gene transfection protocols using electroporation [18], and also allowed sufficient uptake of DNA molecules by the GUVs to be quantified accurately, without loss of stability of the GUVs post electroporation. The DNA uptake by GUVs during elec-

troporation was recorded under a confocal microscope and is shown in Figure 3.3.1. The figure consists of 3 rows and 7 columns showing uptake of DNA molecules corresponding to different DNA sizes. The images in the first row (Figure 3.3.1 (a)) shows images of GUVs before the electric field pulses were applied, for all DNA sizes considered. No fluorescence intensity corresponding to YOYO-1-labelled DNA molecules can be detected inside the GUVs before electroporation. The second row (Figure 3.3.1 (b)) shows images of GUVs and DNA uptake during the period of pulses. The DNA molecules can be seen to enter the GUVs from the cathode facing side of the electrode. The last row (Figure 3.3.1 (c)) shows the images of GUVs with corresponding DNA uptake after the application of 10 pulses. All images are representative of typical experimental observations.

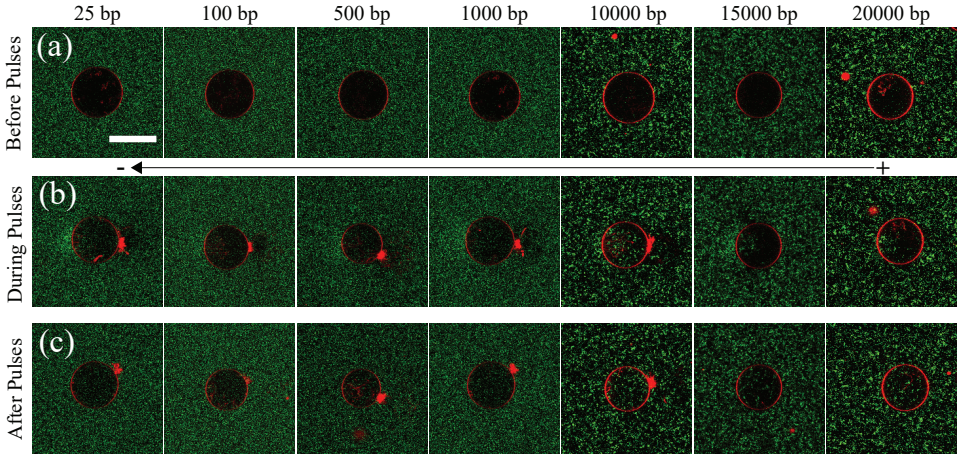

Figure 3.3.1: Confocal images showing uptake of DNA molecules during electroporation of GUVs. DNA molecules are fluorescently labelled using YOYO-1 dye (1:10 dye:bp ratio) and are shown in green. DOPC GUVs are fluorescently labelled with tracer Rhodamine-PE lipids and are shown in red. Images are from representative experiments. (a) or first row shows the state of the GUVs before applying electric field pulses. (b) or second row shows the state of the GUVs during the application of electric field pulses. 10 electric field pulses of 5 ms duration and an amplitude of 0.45 kV/cm were applied at a frequency of 0.33 Hz. The images in (b) correspond to a time (t) between the beginning of the first pulse ($t \sim 0$ s) and the end of the last pulse ($t \sim 30.05$ s) (c) or third row shows the state of the GUVs after the application of electric field pulses. The images in (c) correspond to ($t > 30.05$ s and $t < 120$ s). Scale bar corresponds to 30 μm. For visualization purposes, the images are displayed by adjusting the histograms of the *red* and the *green* channels. Both the histograms are adjusted by setting the minimum intensity to 0+40$^{\text{th}}$ percentile and the maximum intensity to 2^{16}-40$^{\text{th}}$ percentile, of the original histogram.

A representative experiment describing the uptake of DNA molecules by the GUV during electroporation, for a DNA size of 100 bp is shown in Figure 3.3.2. Before the application of electric field pulses, Figure 3.3.2 (a), fluorescence from the DNA molecules (shown in green) could be seen homogeneously distributed outside the GUV (shown in red). The fluorescence intensity of DNA molecules outside the GUV corresponds to a concentration of 2.5 μg/ml and labelled as I_{out}. The negligible green fluorescence that could be seen inside the GUV was attributed to the sensor noise (I_{noise}). On application of electric field pulses at $t \sim 0$ s, the DNA molecules could be seen entering the GUV from

the cathode facing side of the electrode. A simultaneous decrease in the GUV diameter was also observed. A representative snapshot of this process is shown in Figure 3.3.2 (b). After the application of electric field pulses, no uptake of DNA, nor a decrease in GUV diameter was observed. The final state of the GUV is shown in Figure 3.3.2 (c).

From these experiments, the transient data of the effect of electric field pulses on the GUVs and the simultaneous uptake of DNA molecules during electroporation could be extracted from the sequence of images captured for the process. Figure 3.3.2 (d) shows the GUV diameter as a function of time. Before the application of electric field pulses, the diameter was constant at ~ 33 μm (labelled as D_i). The initial diameter, D_i, was calculated by taking the average of the diameters before the application of electric field pulses. During the application of electric field pulses (from $t \sim 0$ s till $t \sim 30$ s, as marked by arrows), the diameter decreased continuously. The decrease in diameter has been observed previously for fluid phase GUVs and is attributed to lipid loss during electroporation [19, 20]. After the application of electric field pulses, the diameter attained a steady-state value of ~ 25 μm (labelled as D_f). The final diameter, D_f, was calculated by taking the average of the diameters after the application of pulses.

Similarly, the uptake of DNA by the GUV during electroporation was determined. The mean fluorescence intensity of the DNA molecules inside the GUV (I_{in}) was determined by calculating the mean fluorescence intensity of the DNA molecules inside a circle having a diameter corresponding to 0.9 times the detected GUV diameter (see Section 3.2.5 in Materials and Methods). This was done to minimize edge effects. The initial mean fluorescence intensity corresponding to sensor noise (I_{noise}) was subtracted from the mean fluorescence intensity of the DNA molecules detected inside the GUV in each frame as $I = I_{in} - I_{noise}$. The sensor noise was also subtracted from the fluorescence intensity of DNA molecules outside the GUV (I_{out}) in each frame as $I_o = I_{out} - I_{noise}$. I_{out} corresponded to the mean fluorescence intensity of the DNA molecules outside a circle having a diameter corresponding to 1.2 times the detected GUV diameter. Normalized mean fluorescence intensity I/I_o was then plotted as a function of time as shown in Figure 3.3.2 (e). Before the application of electric field pulses, no DNA uptake could be observed inside the GUV. During application of electric field pulses (from $t \sim 0$ s till $t \sim 30$ s, as marked by arrows), the mean normalized fluorescence intensity continuously increased linearly. It finally reached a steady state value $(I/I_o)_f = 0.38$ after the end of the electric field pulses. This final steady state value $(I/I_o)_f$ was calculated by taking the average of (I/I_o) values after the application of electric field pulses. Other quantities such as DNA uptake time and the slope of normalized intensity (I/I_o) vs. time during uptake of DNA by the GUV is shown in Section 3.A of Supplementary Information.

The sequence of images representing the electroporation of GUVs were analysed for a number of experiments corresponding to different DNA sizes. The evolution of the diameter of the GUV and the fluorescence intensity corresponding to the uptake of DNA molecules were extracted as shown previously (see Figure 3.3.2). The diameter ratio (D_f/D_i) was calculated for each DNA size and is shown in Figure 3.3.3 (a). The diameter of the GUVs did not decrease by more than ~ 20%, after the application of electric field pulses. Similarly, the uptake of DNA molecule due to electroporation ($(I/I_o)_f$ from Figure 3.3.2 (e)) was determined for each DNA size and is plotted in Figure 3.3.3 (b), as filled squares. Also plotted on the same figure are the theoretical predictions from Yu

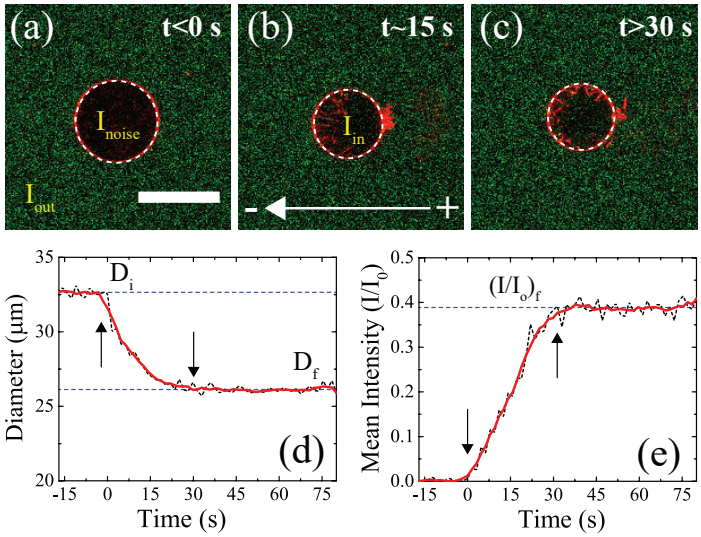

Figure 3.3.2: Quantifying the decrease in GUV diameter and the uptake of DNA molecules during electroporation. (a) State of the GUV before application of electric field pulses (t<0 s). The GUV is shown in red and the DNA molecules are shown in green. The GUV detected is shown using a white-dotted circle (see Section 3.2.5 in Materials and Methods). The mean fluorescence intensity of DNA molecules outside the GUV is depicted as I_{out} corresponding to a concentration of 2.5 μg/ml. The green fluorescence due to sensor noise found inside the GUV is labelled as I_{noise}. Scale bar = 30 μm. (b) State of the GUV during the application of electric field pulses ($t \sim 15$ s). 10 pulses of electric field amplitude of 0.45 kV/cm were applied, each of duration 5 ms and at a frequency of 0.33 Hz. This corresponds to a time frame of $t \sim 0$ s to $t \sim 30$ s. Mean fluorescence intensity inside the GUV due to uptake of DNA molecules during electroporation is depicted as I_{in}. (c) State of the GUV after the application of electric field pulses. For visualization purposes, the images shown in (a)-(c) are enhanced using the same adjustments as for Figure 3.3.1. Detected GUV diameter, and normalized mean fluorescence intensity $I/I_o = (I_{in} - I_{noise})/(I_{out} - I_{noise})$, as a function of time are plotted as black dotted line in (d) and (e), respectively. The beginning and the end of pulses are marked by arrows. The solid red line represents smoothed data using the '*smooth()*' function in MATLAB®.

and Lin [11] (solid line) and Portet *et al.* (2011) [9] (dashed lines). For the theoretical prediction of Yu and Lin [11], final probability of successful translocation ($F - PST$) was used as a measure for translocation efficiency, $(I/I_o)_f$, and for the theoretical prediction of Portet *et al.* (2011) [9], the following equation was used from the proposed theoretical framework:

$$\frac{c}{c_o} = \frac{3\mu E_o t_p N}{4\pi R} f'(0)\theta \tag{3.3.1}$$

Here, c and c_o represent the concentration of DNA molecules inside and outside the GUV, respectively. μ is the electrophoretic mobility of the DNA molecules, t_p is the pulse duration, E_o is the applied electric field, N is the number of the pulses, R is the radius of the GUV, $f'(0)$ is a factor depending on the conductivity ratio of the media inside and outside the GUV and θ represents the angle that the permeabilized spherical cap subtends at the centre of the vesicle. Together, $f'(0)\theta$ is referred to as the flux factor [9]. The normalized concentration c/c_o after the electric field pulses was taken as a measure of

$(I/I_o)_f$. To compute the translocation efficiency $(I/I_o)_f$ from equation 3.3.1, the following values were used; E_o=0.45 kV/cm, t_p =5 ms, N = 10 and R = 15 µm, corresponding to the experimental conditions in this work. Different values of electrophoretic mobility μ were considered. For Tris-acetate Ethylene-diamine-tetra-acetic acid (Tris-acetate EDTA or TAE) buffers, a constant value of electrophoretic mobility of $\mu = 3.75 \times 10^{-8}$ $m^2S^{-1}V^{-1}$ was reported for DNA sizes ranging from 400 bp to 48500 bp [21]. For DNA sizes less than 400 bp, the electrophoretic mobility constantly decreased to a value of $\mu = 3.54 \times 10^{-8}$ $m^2S^{-1}V^{-1}$ for a DNA size of 27 bp [21]. Using these values of electrophoretic mobility for the corresponding DNA sizes used in this work, and a flux factor of $f'(0)\theta$ =0.26, the theoretical prediction according to equation 3.3.1 is plotted in Figure 3.3.3 (b) as a dotted line corresponding to the legend; $f'(0)\theta$ =0.26 TAE Buffer. A value of $\mu = 3.75 \times 10^{-8}$ $m^2S^{-1}V^{-1}$ for the electrophoretic mobility and $f'(0)\theta$ =0.26 for the flux factor was also used by Portet *et al.* (2011) for a DNA size of 4700 bp (pDNA) [9].

The conductivity of the medium has been shown to influence the electrophoretic mobility of the DNA molecules [21–24]. The buffers used in the current experiments consist of 260 mM glucose as the external medium and 240 mM sucrose as the internal medium. This corresponds to very low conductivity or ionic strength compared to TAE buffers. Electrophoretic mobility of DNA molecules in low conductivity buffers can be estimated by systematically reducing the ionic strength, as was done for dsA5 DNA molecules (20 bp) [24]. In this case, the electrophoretic mobility of dsA5 DNA at zero ionic strength was estimated to be $\mu = 4.6 \times 10^{-8}$ $m^2S^{-1}V^{-1}$, by linear extrapolation of electrophoretic mobilities in the range of low ionic strength. A quantitatively similar increase in electrophoretic mobility was observed for dsA5 DNA molecules (20 bp) and pUC19 DNA molecules (2686 bp) with systematic reduction of ionic strength [23]. Therefore, a similar quantitative increase in electrophoretic mobilities was considered for the sizes of the DNA molecules considered in this work corresponding to the low conductive glucose and sucrose buffers. See Section 3.B of Supplementary Information for the exact values of electrophoretic mobilities used, corresponding to TAE (Table 3.B.1) and the low conductive sucrose and glucose buffers (Table 3.B.2), for the different DNA sizes in this work. The theoretical prediction according to equation 3.3.1 with an increased electrophoretic mobility corresponding to the low conductive buffers, and the same flux factor ($f'(0)\theta$ =0.26) is shown in Figure 3.3.3 (b) as a dotted line with a legend; $f'(0)\theta$ =0.26, Glucose/Sucrose Buffer. Also shown in the same figure are the predictions from equation 3.3.1 with the same increased electrophoretic mobility, however a low value of flux factor ($f'(0)\theta$ =0.15) as a dashed line (legend; $f'(0)\theta$ = 0.15, Glucose/Sucrose Buffer) which shows better agreement with the experimental values.

Based on theoretical framework of Portet *et al.* (2011) [9], the electrophoretic mobility can be back calculated using equation 3.3.1. Taking (c/c_o) as $(I/I_o)_f$ and using the electric field parameters from the experiments; E_o=0.45 kV/cm, N = 10, t_p=5 ms and R = 15 µm the electrophoretic mobility can be calculated for each size of the DNA molecule. These values are plotted in Figure 3.3.3 (c), as filled black and open white circles for $f'(0)\theta$ = 0.26 and $f'(0)\theta$ = 0.15, respectively. On the same figure, electrophoretic mobilities determined from the literature (see sectio 3.B of Supplementary Information) are also plotted for TAE buffer and low conductive buffers, as dashed and solid lines, respectively. The close match between the experimentally determined electrophoretic

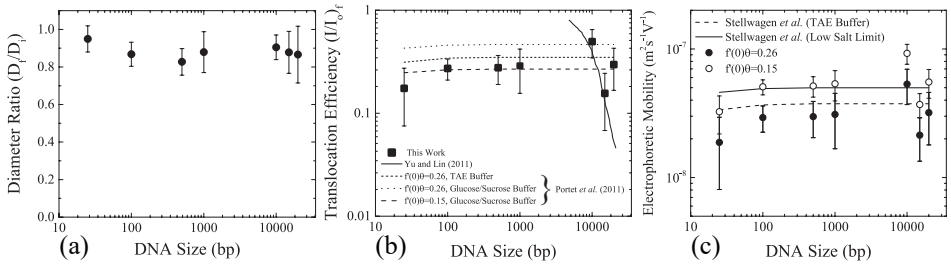

Figure 3.3.3: Size reduction of GUVs and DNA uptake as a function of DNA size. (a) The ratio of the final diameter (D_f), after the application of the electric field pulses, to the initial diameter (D_i), before the application of electric field pulses. The error bars represent the standard deviation. (b) Solid boxes represnent translocation efficiency $(I/I_o)_f$ as a function of the size of the DNA molecules. The error bars represent standard deviation. Also plotted are the theoretical predictions of the translocation efficiency from Yu and Lin (solid line) [11], and Portet *et al.*, (2011) (dashed line) [19]. (c) Electrophoretic mobility as a function of DNA size calculated using equation 3.3.1 taking (c/c_o) as $(I/I_o)_f$ from (b). Two different values of the flux factor were used; $f'(0)\theta$=0.26, corresponding to filled black circles and $f'(0)\theta$=0.15 corresponding to open white circles. Electrophoretic mobilities determined from the literature (see Section 3.B of Supplementary Information for detailed values) is also plotted for TAE buffer [21] and low conductive buffers [24], as dashed and solid lines, respectively.

mobilities to the values determined from the literature further validate the applicability of the theoretical framework of Portet *et al.* (2011) [9] as the dominant mode of DNA translocation during electroporation of GUVs.

3.4. DISCUSSION

To unravel the mechanism of DNA translocation through electropores in GUVs, the DNA size was varied keeping the pulsing parameters constant. The translocation efficiency or the amount of DNA transferred into the GUVs during electroporation as a function the size of the DNA molecules could be compared to predictions from the theoretical frameworks of Yu and Lin [11] and Portet *et al.* (2011) [9]. According to the stochastic model of Yu and Lin [11], the size of the electro-pore is small enough to allow only a single base-pair to translocate at a time. The final probability of successful translocation or F-PST (interpreted as the translocation efficiency, *TE*) should then decrease with the size of the DNA molecules (N), and in particular, should scale with the size of the DNA molecules as $TE \sim N^{-1.5}$. According to figure 3.3.3 (b), no decrease in the translocation efficiency, $(I/I_o)_f$, was observed for the size of the DNA molecules tested. On the same figure, the prediction of Yu and Lin [11] for the translocation efficiency as a function of size is plotted for a pulse duration of 5 ms as a solid line. The experimental results do not match the prediction of Yu and Lin [11], rendering the applicability of their model and mechanism of DNA translocation unlikely for electroporation of GUVs.

The model of Portet *et al.* (2011) [9] suggests that the DNA molecules can cross the electro-pore in their native polymer conformation, or that the electro-pores are large enough to allow the DNA molecules to cross freely. The bulk electrophoretic mobility governs the transport across the pore during electroporation. According to the theoretical framework adapted by Portet *et al.* (2011) [9], the normalized increase in the concen-

tration of DNA molecules inside the GUVs after the application of electric field pulses is given by equation 3.3.1. The prediction is plotted in Figure 3.3.3 (b) for different values of electrophoretic mobility μ and flux factors $f'(0)\theta$, as dashed lines. This prediction matches with the experimental values of normalized mean intensity of DNA molecules inside the GUVs, $(I/I_o)_f$, for values of electrophoretic mobilities of DNA molecules in glucose/sucrose buffer, and for a flux factor of $f'(0)\theta = 0.15$. However, these values are slightly different from the values used in the theoretical framework of Portet *et al.* (2011)[9].

The electrophoretic mobility and the flux factor used in the theoretical framework of Portet *et al.* (2011) were $\mu = 3.75 \times 10^{-8}$ $m^2S^{-1}V^{-1}$ and $f'(0)\theta = 0.26$ [9]. This value of electrophoretic mobility was measured for DNA molecules with size greater than 400 bp and for a TAE buffer (40 mM Tris, 1 mM EDTA, pH 8.0) [21]. The conductivity of TAE buffer is found to be in the range of 0.38 - 3.11 mS cm^{-1} depending upon the concentration of Tris (10-80 mM) [22]. The conductivity of the external buffer used by Portet *et al.* (2011) (260 mM glucose, 1 mM KH_2PO_4/K_2HPO_4, 1 mM NaCl, pH 7) was measured to be 0.45 mS cm^{-1} [9]. This lies within the range of conductivities of the TAE buffers used to measure the electrophoretic mobilities of DNA molecules. Addition of 2 - 50 mM NaCl to TAE buffers has shown to influence the value of the electrophoretic mobility, albeit only slightly for 2 mM NaCl [23]. Therefore, ignoring the effects of addition of 1 mM NaCl to the KH_2PO_4/K_2HPO_4 buffer, a value of electrophoretic mobility of $\mu = 3.75 \times 10^{-8}$ $m^2S^{-1}V^{-1}$ seems to be an appropriate choice for a buffer adopted by Portet *et al.* (2011) [9]. The buffers used in this work correspond to 260 mM as the external solution and 240 mM as the internal solution. The conductivities of 200 mM glucose and 200 mM sucrose solution were measured to be 0.0045 and 0.006 mS cm^{-1} [25], respectively. The conductivity of 240 mM sucrose solutions was measured to be 0.015 mS cm^{-1} [9]. Thus, it can be assumed that the conductivities of the glucose and sucrose solutions used in this work is $O(10^{-3} - 10^{-2})$ mS cm^{-1}. For such low conductive solutions, the electrophoretic mobilities is expected to be higher [21–24]. Using values of electrophoretic mobilities corresponding to the low conductive sucrose/glucose buffers (see Section 3.B of the Supplementary Information for precise values used) and a flux factor $f'(0)\theta = 0.26$, the translocation efficiency or the normalized concentration according to equation 3.3.1 plotted in figure 3.3.3 (b) captures the qualititative trend, however overpredicts the experimental translocation efficiency.

The value of the flux factor in the theoretical framework by Portet *et al.* (2011) was $f'(0)\theta = 0.26$ [9]. The authors determined this value by comparing their experimental results with the theory. According to the theoretical framework, for conductivity ratios (external solution conductivity/internal solution conductivity) between 1 and 10, the experimentally determined flux factor $f'(0)\theta$ should lie between 0.1 - 0.5 [9]. The authors obtained a distribution of experimentally determined $f'(0)\theta$, with a mean value of the distribution as $<f'(0)\theta>$=0.26, thus validating the theoretical framework for a DNA size of 4700 bp. According to Figure 3.3.3 (b), the theoretical prediction (equation 3.3.1) matches with the experimental translocation efficiencies in this work, for electrophoretic mobilities corresponding to low conductive sucrose/glucose buffers, and for a flux factor value of $f'(0)\theta = 0.15$. This value of flux factor $f'(0)\theta$ also lies between 0.1 - 0.5, suggesting the validity of the theoretical framework by Portet *et al.* (2011) [9] for DNA

sizes ranging from 25 bp - 20000 bp.

A lower value of flux factor, $f'(0)\theta = 0.15$ in this work, as opposed to $f'(0)\theta = 0.26$ in Portet *et al.* (2011) [9], could be due to multiple reasons. $f'(0)$ depends on the conductivity ratio, and θ represents the angle that the permeabilized area, accessible to DNA translocation, subtends at the center of the GUV [9]. A constant value of $f'(0)$=2.34 rad^{-1} corresponding to a conductivity ratio of 1 was considered [9]. A similar value of $f'(0) = 3$ rad^{-1} was obtained for the buffers, electric field pulsing conditions and the GUV diameters corresponding to this work (see Section 3.C of Supplementary Information). The distribution, as reported by Portet *et al.* (2011) [9], thus arises due different θ values corresponding to different permeabilized areas [9]. The authors attributed this to different electric field intensities, pulse durations and GUV diameters considered which could lead to different permeabilized areas accessible to DNA translocation [9]. Thus, $f'(0)\theta = 0.15$ for the constant electric field pulsing conditions, GUV diameters and the buffers used in this work could correspond to a value lying in the lower spectrum of the distribution reported by Portet *et al.* (2011) [9].

Considering $f'(0)$=3 rad^{-1}, a permeabilized area subtending an angle $\theta \sim 2.9°$ (for $f'(0)\theta = 0.15$) is obtained. Using $D_{\text{perm}} = R\theta_c$, where D_{perm} is the diameter of the permeabilized area (assuming a circular area), R is the radius of the vesicle and θ_c is the permeabilized angle θ in radians, a permeabilzed area with a diameter $D_{\text{perm}} \sim 0.75$ µm is obtained for $\theta \sim 2.9°$. This permeabilized area could be considered as a single macropore. Although macropores are observed during the electroporation of GUVs [19, 26], they are only observed during the last few µs of a ms pulse, and remain open for tens of milliseconds after the pulse ends [26]. Since diffusion of DNA molecules is negligible compared to electrophoresis [9], majority of the DNA transport thus happens during, and not after the pulse. However, the experiments in this work suggest a mode of transport where the pores are large enough during the electric field pulse to allow DNA molecules to translocate freely in their native polymer conformation. This implies that the pores formed are comparable to the coil size (or radius of gyration R_g) of the DNA molecules. The largest DNA molecule used in this work (20000 bp) has an $R_g \sim 1$ µm (see Section 3.D of Supplementary Information), similar in size to the permeabilized area ($D_{\text{perm}} \sim 0.75$ µm). Thus, a permeabilized area with diameter $D_{\text{perm}} \sim 0.75$ µm, can be considered as a macropore. These results, apart from providing a mechanistic understanding of DNA translocation also provide information on the pore size during electroporation of GUVs.

3.5. CONCLUSIONS

The two theoretical frameworks proposed for DNA translocation, stochastic threading [11] and bulk electrophoretic transfer(2011) [9], were tested by varying the size of the DNA molecules and monitoring the translocation efficiency. It was determined that for the DNA sizes tested (ranging from 25 bp - 20000 bp), the DNA molecules can translocate freely through the electro-pores in their native polymer conformation, suggesting bulk electrophoretic transfer as the dominant mode of transport during electroporation of GUVs. For a given set of pulsing conditions, the bulk electrophoretic mobility of DNA molecules is the key parameter that determines the uptake during electroporation of GUVs. This mechanistic understanding of DNA translocation for model cell membranes not only allows a predictable loading of vesicles with a wide variety of DNA sizes, but

provide also a basis for developing mechanistic models for more complex cell membranes [27], eventually approaching living cells.

APPENDIX

3.A. DETERMINATION OF UPTAKE TIME AND THE SLOPE OF NORMALIZED INTENSITY (I/I_o) VS. TIME DURING UPTAKE OF DNA BY THE GUV

In Figure 3.3.2 (e) of the main text, apart from the final translocation efficiency (I/I_o), the time for DNA uptake (t_{uptake}), and the slope of the curve (I/I_o) vs. time (s) during the application of electric field pulses were extracted. Before showing the time of DNA uptake and the slope corresponding to each DNA size, the process of calculating these quantities is explained below for a representative experiment corresponding to a DNA size of 100 bp (bp=base pairs).

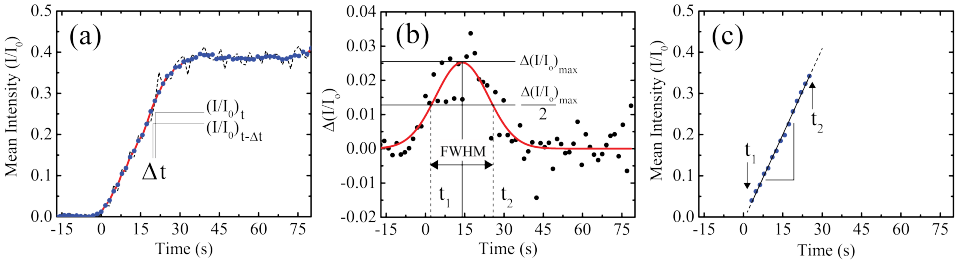

Figure 3.A.1: Process of calculating the time of DNA uptake and the slope of DNA uptake curve (DNA size = 100 bp). (a) Dashed line represents the normalized meant intensity (I/I_o) of DNA molecules inside the GUV as a function of time. This is the same as shown in Figure 3.3.2 (e) of the main text. Filled blue circles connected by a solid red line representing the smoothed data. Consecutive normalized mean intensities are marked as $(I/I_o)_t$ and $(I/I_o)_{t-\Delta t}$ where Δt is the time between consecutive measurements or frames. (b) $\Delta(I/I_o)_t$ as a function of time (s). $\Delta(I/I_o)_t$ is calculated as $\Delta(I/I_o)_t = (I/I_o)_t - (I/I_o)_{t-\Delta_t}$ from the smoothed data in (a). Shown in red is the fitted Gaussian curve $\Delta(I/I_o)_t = Aexp(-0.5(t-t_o)^2/\sigma^2)$, where A, t_o and σ are the fitting parameters and σ represents the standard deviation of the Gaussian. The values of the parameters are A=0.025, $t-$o=13.98 s and σ=10.06. The standard error for A, t_o and σ are 0.0020, 0.86 and 1.02 respectively, as obtained from the best fit. t_1 and t_2 represent the times when $(\Delta(I/I)_o)_t$ attains a value of $(\Delta(I/I)_o)_{max}/2$ where $(\Delta(I/I)_o)_{max}$ is the maximum of the gaussian. t_2-t_1 represents the full width at half maximum ($FWHM$). (c) (I/I_o) vs. time (s) as shown in (a), however for times between t_1 and t_2 only. A straight line $(I/I_o) = mt + c$ is fitted through the data, where m (slope) and c (intercept) are the fitting parameters. m=0.014 s^{-1} and c=-0.010 with standard errors of 2.08 × 10^{-1} s^{-1} and 0.003 respectively.

Figure 3.3.2(e) in the main text is re-plotted below in Figure 3.A.1(a) to describe how the step increment and time were calculated during DNA uptake. The black dotted line represents the normalized mean fluorescence intensity of DNA molecules (I/I_o). The mean intensity of DNA molecules inside the GUV is I and the mean intensity of DNA molecules outside the GUV is I_o. The filled blue points connected by a solid red line

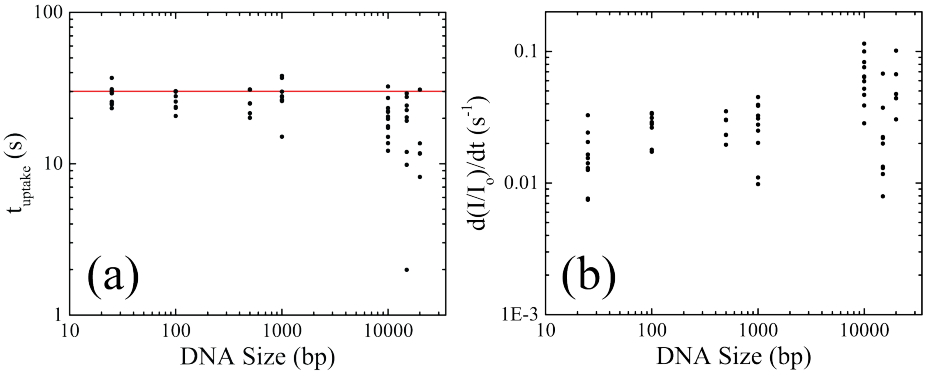

Figure 3.A.2: (a) Time during which DNA uptake was observed (t_{uptake}) potted as a scatter for each DNA size. Each data point (filled black circles) corresponds to a single experiment. Solid red line shown represents the time during which pulses were applied. 10 pulses were applied, each of 5 ms duration and at a frequency of 0.33 Hz, hence the solid line is drawn at t=30.05 s. (b) Slope $m = d(I/I_o)/dt$, as shown in Figure 3.A.1 (c) plotted for each DNA size. Each data point (filled black circles) corresponds to a single experiment.

represents the smoothed data of (I/I_o). The difference in normalized mean fluorescence intensity was calculated as $\Delta(I/I_o)_t = (I/I_o)_t - (I/I_o)_{t-\Delta_t}$, for each time step using the smoothed data, and is plotted in figure 3.A.1 (b) as filled black points. A Gaussian curve shown as a solid red line was fitted to this data. The fitted function was $\Delta(I/I_o)_t = Aexp(-0.5(t-t_o)^2/\sigma^2)$, where A, t_o and σ are the fitting parameters. σ represents the standard deviation of the Gaussian, and the time of DNA uptake is estimated to be $t_{\text{uptake}} \sim 3\sigma$. The full width at half maximum ($FWHM$), was calculated as $FWHM = 2\sqrt{2ln(2)}\sigma$. The times when the Gaussian curve attains a value of $\Delta(I/I_o)_{\max}/2$, where $\Delta(I/I_o)_{\max}$ is the maximum of Gaussian, is shown as t_1 and t_2, such that $FWHM = t_2 - t_1$. The smoothed data of (I/Io) of Figure 3.A.1 (a) is plotted again in Figure 3.A.1 (c) from times t_2 to t_2. A straight line is fitted through this curve in order to find the slope of the curve (I/I_o) vs. time (s). The fitted function was $I/I_o = mt + c$, where m represents the slope and c represents the intercept.

The time during which DNA uptake was observed $t_{\text{uptake}} \sim 3\sigma$, as shown in Figure 3.A.1 (b), was calculated for each experiment and for each DNA size and is plotted in Figure 3.A.2 (a) as a scatter. On the same curve, a solid red line is plotted representing the time during which electric field pulses were applied. Since 10 pulses were applied, each of 5 ms duration and at a frequency 0.33 Hz, therefore this line is plotted at t=30.05 s.

Similarly, the slope of the curve, $m = d(I/I_o)/dt$, was calculated for each experiment and for each DNA size and is plotted in Figure 3.A.2 (b) as a scatter.

3.B. ELECTROPHORETIC MOBILITIES IN DIFFERENT BUFFERS

To calculate the theoretical prediction plotted in Figure 3.3.3 (b) of the main text corresponding to Tris-acetate EDTA (TAE) buffers, the electrophoretic mobility of DNA molecules (μ) used in equation 3.3.1 of main text, were obtained from Stellwagen et al. (1997) [21]. These values are listed in Table 3.B.1 below.

For low conductive buffers, the electrophoretic mobility of dsA5 (20 bp) DNA molecule was estimated to be μ= 4.60 x 10^{-8} $m^2s^{-1}V^{-1}$ [24]. Considering this to be the value of electrophoretic mobility for a 25 bp DNA molecule in a low conductive buffer, this corresponds to an increase of 1.24 x 10^{-8} $m^2s^{-1}V^{-1}$ in the electrophoretic mobility from TAE buffers (Table 3.B.1). A similar increase in in electrophoretic mobility was observed for both dsA5 (20 bp) and pUC19 (2686 bp) DNA molecules upon reducing the conductivity of the buffer [23]. Therefore, considering the same increase in the electrophoretic mobility of DNA molecules of all sizes used in this work, the electrophoretic mobilities corresponding to low conductive glucose/sucrose buffers are listed in Table 3.B.2 below.

Table 3.B.1: Electrophoretic mobility of DNA molecules of different sizes in TAE buffer [21].

DNA Size (bp)	**Electrophoretic Mobility** (μ) ($m^2s^{-1}V^{-1}$)
25	3.36 x 10^{-8}
100	3.67 x 10^{-8}
500	3.75 x 10^{-8}
1000	3.75 x 10^{-8}
10000	3.75 x 10^{-8}
15000	3.75 x 10^{-8}
20000	3.75 x 10^{-8}

3.C. COMSOL SIMULATIONS OF ELECTRIC FIELD THROUGH THE ELECTRO-PORE

To estimate the electric flux through a pore on a giant unilamellar vesicle (GUV) placed in an electric field, E_{app}, finite element numerical calculations were carried out using COMSOL Multiphysics. The numerical calculations were carried out in two dimensions assuming the system is axisymmetric. The GUV is modelled as a spherical shell of radius R as seen in Figure 3.C.1. The electrical conductivity of aqueous solution inside the GUV is σ_i. The GUV is placed in an aqueous solution of electrical conductivity σ_e represented as a rectangle of dimensions 100 µm × 50 µm. It is assumed that aqueous solution inside the GUV and the external medium mix after the formation of the pore and hence σ_i and σ_e are equal. The size of electropore is parameterized as a spherical cap of angle θ on the membrane on the sides facing both anode and the cathode.

To compute the electric potential distribution in the system, Laplace's equation 3.C.1 (shown below) for the electric potential is solved numerically using the *Electric currents(ec)* module.

$$\nabla.\sigma\nabla V = 0 \tag{3.C.1}$$

The GUV membrane is modelled as a thin high resistance region using contact impedance boundary condition [28].

$$\mathbf{n}.\mathbf{J}_1 = \frac{\sigma_m}{d_m}(V_1 - V_2) \tag{3.C.2}$$

$$\mathbf{n}.\mathbf{J}_2 = \frac{\sigma_m}{d_m}(V_2 - V_1) \tag{3.C.3}$$

Here, $\mathbf{n}$ is the unit normal vector to the boundary surface, $\mathbf{J}$ is the electric current density, V_1 is the electric potential inside the GUV and V_2 is the electric potential on the exterior of the GUV, σ_m is the membrane conductivity and d_m is the thickness of the membrane.

After the values of electric potential is obtained, the electric field E is determined by:-

$$\mathbf{E} = -\nabla V \tag{3.C.4}$$

Table 3.B.2: Electrophoretic mobilities of DNA molecules in low conductive glucose/sucrose buffers.

DNA Size (bp)	**Electrophoretic Mobility** (μ) ($m^2s^{-1}V^{-1}$)
25	4.60 x 10^{-8}
100	4.91 x 10^{-8}
500	5.99 x 10^{-8}
1000	5.99 x 10^{-8}
10000	5.99 x 10^{-8}
15000	5.99 x 10^{-8}
20000	5.99 x 10^{-8}

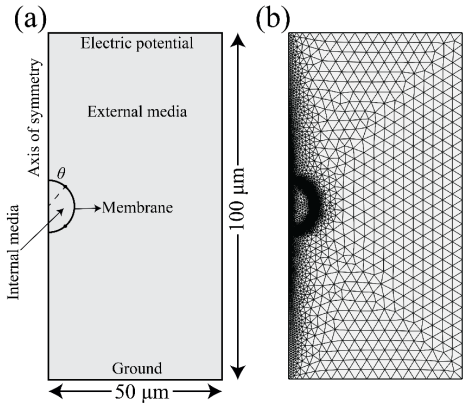

Figure 3.C.1: Geometry of the domain used for finite element numerical calculations. The GUV is modelled as the semicircle enveloped by the membrane and the pore is modelled as the spherical cap of angle θ on the membrane. The external medium is modelled as the rectangle of dimensions 100 μm × 50 μm. The top and bottom sides of the rectangle are modelled as electrodes such that an electric field Eapp exists between the two sides. The axis of symmetry is labelled on the figure. (b) The mesh that is used for numerical calculation of electric potential. The domain is discretized in to approximately 70000 elements through free triangulated meshing in COMSOL Multiphysics. The minimum mesh size is close to the edges of the pores with a mesh size of $5\text{x}10^{-11}$ m. The maximum mesh size is $1\text{x}10^{-9}$ m.

The electric flux through the pore is then calculated numerically by integrating the electric field on the surface of the electropore ($\int \mathbf{E}.\mathbf{ds} = \mathbf{f}(\boldsymbol{\theta}) = \mathbf{f}'(\mathbf{0})\boldsymbol{\theta}$). The electric flux is then calculated as a function of the angle θ.

Table 3.C.1: Model parameters used for numerical calculations.

Symbol	Parameter	Value
R	Vesicle Radius	15 μm
d_{m}	Membrane thickness	4 nm
σ_{e}	External Conductivity	$1.5 \text{ x } 10^{-4}$ S/m
σ_{i}	Internal Conductivity	$1.5 \text{ x } 10^{-4}$ S/m
σ_{m}	Membrane Conductivity	$1.0 \text{ x } 10^{-9}$ S/m
E_{app}	Applied electric field	45 kV/m

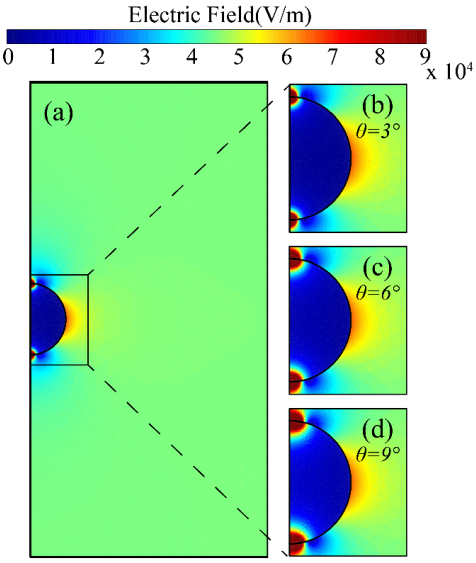

Figure 3.C.2: (a) Electric field distribution for the geometry shown in Figure 3.C.1. The applied electric field is 45 kV/m and the radius of the GUV is 15 µm. (b), (c), (d) The electric field distributions in a small region enveloping the GUV for angle of electro-pore, θ=3°, 6°, 9°. The electric field is higher at the pores and low inside the GUV.

3.D. RADIUS OF GYRATION

The contour length of DNA (L) can be estimated as $L = (no.of base pairs)$Ö0.34 nm, since the inter bp distance is ~ 0.34 nm [29]. The persistence length (l_p) of DNA in physiological salt conditions is l_p ~ 50 nm (150 bp), however it increases with decreasing salt concentrations to l_p ~ 150 nm (~450 bp) [30]. Therefore, DNA molecules of size 25 bp and 100 bp behave as rod-like molecules ($l_p > L$), and DNA molecules of size 1000 bp, 10000 bp, 150000 bp and 20000 bp behave as coil-like molecules ($L > l_p$). The DNA molecules of size 500 bp have are assumed to behave either as coil-like molecules if l_p ~ 150 bp, or rod-like molecules if l_p 450 bp.

In order to calculate the radius of gyration ($R_{g,rod}$) for rod-like molecules ($l_p > L$), the following equation 3.D.1 was used [31].

$$R_{g,rod} = \sqrt{\frac{L^2}{12}} \tag{3.D.1}$$

In order to calculate the radius of gyration ($R_{g,coil}$) for coil like molecules ($L > l_p$), the following equation (3.D.2) was used (end-to-end length for the Kratky-Porod model) [32].

$$R_{g,coil} = \sqrt{2l_pL - 2l_p^2\left[1 - exp\left(-\frac{L}{l_p}\right)\right]} \tag{3.D.2}$$

The radius of gyration according is estimated according to the above equations (3.D.1 and 3.D.2) and is shown in Table3.D.1 below. For rod-like DNA molecules (25 bp, 100 bp),

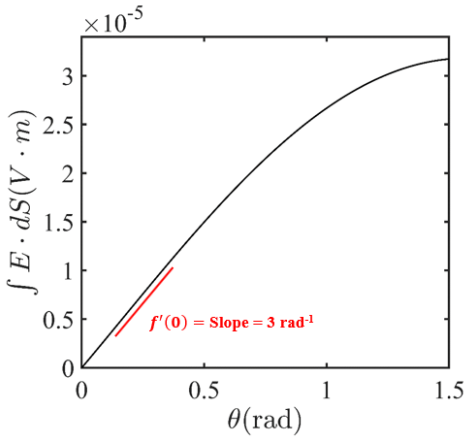

Figure 3.C.3: Electric flux across the electropore ($\mathbf{f}(\boldsymbol{\theta}) = \mathbf{f}'(\mathbf{0})\boldsymbol{\theta}$) given as a function of angle of electropore, θ. The internal and external conductivities are equal and are equal to 0.15 mS/cm [9]. The membrane as a conductivity equal to 1 x 10^{-8} mS/cm [4]. The applied electric field across two electrodes is equal to 45 kV/m and the radius of the vesicle is equal to 15 µm.

equation 3.D.1 was used to estimate R_g. For coil-like DNA molecules (1000 bp, 10000 bp, 15000 bp and 20000 bp), 3 different values of persistence length l_p= 50 nm, 100 nm and 150 nm were used to estimate R_g according to equation 3.D.2. To estimate radius of gyration for DNA molecules of size 500 bp, both equations (3.D.1 and 3.D.2) were used.

Table 3.D.1: Radius of gyration (R_g) values for different DNA sizes used.

DNA Size (bp)	**Contour Length (L) (nm)**	**Equation**	**$R_{g,rod}$ (nm)**	**$R_{g,coil}$ (nm) lp= 50 nm**	**$R_{g,coil}$ (nm) lp= 100 nm**	**$R_{g,coil}$ (nm) lp= 150 nm**
25	8.5	3.D.1	2.4			
100	34	3.D.1	9.8			
500	170	3.D.1,3.D.2	49.1	110.3	132.9	143.1
1000	340	3.D.2		170.3	220.6	248.3
10000	3400	3.D.2		578.8	812.4	987.4
15000	5100	3.D.2		710.6	1000.0	1218.6
20000	6800	3.D.2		821.6	1157.6	1412.4

REFERENCES

[1] S. Sachdev, A. Muralidharan, D. K. Choudhary, D. L. Perrier, L. Rems, M. T. Kreutzer, and P. E. Boukany, *Dna translocation to giant unilamellar vesicles during electroporation is independent of dna size,* Soft matter **15**, 9187 (2019).

[2] C. Rosazza, S. Haberl Meglic, A. Zumbusch, M.-P. Rols, and D. Miklavcic, *Gene electrotransfer: a mechanistic perspective,* Current Gene Therapy **16**, 98 (2016).

[3] M. P. Stewart, R. Langer, and K. F. Jensen, *Intracellular delivery by membrane disruption: mechanisms, strategies, and concepts,* Chemical reviews **118**, 7409 (2018).

[4] D. L. Perrier, L. Rems, and P. E. Boukany, *Lipid vesicles in pulsed electric fields: fundamental principles of the membrane response and its biomedical applications,* Advances in colloid and interface science **249**, 248 (2017).

[5] S. J. Singer and G. L. Nicolson, *The fluid mosaic model of the structure of cell membranes,* Science **175**, 720 (1972).

[6] H. Lodish, J. E. Darnell, A. Berk, C. A. Kaiser, M. Krieger, M. P. Scott, A. Bretscher, H. Ploegh, P. Matsudaira, *et al.*, *Molecular cell biology* (Macmillan, 2008).

[7] L. V. Chernomordik, A. V. Sokolov, and V. G. Budker, *Electrostimulated uptake of dna by liposomes,* Biochimica et Biophysica Acta (BBA)-Biomembranes **1024**, 179 (1990).

[8] P. F. Lurquin and K. Athanasiou, *Electric field-mediated dna encapsulation into large liposomes,* Biochemical and biophysical research communications **267**, 838 (2000).

[9] T. Portet, C. Favard, J. Teissié, D. S. Dean, and M.-P. Rols, *Insights into the mechanisms of electromediated gene delivery and application to the loading of giant vesicles with negatively charged macromolecules,* Soft Matter **7**, 3872 (2011).

[10] M. Breton, L. Delemotte, A. Silve, L. M. Mir, and M. Tarek, *Transport of sirna through lipid membranes driven by nanosecond electric pulses: an experimental and computational study,* Journal of the American Chemical Society **134**, 13938 (2012).

[11] M. Yu, W. Tan, and H. Lin, *A stochastic model for dna translocation through an electropore,* Biochimica et Biophysica Acta (BBA)-Biomembranes **1818**, 2494 (2012).

[12] C. Dekker, *Solid-state nanopores,* Nature Nanotechnology **2**, 209 (2007).

[13] M. I. Angelova and D. S. Dimitrov, *Liposome electroformation,* Faraday Discussions of the Chemical Society **81**, 303 (1986).

[14] K. Günther, M. Mertig, and R. Seidel, *Mechanical and structural properties of yoyo-1 complexed dna,* Nucleic acids research **38**, 6526 (2010).

[15] B. Kundukad, J. Yan, and P. S. Doyle, *Effect of yoyo-1 on the mechanical properties of dna,* Soft matter **10**, 9721 (2014).

[16] T. J. Atherton and D. J. Kerbyson, *Size invariant circle detection,* Image and Vision computing **17**, 795 (1999).

[17] T. Kotnik, G. Pucihar, and D. Miklavčič, *Induced transmembrane voltage and its correlation with electroporation-mediated molecular transport,* The Journal of membrane biology **236**, 3 (2010).

[18] J. C. Weaver, K. C. Smith, A. T. Esser, R. S. Son, and T. Gowrishankar, *A brief overview of electroporation pulse strength–duration space: A region where additional intracellular effects are expected,* Bioelectrochemistry **87**, 236 (2012).

[19] T. Portet, F. C. i Febrer, J.-M. Escoffre, C. Favard, M.-P. Rols, and D. S. Dean, *Visualization of membrane loss during the shrinkage of giant vesicles under electropulsation,* Biophysical journal **96**, 4109 (2009).

[20] D. L. Perrier, L. Rems, M. T. Kreutzer, and P. E. Boukany, *The role of gel-phase domains in electroporation of vesicles,* Scientific reports **8**, 4758 (2018).

[21] N. C. Stellwagen, C. Gelfi, and P. G. Righetti, *The free solution mobility of dna,* Biopolymers: Original Research on Biomolecules **42**, 687 (1997).

[22] N. C. Stellwagen, A. Bossi, C. Gelfi, and P. G. Righetti, *Dna and buffers: are there any noninteracting, neutral ph buffers?* Analytical biochemistry **287**, 167 (2000).

[23] E. Stellwagen and N. C. Stellwagen, *The free solution mobility of dna in tris-acetate-edta buffers of different concentrations, with and without added nacl,* Electrophoresis **23**, 1935 (2002).

[24] E. Stellwagen and N. C. Stellwagen, *Probing the electrostatic shielding of dna with capillary electrophoresis,* Biophysical journal **84**, 1855 (2003).

[25] K. A. Riske and R. Dimova, *Electro-deformation and poration of giant vesicles viewed with high temporal resolution,* Biophysical journal **88**, 1143 (2005).

[26] T. Portet and R. Dimova, *A new method for measuring edge tensions and stability of lipid bilayers: effect of membrane composition,* Biophysical journal **99**, 3264 (2010).

[27] D. L. Perrier, A. Vahid, V. Kathavi, L. Stam, L. Rems, Y. Mulla, A. Muralidharan, G. H. Koenderink, M. T. Kreutzer, and P. E. Boukany, *Response of an actin network in vesicles under electric pulses,* Scientific reports **9**, 8151 (2019).

[28] L. Rems, M. Ušaj, M. Kandušer, M. Reberšek, D. Miklavčič, and G. Pucihar, *Cell electrofusion using nanosecond electric pulses,* Scientific reports **3**, 3382 (2013).

[29] M. Mandelkern, J. G. Elias, D. Eden, and D. M. Crothers, *The dimensions of dna in solution,* Journal of Molecular Biology **152**, 153 (1981).

[30] S. Pan, D. At Nguyen, T. Sridhar, P. Sunthar, and J. Ravi Prakash, *Universal solvent quality crossover of the zero shear rate viscosity of semidilute dna solutions,* Journal of Rheology **58**, 339 (2014).

[31] M. Rubinstein and R. H. Colby, *Polymer physics* (Oxford university press New York, 2003).

[32] B. J. Kirby, *Micro-and nanoscale fluid mechanics: transport in microfluidic devices* (Cambridge university press, 2010).

4

EXTENSIONAL FLOW OF POLYMER SOLUTION

Molecular processes leading to "necking" in extensional flow of polymer solutions: using micro-fluidics and single DNA imaging

We study the necking and pinch-off dynamics of liquid droplets that contain a semi-dilute polymer solution of polyacrylamide close to overlap concentration by combining microfluidics and single DNA observation. Polymeric droplets are stretched by passing them through the stagnation point of a T-shaped microfluidic junction. In contrast with the sudden breakup of Newtonian droplets, a stable neck is formed between the separating ends of the droplet which delays the breakup process. Initially, polymeric filaments experience exponential thinning by forming a stable neck with extensional flow within the filament. Later, thin polymeric filaments develop a structure resembling a series of beads-on-a-string along their length and finally rupture during the final stages of the thinning process. To unravel the molecular picture behind these phenomena, we integrate a T-shaped microfluidic device with advanced fluorescence microscopy to visualize stained DNA molecules at the stagnation point within the necking region. We find that the individual polymer molecules suddenly stretch from their coiled conformation at the onset of necking. The extensional flow inside the neck is strong enough to deform and stretch polymer chains, however, the distribution of polymer conformations is broad and it remains stationary in time during necking. Furthermore, we study the dynamics of single molecules during formation of beads-on-a-string structure. We observe that polymer chains gradually recoil inside beads while polymer chains between beads remain stretched to keep the connection between beads. The present work effectively extends single molecule experiments to free surface flows, which provides a unique opportunity for molecular-scale observation within the polymeric filament during necking and rupture.

This chapter is published in Macromolecules **49**, 9578 (2016) [1].

4.1. INTRODUCTION

The extensional flow and breakup of liquid droplets is strongly affected by the presence of a very small amount of long macromolecules. For instance, during jet breakup, or when a drop of pure water falls from a faucet or a nozzle, it suddenly necks down under the capillary forces and pinches off into smaller droplets [2]. If a small amount of polyacrylamide (PAA) or polyethylene oxide (PEO) is added to water, this sudden rupture (or pinching) is delayed and instead a stable "neck" is formed that thins down slowly over time [3–6]. The process of neck formation is a ubiquitous feature in all extensional flows of polymeric fluids and happens at all length scales [7]. Therefore, characterizing the extensional rheology of polymer solutions is not only of fundamental importance for studying the stable neck formation, but is important also for a large number of commercially relevant processes that are influenced by it. A few examples are fibre spinning, nanowire array formation, roll-coating of adhesive, ink jet printing, spray formation, porous media flows and turbulent drag reduction [8–10].

Extensional flows of free surface polymer solutions were traditionally investigated by filament stretching extensional rheometer (FiSER) [11] or capillary break-up extensional rheometer (CaBER) [12] devices. FiSER devices can produce homogeneous extensional flows by sandwiching a polymer solution between two circular end-plates and moving them apart with the constant imposed extension rate, $\dot{\varepsilon}$ [13]. In CaBER devices, a polymeric fluid is also placed between two circular end-plates (of radius R) and stretched with an exponential profile to form a liquid bridge with the final stretch length $L \approx 3.6R$. The stretch is then stopped, and the developed liquid bridge thins under capillary forces resulting in the generation of an extensional flow within the cylindrical polymeric filament [14]. The shape of the polymeric filament leads to higher capillary pressure inside the filament than in the end regions of the filament which squeezes the polymeric fluid towards the upper and lower end-plates. This creates a self-thinning of the thread and the evolution of the thread diameter is observed while the thread thins and finally breaks [7, 14]. For Newtonian solutions, the extensional viscosity is three times the shear viscosity. However, for polymer solutions, the transient extensional viscosity can be orders of magnitude higher than the shear viscosity at high $\dot{\varepsilon}$ [15]. Recently, Liu *et al.* [16] investigated the origin of strain hardening during the startup uniaxial extension of polymer melts and suggested that this phenomenon may originate from the difference in the kinematics between shear and extension. In addition, they found that the geometric condensation occurs in startup uniaxial extension and can produce noticeable strain hardening [16]. When the flow becomes strong enough (at extension rates larger than the characteristic relaxation time of the polymeric fluid, $\dot{\varepsilon}\tau \geq 0.5$) [17], the effective viscosity of the polymeric fluid can be increased dramatically due to polymeric chain stretching [7]. This high transient extensional viscosity is able to resist the extensional deformation and leads to the formation of a stable neck during extensional flow and capillary thinning [7]. Elastic forces developed within the flow of the polymer solutions are able to resist the capillary forces during jet breakup, giving rise to the high extensional viscosity [7, 13, 18]. From a molecular point of view, these elastic forces originate due to the orientation and stretching of polymer molecules in the direction of the flow or the extensional deformation [7, 13, 18, 19]. Thus, in order to better characterize the extensional rheology of polymer solutions, it is essential to elucidate the molecular picture behind

extensional deformation and stable neck formation.

Using microfluidics integrated with a fluorescence microscope has allowed polymer scientists to study the conformation of fluorescently stained DNA in controlled flow conditions and examine polymer theories directly against experimental observations at the single-chain level [9, 20–27]. In 1974, de Gennes predicted that a sharp coil-stretch transition occurs in a homogeneous extensional flow of dilute polymer solution, if the extension rate exceeds a critical value of the Weissenberg number ($Wi = \dot{\varepsilon}\tau$) [17]. Experimentally, Chu's group at Stanford used a microfluidic cross-slot device to trap single DNA molecules at the stagnation point of an extensional flow and visualized the evolution of individual DNA molecules during the extensional flow to validate this theoretical prediction [9, 28]. They found that most of the DNA molecules are highly aligned and stretched at high $Wi \approx 3$, after sufficient residence time in the extensional flow [28]. So far, the coil-stretch transition has been observed in single phase extensional flow of dilute of linear and circular DNA molecules beyond a critical $\dot{\varepsilon}$ (when $Wi \geq 1$) in the microfluidic cross-slot geometry [21, 23, 24]. However, to address neck formation, and breakup of polymeric fluids, one needs to perform single DNA molecule experiments in free surface flows of polymer solutions inside a microfluidic device.

While considerable effort has been dedicated to characterize the extensional rheology of polymer solutions using microfluidics [29], microfluidics has also been used to study the jet breakup of polymer solutions leading to a stable neck [30–37]. Thus microfluidics, owing to the length scales involved, provides a suitable platform for measuring the bulk flow behaviour of the stable neck and simultaneously observing the individual molecules inside it [38]. Recently, co-flowing microfluidic geometries have been used to study the polymeric jet breakup and stable neck formation and observe the conformation of DNA molecules inside them [36, 37]. An inherent disadvantage with these geometries is the lack of a stagnation point. Therefore, either it is not possible to make molecular observations in the stable neck due to high velocities and motion blur [36], or the observations have to be corrected for the motion blur [37]. To overcome this limitation, we propose to employ a microfluidic T-junction to visualize single DNA molecules inside polymeric filaments by generating polymeric droplets and passing them through the stagnation point at a T-junction.

In this work, we integrate a T-junction microfluidic geometry with DNA imaging to capture the molecular picture behind the neck formation in extensional flow of aqueous polymer solutions. In particular, we use semi-dilute solution of long-chain PAA molecules seeded with fluorescently stained DNA molecules (T4-DNA with similar contour length) to link between the microscopic properties of the solution and the thinning dynamics of polymeric filaments during extensional flow. The presence of a stagnation point in microfluidic T-junctions allows for the observation of individual DNA molecules in the stable neck. Since DNA molecules are seeded or dissolved in the polymer solution, they act as markers or probes for the polymers in the solution and hence reflect the conformation of polymer molecules. With this argument, we find that the initially coiled polymer molecules elongate suddenly at the onset of the neck formation giving rise to a high extensional viscosity in polymer solutions. We find nearly full extension of polymer molecules in the bulk of the neck, however, they display a broad distribution of the molecular extensions due to molecular individualism. Furthermore, beads-on-

a-string morphology observed at the very last stage of the polymeric droplet breakup is also explored using single molecule observations. As such, we demonstrate a simple and effective microfluidic tool which has the capability to characterize the extensional flow of polymer solutions at both microscopic and macroscopic level.

4.2. EXPERIMENTAL SECTION

To analyze the filament thinning and droplet deformation, a T-shaped microfluidic chip is fabricated from polydimethylsiloxane (PDMS) using standard soft lithography technique [39, 40]. Microfluidic channels are sealed with a glass slide coated with a thin layer of PDMS after treating both top and bottom surfaces with an oxygen plasma. The assembled microfluidics is baked in the oven for 12 h at 68° C to complete the curing process. To ensure that the walls are more hydrophobic, the baked chips are also exposed to tricholoro (1H,1H,2H,2H-perflurooctyl) silane inside a dessicator for at least 12 hours. A schematic picture of the entire geometry is shown Figure 4.2.1. Silicone oil (50 cst, Sigma Aldrich) constitutes the continuous phase and enters the microfluidic geometry through channel (i). The polymer solution constitutes the dispersed phase and enters the microfluidic geometry through channel (ii). At the intersection of channel (i) and channel (ii), the stable polymeric droplet is formed (without using a surfactant). An additional continuous phase inlet for silicone oil is provided (channel iii). This is used to adjust the spacing between the droplets. This droplet then travels downstream at constant velocity (≈ 3300 μm/s) and reaches the T-junction where it is pulled into the two arms. The droplet then starts to thin due to a build-up of pressure at the upstream of the two arms and low pressure at the downstream of the two arms (see zoomed image of the T-junction). Two bypass junctions are provided to equalize the pressure downstream of the two arms. The continuous phase inlet flow rate is 0.2 μl/min and the dispersed phase inlet flow rate is 0.1 μl/min. The additional continuous phase inlet flow rate is 1 μl/min. The combination of these flow rates gives the best droplet production stability.

The flow images, or droplet thinning dynamics, are captured in bright-field using a Zeiss Axiovert 100M microscope connected with a high-speed camera (Phantom V9.1, 1600 x 1200 pixels). The bright-field images are obtained at 20X magnification and 1000 frame per seconds (fps) with an exposure time of 150 μs. For the DNA imaging, a tiny amount of T4-DNA as tracer molecules is added to the polymer solution. First, 10 μl T4-DNA solution (used as received from Nippon Gene Co. Ltd. at a concentration of 440 μ g/ml in 10 mM Tris (pH=8.0) and 1 mM EDTA) is stained using the YOYO-1 dye (Molecular Probes Inc.) at a base-pair:dye ratio of 5:1. The solution is then diluted to 4.4 μg/ml in Milli-Q. Finally, ≈ 20 μl of this solution is added to 5 ml of the polymer solution thus making the final concentration of tracer T4-DNA as ≈ 0.01 ppm. We find that the presence of DNA tracers does not affect the thinning and breakup dynamics of our solutions (see Figure 4.A.1). The reason for choosing T4-DNA is that it has a similar contour length (≈ 56 μm) as PAA (≈ 53 μm) which allows for a direct correlation between molecular conformations of T4-DNA and PAA. DNA imaging is carried out on a fluorescence microscope (Zeiss AxioObserver-Z1) coupled with an EMCCD camera (ANDOR ixon3). A 63X objective lens with water immersion is used for an optimal magnification with a numerical aperture (NA) of 1.0 and working distance of 2.1 mm. The field of view is 110 μm × 110 μm with a resolution of 512 × 512 or 128 × 128 pixels using frame rates varying

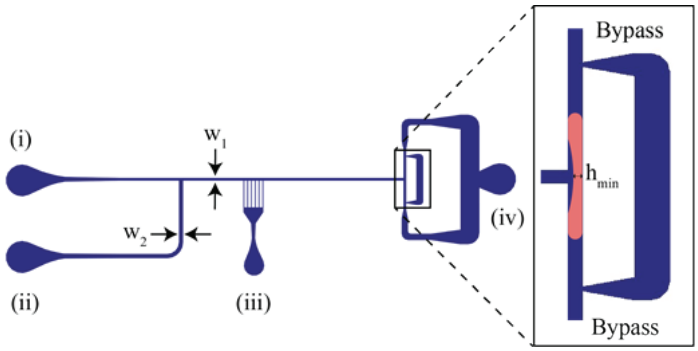

Figure 4.2.1: Microfluidic T-junction geometry used to study polymeric droplet breakup. (i) Inlet channel for the continuous phase, 50 cst Silicone oil. (ii) Inlet channel for the dispersed phase, aqueous polymer solution. (iii) Additional inlet for the continuous phase to adjust the spacing between the droplets. (iv) Outlet. The width of the main channel, W_1, is 100 μm and W_2 is 150 μm. The height of the microfluidic chip (H) is 100 μm.

between 33 fps up to 125 fps, which is fast enough to capture the DNA dynamics without motion blur.

We focus on the extensional flow behaviour of PAA (Polysciences Inc., average molecular weight M_w = 18 × 10^6 g/mol) at a concentration of 200 μg/ml in two different solvents. Radius of gyration R_g of this polymer molecule in water is around 0.33 μm with a contour length (L_c) of 53 μm [32, 37, 41]. The overlap concentration of this polymer in water (C^*) is also around 200 μg/ml calculated as $C^* = \frac{3M_w}{4\pi N_A (R_g)^3}$, where M_w is the molar mass of the chain, N_A is the Avagadro number, and R_g is the radius of gyration of polymer in a dilute solution [42]. Note that, PAA is a charged polymer, meaning that the polymer coils could be extended beyond the random coil configuration in pure water and the above expression is probably an overestimate of the coil overlap concentration [43]. To prepare polymer solutions as the dispersed phase, we dissolve the PAA polymer (used as received from Polymer sciences Inc.) at a concentration of 200 μg/ml ($C \approx C^*$) in two different solvents including, pure water (Milli-Q), or glycerol-Milli-Q (25%-75% in volume). We also tested concentrations of PAA solutions less than 200 μg/ml. PAA solutions made with 200 μg/ml provided a stable neck that persisted for a sufficient amount of time to allow for molecular observations (see Figure 4.A.1 for more details). We note that for samples at low polymer concentrations (C < 100 μg/ml), droplets rupture like Newtonian droplets without exhibiting a stable neck formation, due to their lower viscoelasticities.

To characterize the viscoelastic properties of polymer solutions, rheological measurements are performed. All rheological measurements are carried out on a TA AR2000 rheometer with Couette configuration (with a cup of 30 mm and a bob of 28 mm) at room temperature. To check reproducibility of our measurements, all rheological and thinning experiments are carried out at least in triplicate. The viscosity of the Newtonian solvent (η_{sol}) is 1 mPas and 2.5 mPas for only Milli-Q and 25% glycerol-Milli-Q (v/v) respectively. The two polymer solutions, PAA in only Milli-Q and PAA in 25% Glycerol-Milli-Q (v/v),

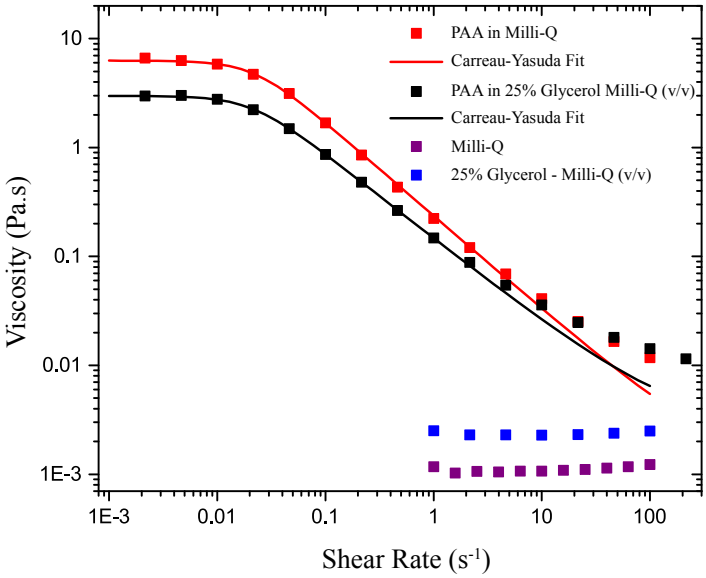

Figure 4.2.2: Steady shear viscosity curves for Newtonian solvents (Milli-Q and 25% glycerol-Milli-Q (v/v)) and rheology of the PAA solutions (C = 200 µg/ml) used in this study. All shear experiments are carried out at room temperature.

show strong shear thinning with zero shear viscosity of 6 Pa.s and 3 Pa.s respectively (see Figure 4.2.2). The variation of shear viscosity (η) with imposed shear rate can be fitted with the Carreau-Yasuda model: $\frac{\eta-\eta_\infty}{\eta_o-\eta_\infty} = [1+(\tau\dot{\gamma})^a]^{\frac{n-1}{a}}$. Here η is the measured shear viscosity, η_o is the zero shear viscosity, η_∞ is the shear viscosity at infinite shear rate (close to solvent viscosity), $\dot{\gamma}$ is the imposed shear rate, τ is a characteristic relaxation time (close to the reciprocal shear rate at which shear thinning occurs during shear), n is the power-law exponent and a represents the width of the transition region from the zero shear viscosity η_o to the shear thinning or the power-law region. The fittings of the Carreau-Yasuda model to the experimental measurements of the steady shear rheology are displayed in Figure 4.2.2. These solutions are shear thinning fluids with power law index around $n \approx 0.13$ and $n \approx 0.25$ for water and glycerol-water mixtures respectively. It is well established that PAA solutions exhibit strong shear thinning in the non-ionic solvents (in the absence of salt) [43]. The relaxation time from the Carreau-Yasuda model gives $\tau_{CY} \approx 45$ s and $\tau_{CY} \approx 53$ s for water and glycerol-water mixtures respectively. Such a high relaxation times were reported for PAA solutions, which could be attributed to the non-ionic solvent and polydispersity of PAA [43, 44]. Typically, the persistence length of PAA in high ionic solvent is 2.7 ± 0.9 nm [41, 45]. In the absence of salt, the persistence length of PAA can be of ≈ O(100 nm) [41]. This can probably increase the relaxation time of the polymer system since it has been shown previously that the onset of shear thinning regime in steady shear flows happens at lower shear rates for hydrolysed polyacrylamides (HPAM) in non-ionic solvents as opposed to ionic solvents [46, 47]. We also

investigate the flow response of PAA solutions (200 µg/ml) in the presence of salt (10 mM NaCl), and the steady shear rheology of PAA solutions with addition of salt (10 mM NaCl) is shown in Figure 4.C.1.

Zimm relaxation time of polymer solutions τ_Z is approximately 0.01 s and 0.03 s for pure Milli-Q and 25% glycerol-Milli-Q (v/v) solutions, respectively, estimated as $\tau_Z = \frac{\eta_{sol}(R_g)^3}{k_B T}$, where η_{sol} is the solvent viscosity, k_B is the Boltzmann's constant, and T is the absolute temperature of the solution [48]. The interfacial surface tension of solutions (with employed silicone oil) determined by the pendant drop technique, are $\gamma \approx 35$ mN/m and $\gamma \approx 12$ mN/m for pure Milli-Q and a 25% glycerol-Milli-Q (v/v) solutions, respectively (see Figure 4.B.1). All measurements are carried out at room temperature. For these set of conditions, the Reynold's number based on the zero shear viscosity is, Re $\approx O(10^{-4} - 10^{-3})$ and the Capillary number is, Ca $\approx O(10^{-3} - 10^{-2})$. The Reynolds number ($Re$) is defined as $Re = \rho U l/\eta$, where ρ is the fluid density, U is the velocity of the flow, η is the fluid viscosity, and $l = 2WH/(W+H)$ is the characteristic length ($l \approx W$, when $W \approx H$); here W =100 µm and H= 100 µm are the characteristic width and depth of the microchannel respectively [38]. The Ca is defined as $Ca = \eta U/\gamma$, where γ is the interfacial tension between the continuous and dispersed phases.

4.3. RESULTS AND DISCUSSION

First, we monitor the change in the thickness of the filament that holds the droplet as a function of time during the droplet stretching or pinch-off at the T-junction. Representative snapshots of the stretched liquid droplets at the stagnation point and the necked region undergoing thinning in Newtonian and polymer solutions are shown in Figure 4.3.1 (a-d). In the first case, we investigate the breakup of a Newtonian droplet for comparison and reference purposes (see Figure 4.3.1 b). The Newtonian system considered here is an aqueous glycerol solution (25% glycerol-Milli-Q (v/v)). Figure 4.3.1 (b) shows the breakup as a function of t/t_b, where t_b is the breakup time of the droplet ($t_b \approx 0.05$ s). $t = 0$ is taken as the instant when the droplet completely occupies the two arms of the T-junction and the width of the droplet is equal to the width of the channel of the T-junction. There is a build-up of pressure at the upstream end of the droplet because of the flowing outer phase (50 cst silicone oil). Since the droplet completely occupies the two arms of the T-junction, the pressure downstream in the two arms of the droplets is reduced. Thus a pressure drop is created, with high pressure at the center of the droplet and low pressure at the two ends of the T-junction. This pressure drop squeezes the droplet until it eventually breaks. As can be seen from Figure 4.3.1 (b), the Newtonian droplet pinches off suddenly without exhibiting a stable neck formation at $t/t_b \approx 0.9$ (see movie S1).

The breakup of polymeric droplets at the microfluidic T-junction is shown in Figure 4.3.1 (c-d). The polymeric droplet initially starts to thin by a similar mechanism as the Newtonian droplet. However, these droplets do not pinch off suddenly and the breakup is delayed. Figures 4.3.1 (c-d) reveal that the droplet behaves differently from its Newtonian counterpart (at $t/t_b \approx 0.5$). A stable neck is formed between the breaking ends which significantly delays the breakup (see movies S2-3). While the formation of a neck could be observed in both polymeric systems, we focused on PAA dissolved in 25%

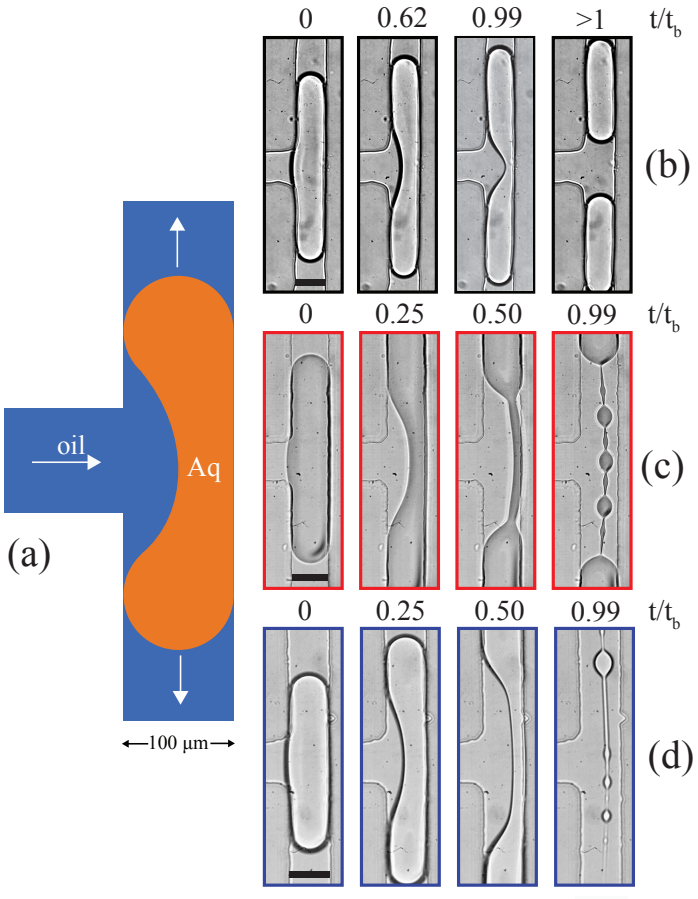

Figure 4.3.1: (a) Microfluidic T-junction geometry used to stretch liquid droplets. Sequences of images comparing the breakup of Newtonian and polymeric droplets. (b) Breakup of Newtonian (25% glycerol-Milli-Q (v/v)) droplets (with $t_b \approx 0.05$ s). Stretching and thinning of PAA fluids in (c) Milli-Q (with $t_b \approx 0.19$ s), and (d) 25% glycerol-Milli-Q (v/v) (with $t_b \approx 0.47$ s) at the T-junction. The scale bar is 100 μm.

glycerol-Milli-Q (v/v) solution, as the necking process is slower and easier to analyze for DNA imaging. In both polymeric solutions, beads-on-a-string structure has been observed at the late stage of the pinch-off process ($t/t_b \approx 1$).

To quantify the breakup event, the breakup dynamics are measured for both the Newtonian droplets and the polymeric droplets (see Figure 4.3.2 a). The breakup dynamics is measured by tracking the interface of the thinning droplet. The interface is tracked where the thickness of the droplet is minimal which occurs at the middle of the T-junction. This minimum thickness is referred to as h_{min}. From the breakup dynamics of the Newtonian droplet it is clear that the droplet snaps off instantly when the minimum thickness reaches a value around 70 μm. This sudden snap-off behaviour is com-

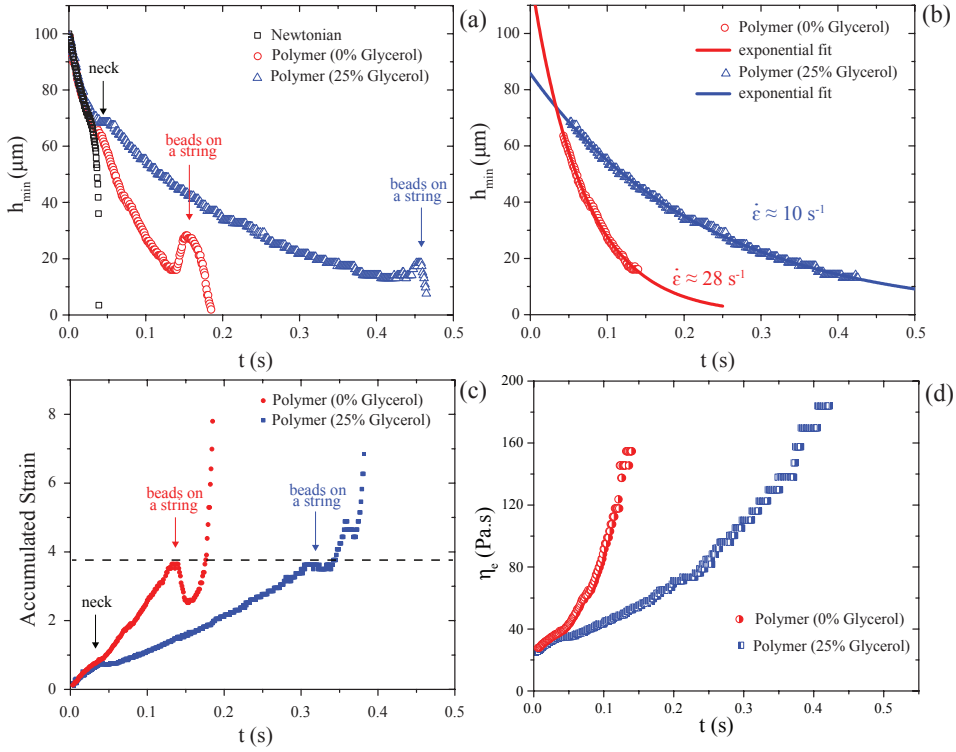

Figure 4.3.2: (a) The breakup dynamics calculated by measuring the $h_{\min}$ as a function of time for both Newtonian and polymeric droplets (approximately 5-10 droplets are analyzed for each set of operating conditions). (b) Strain rate ($\dot{\varepsilon}$) is estimated by exponential fitting of the breakup dynamics during necking. $\dot{\varepsilon} = 27.3 \pm 3.3\ s^{-1}$ and $\dot{\varepsilon} = 9.8 \pm 1.1\ s^{-1}$ for PAA solution in Milli-Q and 25% glycerol-Milli-Q (v/v), respectively. (c) Accumulated Hencky strain is calculated as $\varepsilon = -2ln(\frac{h_{\min}(t)}{h_o})$ for both PAA solutions. [18] (d) Transient extensional viscosity of PAA solutions against time.

mon for Newtonian systems and has also been observed previously, and is referred to as the singular behaviour or finite time singularity [6, 49]. For polymeric droplets, it can be seen that the breakup dynamics are exactly similar to the Newtonian droplet for early times ($t < 0.05$ s). However, after $t \approx 0.05$ s, the breakup dynamics start to diverge. The polymeric droplet forms a stable neck that thins down slowly with time.

The necking part (from $t \approx 0.05$ s to beads-on-a-string regime) of the thinning dynamics of the polymeric droplet is subjected to an exponential fit of the form $h_{min} \propto exp(-\frac{1}{2}\dot{\varepsilon}t)$, where $\dot{\varepsilon}$ is the extensional strain rate. From Figure 4.3.2 (b), it can be seen that the exponential fit well approximates the thinning dynamics of the droplet in the neck with $\dot{\varepsilon} \approx 28\ s^{-1}$ and $10\ s^{-1}$ for PAA solution in Milli-Q and 25% glycerol-Milli-Q (v/v) respectively. Such an exponential decay of $h_{\min}$ with time is characteristic of a pure extensional flow and has been previously observed in various configurations producing an extensional flow [6, 13, 18, 50] and has also been predicted by theory [19]. This suggests

that the flow inside the stable neck observed in microfluidic T-junction is extensional. By assuming that $Wi = \dot{\varepsilon}\tau_{\text{eff}} = 2/3$, we can estimate the effective relaxation of $\tau_{\text{eff}} \approx 0.02$ and 0.06 s corresponding to the PAA solution in Milli-Q and aqueous glycerol (25% glycerol-Milli-Q (v/v)), respectively [18]. Our estimated τ_{eff} is of the same order of magnitude as the estimated τ_Z. Furthermore, the accumulated Hencky strain can be calculated as $\varepsilon = -2ln(\frac{h_{\min}(t)}{h_o})$, where h_0 is the initial thickness of droplet (at $t = 0$) [18]. Figure 4.3.2 (c) displays that beads-on-a-string structure has been formed, at $\varepsilon \approx 4$ in both PAA solutions. Figure 4.3.2 (d) displays the estimated transient extensional viscosity calculated as $\eta_e = \frac{2\gamma}{\dot{\varepsilon} h_{\min}(t)}$ for both solutions [18]. It is well-established that transient η_e can be orders of magnitude larger than shear viscosity and, it is strongly dependent on time (or ε), as shown in Figure 4.3.2 (d). In addition, we investigate the thinning dynamics of PAA solution (with 10 mM NaCl). With this salt concentration, we expect that polymer chains are fully neutralized and electrostatic effects are minimized [51]. Qualitatively, similar thinning behaviour has been observed in PAA solution with 10 mM NaCl (see Figure 4.C.2).

Having validated the microfluidic T-junction for producing a stable neck with an extensional flow inside, we continued investigating the conformations of the polymer molecules by direct visualization inside this neck. Since, it is currently difficult to directly stain the polymer (PAA) molecules [37], stained T4-DNA molecules of comparable contour length are added to the solution. We assumed that the individual dynamics of the T4-DNA molecules would be representative of the polymer molecules producing the neck [9, 37, 52–55]. The dynamics of individual DNA molecules at different stages of thinning is shown in Figure 4.3.3 (b). During the initial stages of the breakup, the thinning dynamics of the polymer and the Newtonian droplet are the same, which implies that the role of the polymer molecules is absent during this stage. The macromolecules remain coiled and are not influencing the breakup dynamics (see Figure 4.3.3 a-b). However, at the onset of necking, the macromolecules elongate suddenly, as shown by the last two snapshots of Figure 4.3.3 (b). The extensions of the DNA molecules are measured both before and during stable neck formation (see Figure 4.3.3 c-d), respectively, as the probability density of normalized lengths. Figure 4.3.3 (c) confirms that before necking, majority of the DNA molecules are in their equilibrium coiled conformation. In contrast, during the neck formation, majority of these polymer molecules are stretched due to the extensional flow inside the stable neck. The Wi number can be calculated as $Wi = \dot{\varepsilon}\tau_{\text{CY}} \approx 530$, where $\dot{\varepsilon} \approx 10\ \text{s}^{-1}$ and $\tau_{\text{CY}} \approx 53$ s from shear rheology. The strain accumulated over the entire process of necking is $\varepsilon \approx 4$ (as shown in Figure 4.3.2 (c)) before the neck transforms into a beads-on-a-string morphology. Such a high Wi number and accumulated strain is enough to stretch the polymer molecules from their equilibrium coiled conformation. Despite such high Wi, the the level of stretch or the molecular extension of individual DNA molecules is rather heterogeneous with a broad distribution as shown in Figure 4.3.3 (d). The level of this heterogeneity could possibly be explained by molecular individualism and different pre-shear conditions and has been previously observed as well [26, 28, 36]. Apart from this, a few DNA molecules are pre-stretched beyond their equilibrium coiled conformation before the formation of stable neck (see Figure 4.3.3 c). The inset of Figure 4.3.3 (d) confirms that the variation of the extensions during necking is insensitive to the necking time, and the probability distribution is almost the same when the data is separated into two groups. Similar distribution has been

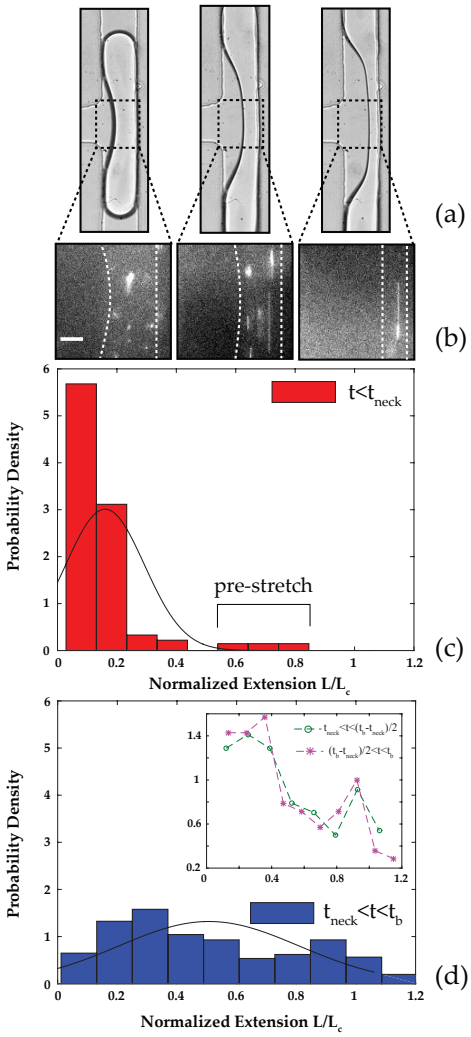

Figure 4.3.3: (a) and (b) Snapshots showing how DNA molecules behave during the neck formation (the snapshots are separated by an interval of 15 ms). Scale bar is 35 μm. Probability density of the extension of the DNA molecules is shown in (c) before and (d) after the neck formation. The Probability density functions (PDF) are constructed using 600 measurements. The inset shows that PDF is almost insensitive to the time during necking.

observed in PAA solution in 50% glycerol (see Figure 4.D.1) and also for PAA solution (200 μg/ml dissolved in 25% glycerol-Milli-Q (v/v)) with 10 mM NaCl (see Figure 4.C.3). Thus, it can be concluded that the electrostatic effects are negligible, or at least small compared to the effect of extension in our PAA solutions (in the range we studied). The stretching and deformation of macromolecules contribute additional tensile elastic stresses, which

stabilize the neck formation by opposing capillary stress during thinning.

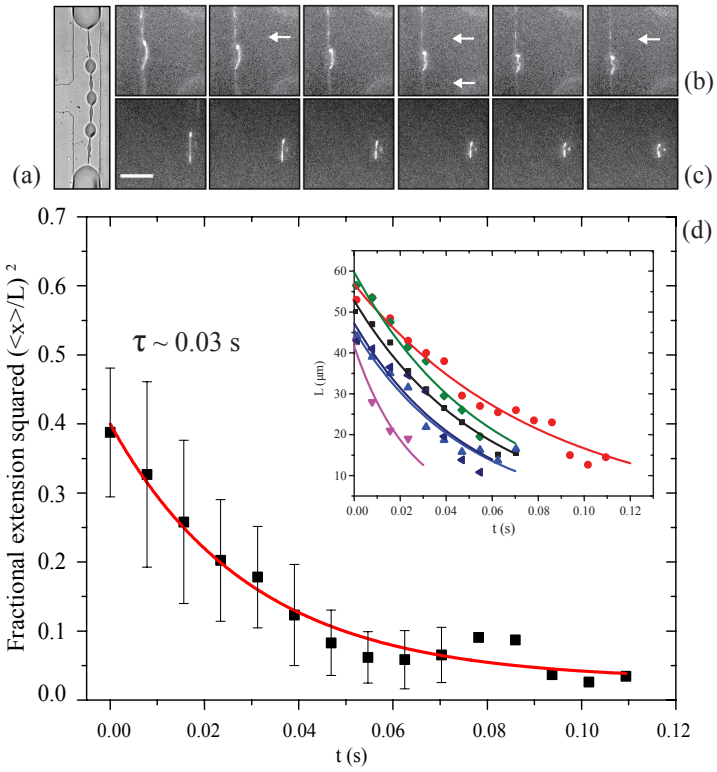

Figure 4.3.4: (a) A bright field image of beads-on-a-string morphology in PAA solution. Sequence of fluorescence images showing how single molecules behave during formation of beads on a string morphology in the solution of PAA in (b) Milli-Q water, and (c) 25% glycerol. Single polymers gradually recoil inside a bead, and polymeric chains between beads remained stretched (highlighted by white arrows) during this process (the snapshots are after an interval of 15 ms). Scale bar is 50 μm. (d) Time evolution of recoiling-process in the solution of PAA in 25% glycerol. The symbols are average experimental data and represent the time evolution of the square of the fractional extension of 6 individual DNA molecules relaxing during the beads-on-a-string process. Error bars represent the standard deviation calculated from a set of six measurements. The solid line represents an exponential fit of the form $((< x > /L)^2 = C_1 exp(-t/\tau) + C_2$, where C_1 and C_2 are fitting parameters, and the <> represent an average over 6 DNA molecules). The characteristic relaxation time (τ) obtained from the fitting is 0.03 s. The inset shows the DNA length versus time, suggesting that the recoiling-process occurs for 6 individual DNA molecules during beads-on-a-string formation.

During the last stages of the breakup, the stable neck transforms into beads-on-a-string morphology (see Figure 4.3.4 a). The microfluidic T-junction also provides an opportunity to investigate the beads-on-a-string morphology at the molecular level. During the last stages of the breakup, the DNA molecules are found to be coiled in the beads, while they are stretched in the strings connecting the beads (see Figure 4.3.4 b-c). These observations suggest a molecular mechanism in which the fully stretched DNA/polymer molecules coil back to form the beads-on-a-string morphology. Figure 4.3.4 (d) displays

the time evolution of recoiling process inside a bead for the PAA solution in 25% glycerol-Milli-Q (v/v). Characteristic relaxation time ($\tau \approx 0.03$ s) of this process is extracted by exponential fitting of square of fractional extension against time [28, 51]. The characteristic relaxation time obtained in Figure 4.3.4 (d) is very close to the effective relaxation time estimated from thinning dynamics of PAA solution ($\tau_{\text{eff}} \approx 0.06$ s). The estimated relaxation time from shear rheology and Carreau-Yasuda fitting is $\tau_{\text{CY}} \approx 53$ s, which is significantly slower than our observed relaxation time based on thinning dynamics and single molecule observation during beads formation process. Recently Sousa *et al.* [44], used CaBER rheometer to extract the relaxation time of PAA solutions for investigation of polymeric fluid flow in microscale cross-slot devices. They found that CaBER relaxation time (τ_{Ca}) is also significantly faster than a relaxation time determined from a shear flow (τ_{CY}). Note that the process of polymer/DNA molecules coiling back into the beads of the beads-on-a-string morphology is not a pure relaxation process and it is possible that it is influenced by fluid flow from the strings into the beads.

4.4. CONCLUSION

In conclusion, we have investigated and described the conformation of polymer molecules during thinning and necking of polymeric droplets in an extensional flow provided by a T-shaped microfluidic device. In contrast to the breakup of Newtonian droplets, a stable neck is formed between the separating ends of polymeric droplet that thins down slowly in time. The rate of thinning of the neck is exponential in time suggesting that the primary flow occurring during the breakup of the droplet is extensional. The overall distribution of molecular extensions in the neck is obtained for the established extensional rate using DNA imaging. This distribution is heterogeneous indicating that, in the neck, individual DNA molecules unravel and evolve with different rates and have different steady state extensions. The stretched molecules provide the elastic stresses which stabilize the neck formation during thinning. Moreover, the stretched macromolecules coil back to their equilibrium conformation during the formation of the beads-on-a-string morphology. The present work is only the first step toward understanding a realistic molecular picture for macromolecular solutions under strong extensional flow. We believe that our developed T-shaped microfluidics combined with single molecule experiments can provide a unique opportunity to study the dynamics of single chains in extensional flow fields of polymer solutions (ranging from dilute to well-entangled solutions) with different architectures (from linear to branched polymers) [56, 57]. These single molecule experiments are required for developing a realistic theoretical picture of polymer solutions in extensional flow fields.

APPENDIX

4.A. DEPENDENCE OF THINNING DYNAMICS OF THE BREAKING DROPLETS ON THE CONCENTRATION OF PAA SOLUTIONS

Experiments were performed for different concentrations of PAA solutions to determine the concentration that would produce a stable neck for a sufficient amount of time allowing for observation of DNA molecules. From the figure (Figure 4.A.1) below, 200 µg/ml PAA dissolved in Milli-Q, with a breakup time (t_b) of around 0.15 s was just sufficient. After 25% (v/v) glycerol to the solvent (200 µg/ml PAA dissolved in 25% glycerol-Milli-Q (v/v)), the breakup time (t_b) increased to about 0.45 s and was enough to observe the conformations of DNA molecules inside the neck. Solutions with 25 µg/ml PAA and 50 µg/ml PAA did not show any stable neck formation.

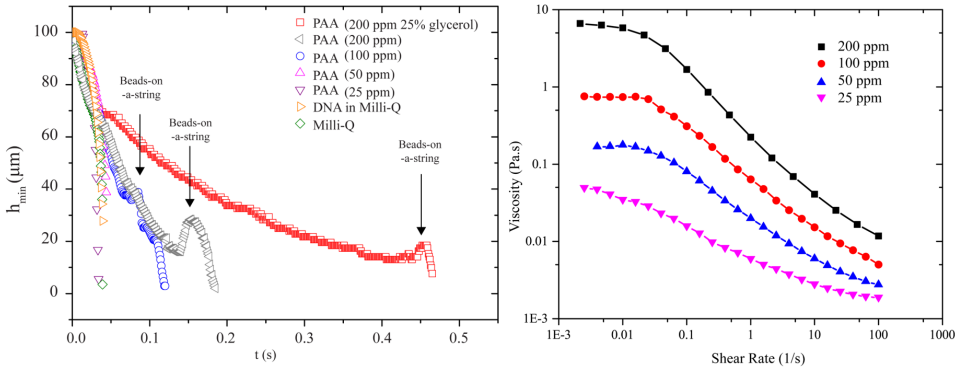

Figure 4.A.1: (Left) Breakup profiles of the thinning droplets at the microfluidic T-junction for different concentrations of the PAA solutions. (Right) Shear rheology of the different PAA solutions (no glycerol or salt added).

4.B. INTERFACIAL TENSION MEASUREMENTS

Interfacial tension of the two aqueous polymer solutions with 50 cst silicone oil is measured using the pendant drop method (as shown in Figure 4.B.1). The interfacial tension between 50 cst silicone oil and PAA dissolved in only Milli-Q is approximately 35 mN/m (Figure 4.B.1 a) and between 50 cst silicone oil and PAA dissolved in 25% Glycerol-Milli-Q solution is 12 mN/m (see Figure 4.B.1 (b)).

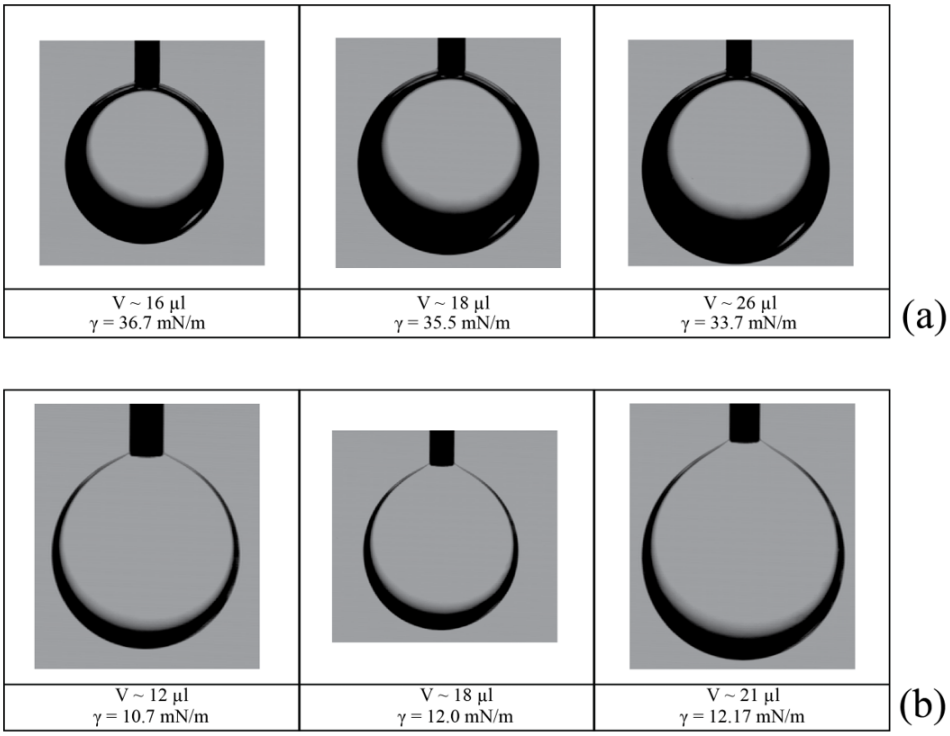

Figure 4.B.1: Measurement of interfacial tension between 50 cst silicone oil and the two polymer solutions. (a) Drop of PAA dissolved in Milli-Q suspended in 50 cst silicone oil. The snapshots represent different drop volumes considered to measure the interfacial tension. (b) Drop of PAA dissolved in 25% Glycerol-Milli-Q solution suspended in 50 cst silicone oil. The snapshots represent different drop volumes considered to measure the interfacial tension. The interfacial tension was measured using the droplet analysis method [58].

4.C. DROPLET THINNING DYNAMICS AND DISTRIBUTION OF DNA EXTENSIONS FOR PAA SOLUTIONS IN 10 MM NACL

Shear rheology of PAA solutions with and without the addition of salt (10 mM NaCl) is shown in Figure 4.C.1. After the addition of salt, the polymer solutions show less shear thinning when compared to the polymer solutions without salt. The polymer solutions without salt are subject to a Carreau-Yasuda fit (the details of the fitting and the fitting parameters can be found in the main text in Figure 2 and also mentioned below). The polymer solutions with 10 mM NaCl added are subject to a power law fit of the form $\eta = K\dot{\gamma}^{n-1}$, where η is the shear viscosity, $\dot{\gamma}$ is the imposed shear rate and n is the power-law exponent. The fitting parameters for the Carreau-Yasdua fit and the Power-Law fit are also shown in Table 4.C.1 and 4.C.2 below.

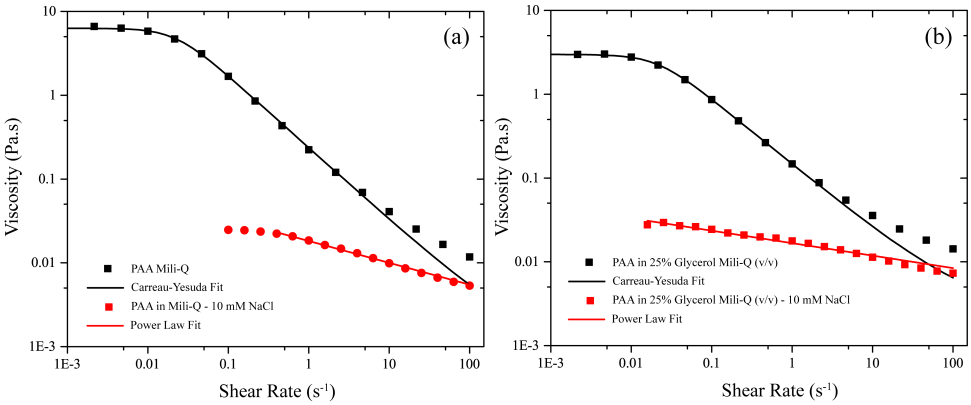

Figure 4.C.1: Effect of salt on the shear rheology for 200 µg/ml PAA dissolved in (a) Milli-Q and (b) 25% glycerol-Milli-Q (v/v). The solid black lines represents a Carreau-Yasdua fit to the shear rheology data and the solid black line represents a power-law fit of the form $\eta = K\dot{\gamma}^{n-1}$, to the shear rheology data.

Table 4.C.1: Fitting parameters for the Carreau-Yasdua Fitting

PAA Solution	Carreau-Yasuda Fit $\frac{\eta-\eta_\infty}{\eta_0-\eta_\infty} = [1+(\tau\dot{\gamma})^a]^{\frac{n-1}{a}}$		
	τ	η	a
200 (η_0 = 6.28 Pa.s, η_∞ = 1.00 mPa.s)	45.42	0.13	2.11
200 µg/ml (η_0 = 2.98 Pa.s, η_∞ = 2.49 mPa.s)	53.21	0.25	2.27

Polymer solutions with salt show significantly less shear thinning (n=0.73 and n=0.85) compared to polymer solutions without salt (n=0.13 and n=0.25).

The exponential part for the breakup of 200 µg/ml in 25% glycerol-Milli-Q (v/v) is shown below in Figure 4.C.2 (a) without salt and (b) with salt (10 mM NaCl). The thinning

Table 4.C.2: Fitting parameters for the Power-Law Fitting

PAA Solution (with 10 mM NaCl)	Power-Law Fit $\eta = K\dot{\gamma}^{n-1}$	
	K	n
200 μg/ml	0.01	0.73
200 μg/ml (glycerol)	0.01	0.85

dynamics (or extensional strain rate,$\dot{\epsilon}$) changes slightly by the addition of 10 mM NaCl. For PAA solution without salt $\dot{\epsilon} \sim 10\ s^{-1}$ and for PAA solution with salt $\dot{\epsilon} \sim 13\ s^{-1}$.

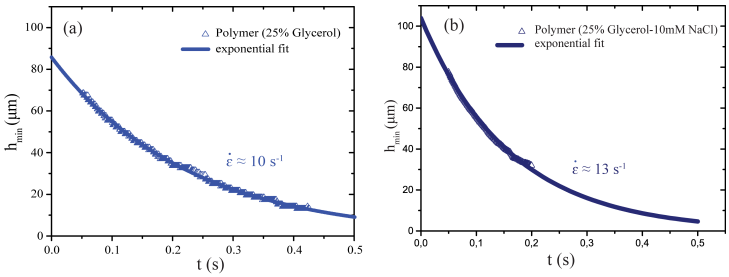

Figure 4.C.2: Exponential part for the thinning of PAA (200 μg/ml in 25% glycerol-Milli-Q (v/v)) droplets at the microfluidic T-junction for (a) without salt and (b) with salt (10 mM NaCl). Approximately 10 droplets are analysed for both solutions. The exponential part of the thinning dynamics is subject to an exponential fit of the form, $h_{\text{min}} = h_o exp(-\frac{\dot{\epsilon}t}{2})$ where $\dot{\epsilon}$ and h_o are the fitting parameters. $\dot{\epsilon}$=9.8 ± 1.1 s^{-1} for (a) and $\dot{\epsilon}$=13.37 ± 3.9 s^{-1} for (b).

The distribution of DNA extensions was measured for 200 μg/ml in 25% glycerol-Milli-Q (v/v) with the addition of 10 mM NaCl and it is shown below in Figure 4.C.3. The distribution of DNA extensions remains broad similar to the polymer solution without the addition of salt.

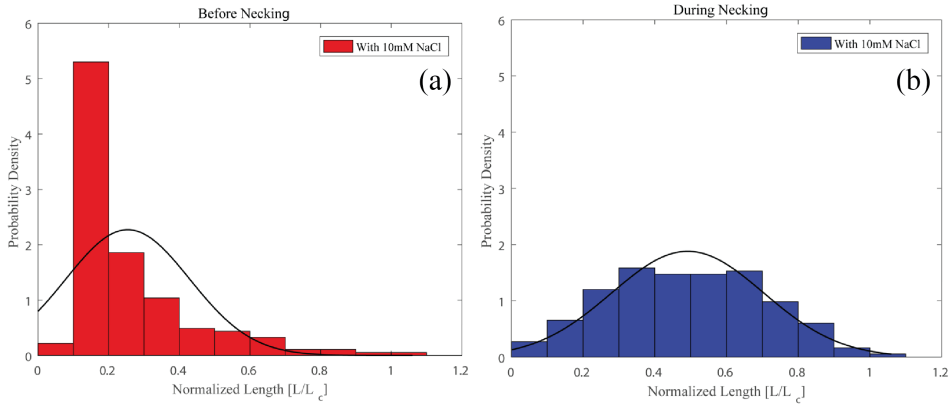

Figure 4.C.3: Probability density of molecular extension of DNA molecules for 200 μg/ml in 25% glycerol-Milli-Q (v/v) with 10 mM NaCl for both (a) before necking and (b) during necking. The histograms have been constructed using more than 400 measurements.

4.D. DISTRIBUTION OF DNA EXTENSIONS FOR PAA SOLUTION IN 50% GLYCEROL

The distribution of DNA extensions is also measured for another system, which comprises of 500 cst silicone oil as the outer solution and PAA solution (C = 200 μg/ml) in 50% glycerol. The extensional strain rate measured from droplet thinning is approximately 5 s^{-1}. The distribution of DNA extension for this system is shown below in Figure 4.D.1.

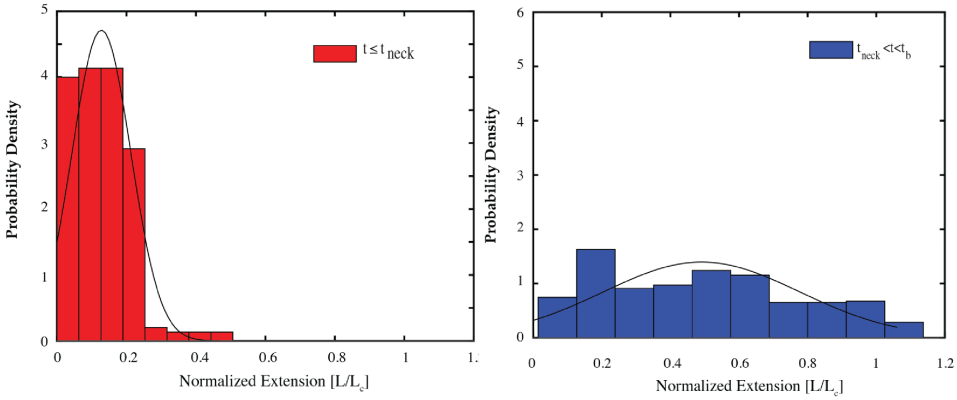

Figure 4.D.1: Distribution of DNA extensions represented as a probability density of normalized extensions (left) before necking and (right) after necking.

REFERENCES

[1] S. Sachdev, A. Muralidharan, and P. E. Boukany, *Molecular processes leading to "necking" in extensional flow of polymer solutions: Using microfluidics and single dna imaging,* Macromolecules **49**, 9578 (2016).

[2] J. W. Strutt and L. Rayleigh, *On the instability of jets,* Proc. London Math. Soc **10** (1878).

[3] M. Goldin, J. Yerushalmi, R. Pfeffer, and R. Shinnar, *Breakup of a laminar capillary jet of a viscoelastic fluid,* Journal of Fluid Mechanics **38**, 689 (1969).

[4] D. Bousfield, R. Keunings, G. Marrucci, and M. Denn, *Nonlinear analysis of the surface tension driven breakup of viscoelastic filaments,* Journal of non-newtonian fluid mechanics **21**, 79 (1986).

[5] W. Jones, N. Hudson, and J. Ferguson, *The extensional properties of m1 obtained from the stretching of a filament by a falling pendant drop,* Journal of Non-Newtonian Fluid Mechanics **35**, 263 (1990).

[6] Y. Amarouchene, D. Bonn, J. Meunier, and H. Kellay, *Inhibition of the finite-time singularity during droplet fission of a polymeric fluid,* Physical Review Letters **86**, 3558 (2001).

[7] G. H. McKinley, *Visco-elasto-capillary thinning and break-up of complex fluids,* in Rheology Reviews, edited by D. M. Binding and K. Walters (British Society of Rheology, Aberystwyth, UK , 1 (2005).

[8] F. J. Galindo-Rosales, M. Alves, and M. Oliveira, *Microdevices for extensional rheometry of low viscosity elastic liquids: a review,* Microfluidics and nanofluidics **14**, 1 (2013).

[9] L. Rems, D. Kawale, L. J. Lee, and P. E. Boukany, *Flow of dna in micro/nanofluidics: From fundamentals to applications,* Biomicrofluidics **10**, 043403 (2016).

[10] P. J. Glazer, L. Bergen, L. Jennings, A. J. Houtepen, E. Mendes, and P. E. Boukany, *Generating aligned micellar nanowire arrays by dewetting of micropatterned surfaces,* Small **10**, 1729 (2014).

[11] J. Matta and R. Tytus, *Liquid stretching using a falling cylinder,* Journal of Non-Newtonian Fluid Mechanics **35**, 215 (1990).

[12] A. Bazilevsky, V. Entov, and A. Rozhkov, *Liquid filament microrheometer and some of its applications,* in *Third European Rheology Conference and Golden Jubilee Meeting of the British Society of Rheology* (Springer, 1990) pp. 41–43.

[13] G. H. McKinley and T. Sridhar, *Filament-stretching rheometry of complex fluids,* Annual Review of Fluid Mechanics **34**, 375 (2002).

[14] G. H. McKinley and A. Tripathi, *How to extract the newtonian viscosity from capillary breakup measurements in a filament rheometer,* Journal of Rheology (1978-present) **44**, 653 (2000).

[15] R. B. Bird, R. C. Armstrong, and O. Hassager, *Dynamics of polymeric liquids. vol. 1: Fluid mechanics,* (1987).

[16] G. Liu, H. Sun, S. Rangou, K. Ntetsikas, A. Avgeropoulos, and S.-Q. Wang, *Studying the origin of "strain hardening": Basic difference between extension and shear,* Journal of Rheology **57**, 89 (2013).

[17] P. De Gennes, *Coil-stretch transition of dilute flexible polymers under ultrahigh velocity gradients,* The Journal of Chemical Physics **60**, 5030 (1974).

[18] S. L. Anna and G. H. McKinley, *Elasto-capillary thinning and breakup of model elastic liquids,* Journal of Rheology (1978-present) **45**, 115 (2001).

[19] V. Entov and E. Hinch, *Effect of a spectrum of relaxation times on the capillary thinning of a filament of elastic liquid,* Journal of Non-Newtonian Fluid Mechanics **72**, 31 (1997).

[20] D. J. Mai, C. Brockman, and C. M. Schroeder, *Microfluidic systems for single dna dynamics,* Soft Matter **8**, 10560 (2012).

[21] D. E. Smith and S. Chu, *Response of flexible polymers to a sudden elongational flow,* Science **281**, 1335 (1998).

[22] H. P. Babcock, R. E. Teixeira, J. S. Hur, E. S. G. Shaqfeh, and S. Chu, *Visualization of molecular fluctuations near the critical point of the coil-stretch transition in polymer elongation,* Macromolecules **36**, 4544 (2003).

[23] C. M. Schroeder, H. P. Babcock, E. S. Shaqfeh, and S. Chu, *Observation of polymer conformation hysteresis in extensional flow,* Science **301**, 1515 (2003).

[24] Y. Li, K.-W. Hsiao, C. A. Brockman, D. Y. Yates, R. M. Robertson-Anderson, J. A. Kornfield, M. J. San Francisco, C. M. Schroeder, and G. B. McKenna, *When ends meet: Circular dna stretches differently in elongational flows,* Macromolecules **48**, 5997 (2015).

[25] R. E. Teixeira, H. P. Babcock, E. S. G. Shaqfeh, and S. Chu, *Shear thinning and tumbling dynamics of single polymers in the flow-gradient plane,* Macromolecules **38**, 581 (2005).

[26] R. E. Teixeira, A. K. Dambal, D. H. Richter, E. S. G. Shaqfeh, and S. Chu, *The individualistic dynamics of entangled dna in solution,* Macromolecules **40**, 2461 (2007).

[27] P. E. Boukany, O. Hemminger, S.-Q. Wang, and L. J. Lee, *Molecular imaging of slip in entangled dna solution,* Phys. Rev. Lett. **105**, 027802 (2010).

[28] T. T. Perkins, D. E. Smith, and S. Chu, *Single polymer dynamics in an elongational flow,* Science **276**, 2016 (1997).

[29] S. Haward, *Microfluidic extensional rheometry using stagnation point flow,* Biomicrofluidics **10**, 043401 (2016).

[30] J. Husny and J. J. Cooper-White, *The effect of elasticity on drop creation in t-shaped microchannels,* Journal of non-newtonian fluid mechanics **137**, 121 (2006).

[31] B. Steinhaus, A. Q. Shen, and R. Sureshkumar, *Dynamics of viscoelastic fluid filaments in microfluidic devices,* Physics of Fluids (1994-present) **19**, 073103 (2007).

[32] P. E. Arratia, J. P. Gollub, and D. J. Durian, *Polymeric filament thinning and breakup in microchannels,* Physical Review E **77**, 036309 (2008).

[33] P. E. Arratia, L. Cramer, J. P. Gollub, and D. J. Durian, *The effects of polymer molecular weight on filament thinning and drop breakup in microchannels,* New Journal of Physics **11**, 115006 (2009).

[34] G. Christopher and S. Anna, *Passive breakup of viscoelastic droplets and filament self-thinning at a microfluidic t-junction,* Journal of Rheology (1978-present) **53**, 663 (2009).

[35] W. Lee, L. M. Walker, and S. L. Anna, *Competition between viscoelasticity and surfactant dynamics in flow focusing microfluidics,* Macromolecular Materials and Engineering **296**, 203 (2011).

[36] G. Juarez and P. E. Arratia, *Extensional rheology of dna suspensions in microfluidic devices,* Soft Matter **7**, 9444 (2011).

[37] F. Ingremeau and H. Kellay, *Stretching polymers in droplet-pinch-off experiments,* Physical Review X **3**, 041002 (2013).

[38] X. Hu, P. E. Boukany, O. L. Hemminger, and L. J. Lee, *The use of microfluidics in rheology,* Macromolecular Materials and Engineering **296**, 308 (2011).

[39] D. C. Duffy, J. C. McDonald, O. J. Schueller, and G. M. Whitesides, *Rapid prototyping of microfluidic systems in poly (dimethylsiloxane),* Analytical chemistry **70**, 4974 (1998).

[40] Y. Xia and G. M. Whitesides, *Soft lithography,* Annual review of materials science **28**, 153 (1998).

[41] J. Francois, D. Sarazin, T. Schwartz, and G. Weill, *Polyacrylamide in water: molecular weight dependence of $<R^2>$ and [η] and the problem of the excluded volume exponent,* Polymer **20**, 969 (1979).

[42] M. Doi and S. F. Edwards, *The theory of polymer dynamics*, Vol. 73 (oxford university press, 1988).

[43] L. Campo-Deaño, F. J. Galindo-Rosales, F. T. Pinho, M. A. Alves, and M. S. Oliveira, *Flow of low viscosity boger fluids through a microfluidic hyperbolic contraction,* Journal of Non-Newtonian Fluid Mechanics **166**, 1286 (2011).

[44] P. C. Sousa, F. T. Pinho, M. S. N. Oliveira, and M. A. Alves, *Purely elastic flow instabilities in microscale cross-slot devices,* Soft Matter **11**, 8856 (2015).

[45] W. F. Reed, S. Ghosh, G. Medjahdi, and J. Francois, *Dependence of polyelectrolyte apparent persistence lengths, viscosity, and diffusion on ionic strength and linear charge density,* Macromolecules **24**, 6189 (1991).

[46] A. Ait-Kadi, P. Carreau, and G. Chauveteau, *Rheological properties of partially hydrolyzed polyacrylamide solutions,* Journal of Rheology (1978-present) **31**, 537 (1987).

[47] A. Magueur, M. Moan G, and G. Chauveteau, *Effect of Successive Contractions and Expansions on the Apparent Viscosity of Dilute Polymer Solutions,* Chemical Engineering Communications **36**, 351 (1985).

[48] M. Rubinstein and R. H. Colby, *Polymer physics* (Oxford university press New York, 2003).

[49] J. Eggers, *Nonlinear dynamics and breakup of free-surface flows,* Reviews of modern physics **69**, 865 (1997).

[50] V. Tirtaatmadja and T. Sridhar, *A filament stretching device for measurement of extensional viscosity,* Journal of Rheology (1978-present) **37**, 1081 (1993).

[51] Y. Liu, Y. Jun, and V. Steinberg, *Concentration dependence of the longest relaxation times of dilute and semi-dilute polymer solutions,* Journal of Rheology (1978-present) **53**, 1069 (2009).

[52] S. Gerashchenko, C. Chevallard, and V. Steinberg, *Single-polymer dynamics: Coil-stretch transition in a random flow,* EPL (Europhysics Letters) **71**, 221 (2005).

[53] N. François, D. Lasne, Y. Amarouchene, B. Lounis, and H. Kellay, *Drag enhancement with polymers,* Physical review letters **100**, 018302 (2008).

[54] N. François, Y. Amarouchene, B. Lounis, and H. Kellay, *Polymer conformations and hysteretic stresses in nonstationary flows of polymer solutions,* EPL (Europhysics Letters) **86**, 34002 (2009).

[55] M. Smith and V. Bertola, *Effect of polymer additives on the wetting of impacting droplets,* Physical review letters **104**, 154502 (2010).

[56] D. J. Mai, A. B. Marciel, C. E. Sing, and C. M. Schroeder, *Topology-controlled relaxation dynamics of single branched polymers,* ACS Macro Letters **4**, 446 (2015).

[57] J. Dinic, Y. Zhang, L. N. Jimenez, and V. Sharma, *Extensional relaxation times of dilute, aqueous polymer solutions,* ACS Macro Letters **4**, 804 (2015).

[58] A. Daerr and A. Mogne, *Pendent_drop: an imagej plugin to measure the surface tension from an image of a pendent drop,* Journal of Open Research Software **4** (2016).

5

CONCLUSION AND OUTLOOK

Research objectives, as stated in Chapter 1, were formulated in order to probe specific aspects of electric field mediated DNA delivery and extensional flow of polymer solutions. The corresponding findings in pursuit of these objectives are presented below in this chapter, along with an outlook and recommendations for future research.

In Chapter 2, it was established that DNA-membrane complex formation (or DNA aggregation) during electropermeabilization is dependent on the size of the DNA. No DNA aggregates were observed for a DNA size of 15 bp, whereas larger DNA molecules of size 25 bp, 50 bp, 100 bp and 1000 bp formed aggregates at the cell membrane. Such a dependency of DNA size on its phase separated, or aggregated behaviour, is consistent with Onsager's theory of DNA condensation. For all the DNA sizes tested, direct access to the cytsoskeleton was observed. The amount of translocated DNA, however decreased with increasing size of the DNA molecule.

DNA forms aggregates, and the process depends on the size of the DNA. Still, the size of the aggregates that are formed remains elusive. Estimates of size of DNA aggregates, or the amount of DNA in them, as a function of DNA size will enable further understanding of DNA uptake during electropermeabilization. For instance, these estimates will help predict the amount of DNA loaded, and the time for DNA molecules to reach their target destination. Therefore, future direction along this line of research would be to estimate the size of these aggregates and this can be achieved by tracking their intra-cellular motion via passive diffusion [1].

The various modes of DNA translocation as shown in Figure 1.1.5 (b-d) were tested and discussed in Chapter 3. Instead of employing cells, experiments were performed on GUVs in order to obtain mechanistic insights over phenomenological observations. The model cell membrane systems allowed a direct comparison of experimentally determined translocation efficiencies with the theoretical predictions of bulk electrophoretic transport (Figure 1.1.5 (b)-(c)) [2] and stochastic threading (Figure 1.1.5 (d)) [3]. The translocation efficiency remained constant as a function of DNA size (25 bp - 20000 bp), suggesting that DNA molecules can translocate across electro-pores in their coiled configuration. This supports bulk electrophoretic transport as the dominant mechanism of

DNA translocation across cell membrane during electropermeabilization.

GUVs used in this research were made of zwitter-ionic DOPC lipids along with trace amounts of Rhodamine-PE lipids for fluorescence visualization. This constitutes a rudimentary model of the real cell. Hence, a first step towards approaching a mechanistic understanding of DNA translocation in real cells, via the model cell membrane pathway, would be to systematically increase the complexity of the GUV. The active mechanisms currently missing from the simplistic GUV could be incorporated by adding entities like cationic lipids that can induce a DNA-membrane interaction [4–6] and an endocytic like invagination [7].

In order to probe the molecular conformations during stable neck formation, polymer droplet breakup was investigated at microfluidic T-junctions as described in Chapter 4. Extensional flow created in the droplet during break-up at the T-junction, led to the formation of a stable neck between the separating ends of the droplet. The stable neck followed exponential thinning and the inherent stagnation point at the T-junction allowed for observation of polymer (fluorescently labelled DNA) molecules inside this stable neck. Polymer molecules were coiled in the initial stages of the thinning. However upon transitioning to a stable neck, polymer molecules suddenly stretched. These stretched polymer molecules generated elastic stresses that were able to resist the capillary thinning and breakup of droplets, giving rise to a stable neck. The stretching distribution of polymer molecules was heterogeneous, with a fraction of polymer molecules reaching full extension. The full extension of polymer molecules during exponential thinning was not observed previously and can be attributed to the lack of a stagnation point in corresponding geometries [8].

The stagnation point in the microfluidic T-junction also provided the opportunity to investigate the molecular behaviour of beads-on-a-string (BOAS) morphology that was observed at the final stages of the droplet breakup. The polymer molecules were found coiled in the beads, whereas they were in an extended conformation in the strings connecting the beads. This provides a molecular snapshot of the behaviour of molecules in the BOAS morphology, but does not explain this behaviour of the polymer molecules. Slowing down the thinning dynamics, by increasing the solvent viscosity for instance, combined with the stagnation point of the T-junction geometry can provide sufficient time to observe and follow the behaviour of polymer molecules leading to BOAS morphology. This would help resolve the proposed mechanism for BOAS formation, such as inertia during the final stages of breakup and represented by ever stretching polymer molecules (Oldroyd-B models) [9], or blistering in polymer solutions due to finite extensibility of polymer molecules (FENE models) [10, 11].

REFERENCES

[1] C. Rosazza, A. Buntz, T. Rieß, D. Wöll, A. Zumbusch, and M.-P. Rols, *Intracellular tracking of single-plasmid dna particles after delivery by electroporation,* Molecular Therapy **21**, 2217 (2013).

[2] T. Portet, C. Favard, J. Teissié, D. S. Dean, and M.-P. Rols, *Insights into the mechanisms of electromediated gene delivery and application to the loading of giant vesicles with negatively charged macromolecules,* Soft Matter **7**, 3872 (2011).

[3] M. Yu, W. Tan, and H. Lin, *A stochastic model for dna translocation through an electropore,* Biochimica et Biophysica Acta (BBA)-Biomembranes **1818**, 2494 (2012).

[4] C. Herold, P. Schwille, and E. P. Petrov, *Dna condensation at freestanding cationic lipid bilayers,* Physical Review Letters **104**, 148102 (2010).

[5] C. Herold, P. Schwille, and E. P. Petrov, *Single dna molecules on freestanding and supported cationic lipid bilayers: diverse conformational dynamics controlled by the local bilayer properties,* Journal of Physics D: Applied Physics **49**, 074001 (2016).

[6] A. G. Cherstvy and E. P. Petrov, *Modeling dna condensation on freestanding cationic lipid membranes,* Physical Chemistry Chemical Physics **16**, 2020 (2014).

[7] M. I. Angelova, N. Hristova, and I. Tsoneva, *Dna-induced endocytosis upon local microinjection to giant unilamellar cationic vesicles,* European Biophysics Journal **28**, 142 (1999).

[8] F. Ingremeau and H. Kellay, *Stretching polymers in droplet-pinch-off experiments,* Physical Review X **3**, 041002 (2013).

[9] P. P. Bhat, S. Appathurai, M. T. Harris, M. Pasquali, G. H. McKinley, and O. A. Basaran, *Formation of beads-on-a-string structures during break-up of viscoelastic filaments,* Nature Physics **6**, 625 (2010).

[10] R. Sattler, C. Wagner, and J. Eggers, *Blistering pattern and formation of nanofibers in capillary thinning of polymer solutions,* Physical review letters **100**, 164502 (2008).

[11] R. Sattler, S. Gier, J. Eggers, and C. Wagner, *The final stages of capillary break-up of polymer solutions,* Physics of Fluids **24**, 023101 (2012).

SUMMARY

DNA delivery into cells using permeabilizing pulsed electric field, or electropermeabilization, has shown promise in clinical trials involving therapeutic applications such as immunotherapy, vaccination against cancer and vaccination against other infectious diseases. However, its complete translation into clinics is incumbent upon further enhancement in terms of increased efficiency of DNA delivery and predictable loading. This is not possible via the current approach of empirical optimization using trial and error. An understanding of the underlying mechanisms behind electropermeabilization and DNA delivery at the cellular and the molecular level is needed. Thus, a major part of this this thesis was to probe mechanisms of DNA-membrane interaction and DNA translocation across the cell membrane during electropermeabilization.

Experiments were done on mammalian cells to investigate the mechanism of DNA-membrane interaction during electropermeabilization (Chapter 2). This interaction is observed as DNA-membrane complex formation or DNA aggregation at the cell membrane. During application of permeabilizing electric field pulses, small DNA molecules of size 15 base pairs (bp) did not form DNA aggregates whereas DNA molecules of size of 25 bp, 50 bp, 100 bp and 1000 bp did form aggregates at the cell membrane. This size dependent DNA aggregation, being consistent with Onsager's theory of DNA condensation, provides a bio-physical basis to DNA aggregation at the cell membrane during electropermeabilization.

In order to identify the mechanism of DNA translocation across the cell membrane, experiments were done on Giant Unilamellar Vesicles, or GUVs (Chapter 3). By doing experiments on model cell membranes such as GUVs, instead of cells, observed translocation efficiency as a function of DNA size could be compared to existing models of DNA translocation (bulk electrophoresis *vs.* stochastic threading). It was inferred that DNA molecules can translocate freely through the electro-pores in their coiled configuration during electric field pulses. Thus, bulk electrophoresis was the dominant mechanism of DNA translocation as opposed to stochastic DNA threading through the electro-pore.

By investigating the effect of DNA size, much needed insights were generated on the mechanisms of DNA-membrane interaction and DNA translocation during electropermeabilization. This mechanistic understanding can be utilized in devising strategies that can by-pass the limiting pathways and also offer predictions on DNA loading and time for the therapeutic action.

Another aspect of this thesis was to investigate stable neck formation during extensional flow of polymer solutions from a molecular perspective (Chapter 4). A microfluidic T-junction was employed for this purpose. Pinching of polymer droplets at a microfluidic T-junction created an extensional flow that led to a stable neck during thinning, prior to breakup. The exponential thinning of the stable neck could be quantified to extract the extensional strain rate, and the inherent stagnation point in the T-junction allowed for simultaneous observations of polymer molecules inside the stable neck.

Polymer molecules elongated suddenly at the onset of stable neck formation. Elastic stresses generated due to the stretching of polymer molecules were able to resist the capillary stresses, leading to a stable neck between the separating ends of the droplet. Conformations of polymer molecules were also investigated in the beads-on-a-string morphology observed during the final stages of the droplet break-up.

The stagnation point of the microfluidic T-junction allows for molecular observations without the limitation of motion-blur as observed in cross-flow and co-flow microfluidic geometries for droplet pinch-off. Hence, it provides a suitable platform for investigating polymeric filament thinning and extensional rheological properties of polymer solutions from a macroscopic and as well as a microscopic perspective, simultaneously.

SAMENVATTING

Het inbrengen van DNA in cellen met een permeabiliserend pulserend elektrisch veld, ook wel elektropermeabilisatie genoemd, levert hoopgevende resultaten in klinisch onderzoek naar therapeutische toepassingen zoals immunotherapie, vaccinatie tegen kanker en vaccinatie tegen andere infectieziekten. Volledige toepassing in de praktijk is echter afhankelijk van verdere verbetering van de efficiëntie van het inbrengen van DNA en de voorspelbaarheid van de hoeveelheid DNA die wordt ingebracht. Dit is niet mogelijk met de huidige aanpak van proefondervindelijke, empirische optimalisatie. Begrip van de onderliggende mechanismen van elektropermeabilisatie en DNA-inbreng op zowel cellulair als moleculair niveau is vereist. Daarom wordt een groot deel van dit proefschrift gewijd aan het onderzoek naar DNA-membraaninteractie en verplaatsing van DNA door het celmembraan tijdens elektropermeabilisatie.

De experimenten om het mechanisme van DNA-membraaninteractie tijdens elektropermeabilisatie te bestuderen zijn uitgevoerd op zoogdiercellen (Hoofdstuk 2). De interactie komt tot uitdrukking als de vorming van een DNA-membraancomplex of de opeenhoping van DNA bij het celmembraan. Tijdens het aanbrengen van permeabiliserende pulsen van het elektrisch veld vormen zich bij het celmembraan geen opeenhopingen van DNA-moleculen van 15 baseparen (bp), maar wel van DNA-moleculen van 25 bp, 50 bp, 100 bp en 1000 bp. Het feit dat de opeenhoping van DNA afhankelijk is van de grootte van het molecuul is in overeenstemming met de theorie van Onsager over DNA-condensatie en levert een biofysische basis voor de opeenhoping van DNA bij het celmembraan tijdens elektropermeabilisatie.

Om het mechanisme achter de verplaatsing van DNA door het celmembraan te bepalen zijn experimenten uitgevoerd met Giant Unilamellar Vesicles, ook wel GUV's (Hoofdstuk 3). Door experimenten met modelcelmembranen zoals GUV's uit te voeren, in plaats van aan echte cellen, kan de afhankelijkheid van de DNA-grootte op de verplaatsings efficiëntie worden vergeleken met bestaande modellen van DNA-verplaatsing (bulkelektroforese vs. stochastisch threaden). Hieruit is afgeleid dat DNA-moleculen zich tijdens pulsen van het elektrische veld in opgerolde toestand vrij door de elektroporiën kunnen verplaatsen. Hieruit volgt dat bulkelektroforese en niet het stochastisch threaden het belangrijkste mechanisme van DNA-verplaatsing door elektroporiën is.

Door het effect van DNA-grootte te onderzoeken zijn noodzakelijke inzichten verkregen in de mechanismen van DNA-membraaninteractie en DNA-verplaatsing tijdens elektropermeabilisatie. Dit mechanistische begrip kan worden gebruikt om strategieën te bedenken die de beperkende factoren kunnen omzeilen en die voorspellingen kunnen doen over het ingebrachte DNA en de therapeutische werking.

Een ander onderdeel van dit proefschrift behelst onderzoek vanuit moleculair perspectief naar de vorming van een stabiele hals tijdens uitrekkende stroming van polymeeroplossingen (Hoofdstuk 4). Hiervoor werd een microfluïdische T-splitsing gebruikt. Het afknijpen van polymeerdruppels in een microfluïdische T-splitsing resulteert in een

uitrekkende stroming die leidt tot een stabiele hals terwijl de druppel dunner wordt, waarna de druppel uiteenvalt. De exponentiële verdunning van de stabiele hals kon worden gekwantificeerd om de uitrekkings snelheid te bepalen en het stagnatiepunt in de T-splitsing maakte het mogelijk tegelijk de polymeermoleculen in de stabiele hals te observeren.

Polymeermoleculen rekken plotseling uit wanneer de stabiele hals begint te vormen. Elastische spanningen die ontstaan door het uitrekken van polymeermoleculen kunnen capillaire spanningen tegenwerken, waardoor een stabiele hals ontstaat tussen de uiteenbewegende uiteinden van de druppel. Voorts zijn structuren van polymeermoleculen bestudeerd die zich voordoen in de parelketting morfologie in de laatste stadia van het uiteenvallen van de druppel.

Het stagnatiepunt van de microfluïdische T-splitsing maakt het mogelijk moleculen te observeren zonder de bewegingsonscherpte die zich bij druppel afknijping in microfluïdische dwarsstromings- en meestromingsgeometriën voordoet. Daarom biedt het een geschikte omgeving voor de gelijktijdige bestudering van zowel polymeer filament verdunning als uitrekkings stromingseigenschappen van polymeeroplossingen op zowel microscopisch als macroscopisch niveau.

ACKNOWLEDGEMENTS

As I write the acknowledgements, I find that I am in a slightly anxious state of mind. Not because I do realise that is the most read part of any thesis, and perhaps the first read part of the thesis as well, but because I would like to do justice in expressing my sincerest gratitude to everyone who has helped me reach here.

Pouyan, first of all I would like to thank you for giving me an opportunity to work on this PhD project. My gratitude, however, goes far beyond this opportunity. Apart from shaping me as a scientific researcher, there are many more things that I would like to thank you for. These things in my opinion have been so subtle yet so influential in developing me as a person, that I might not have explicitly mentioned it to you, or you might not have recognized it. The fact that you valued active communication and discussion never gave me any qualms or apprehensions discussing anything with you. You made me realise that as long as we discuss and communicate, we are heading in the right direction. While this is necessary for a good professional conduct, it is also applicable to inter-personal relationships, and I shall cherish it forever. As much as I learnt how to do good research under your supervision, I also learnt how to be a good family man. The stories and anecdotes you recited over a few drinks at conferences and PPE outings were always refreshing and also re-assuring of a life outside of work. It was only over time that I got to realize how busy you were with ever increasing responsibilities, yet you always took out time to address my queries and concerns whenever I knocked on your door. This is a luxury that not many PhD students enjoy and I am forever grateful to it. It played a huge role in the successful and timely completion of this thesis.

Michiel, I have to admit that it was difficult to convince you and get your approval. But in the pursuit, the end product was so elegant and clear, that it made all the effort worth it. Your questions, instead of harbouring obscurity always resulted in clarity, and as a result an increase in confidence on my own work. It was always a delight for me to be at the receiving end of your interrogation. You taught me that in order to crack down a problem, it would be most yielding and fruitful to target the Achilles heal. You also helped me refine my vision, through the art of questioning, to identify that Achilles heal. Although our interaction was limited to only the progress meetings, your experience and brilliance made sure I gained tremendous help and learnt significantly during these interactions.

I wish to thank **Prof. dr. D. Miklavčič**, **Dr. M. Tarek**, **Prof. dr. ir. J. T. Padding**, **Dr. V. Garbin** and **Prof. dr. S. J. Picken** for taking the time out to be a part of my doctoral defence committee and for critically evaluating and approving my thesis.

After spending 5 years at PPE, first as an M.Sc. and then as a Ph.D. student, I have had the opportunity to have many colleagues. But I am having troubles addressing all you as colleagues. Oxford dictionary defines a colleague as "*a person that you work with, especially in a profession or a business*". There is nothing wrong with this definition nor is there anything wrong with addressing all of you as colleagues, as per this definition.

Well, one could argue that despite our best efforts, there was nothing professional in our conduct at the work space we co-inhabited, and for the business that we were in. We were hardly successful in that pursuit. But this is not my bone of contention in referring all of you as colleagues. I feel that the word is too restrictive in the role that all of you have played in not only in making my working hours, but also my post working hours, *i.e.* if you can distinguish between the two, one hell of a ride that I would gladly buy the tickets too, again and again.

Lea, I always regarded you as a mentor for life. You are my role model of how a researcher should be; vast and immense knowledge of the subject and also a far reaching depth of understanding, relentless passion and dedication towards work and lastly but by no means least important, and in my opinion a significantly important trait, an abundance of empathy. Your ability to tame and calm my chaotically vibrating mind and then to steer it in the right direction is what pulled me through the most difficult and hopeless moments of my PhD. I cannot even imagine to enumerate the variety of ways in which you have helped me out during my PhD, and not for the sake of brevity but because a heart felt gratitude requires no quantification, I will not list them out. I am grateful to have known you as a colleague, as a researcher, as a mentor but most importantly as a friend too. Now that you are going back to Slovenia to start your research group, it gives immense hope to know that academia is in good hands.

Maulik and **Kartik**, I have known you for as long as I have been in the Netherlands. I still vividly remember the the first time I met the both of you. At that time I did not imagine that the acquaintanceship would turn into a profound relationship that it is today, and I would be asking you to stand beside me on this big day. As hard as I am trying not to make this sound romantic, and as embarrassed as you might get after reading this, I find no other way to express my gratitude towards you.

Maulik, many have found solace in your highly accommodating personality and your calming presence. In this world full of people who want to talk, suggest and give their opinions, you are the person who truly *listens* and *understands*, and that makes a world of a difference for those in need of help, a cause that is instinctive, and also inherent in you. I have been through the toughest times knowing that you would be there, whenever the need be. However, you were there even more often than that. Your help towards me and my struggles have been all-pervasive and have transcended all levels; personal and professional, that I just cannot list specific examples. But I guess that is the beauty of our relationship, it doesn't need any exemplification. Thank you for giving me the strength, courage and support all throughout my M.Sc. and Ph.D. You made the hard times feel like a minor blip, and amplified the good times to create the best of the memories that I shall cherish forever. I was lucky to have you by my side during my M.Sc. and my Ph.D, not only as a colleague and as a friend, but also as an elder brother. Thank you for being there, *always!*

Kartik, talking to you has always helped me prioritize the important things in life. Your ability to have effortless clarity on the topics that baffles most of the academics is inspiring. You taught me to have conviction, that pondering over a decision is often pointless, since there is no right or wrong decision. Apart from the profundity of your contribution towards the development of me as a Ph.D., it was also fun to discuss politics and comedy with you. As naive as it may sound to call politics and comedy less profound,

using the two in the same sentence makes up for the lack of good sense.

Dayinta, **Durgesh** and **Piotr** I couldn't have asked for a smoother initiation to the PPE group and my PhD project. You made sure that all my questions, both rational and irrational, with the balance tending towards the latter, were answered thoroughly and with all the patience. I had the warmest welcome into the office and the most encouraging and motivating environment that a new student at the start of his PhD journey could ask for.

Piotr, I was lucky to be trained by you in the initial years. To see the level of ease, precision and detailed organisation with which you did experiments really inspired me and removed my inhibitions from approaching complex experiments. I would also like to thank you for being highly approachable, even long after you left PPE, to answer my questions about the tweezers and clean room. You saved me lot of time and effort.

Dayinta, thanks for giving me a perfect start to the electroporation experiments. The fact that an efficiently managed and robust set up was already in place when I started, gave me enough time to focus on the research questions. I also learnt a great deal from you about organising and documenting, which soon transcended beyond the experiments in the lab to my personal endeavours as well. More importantly, I soon realised that there was so much to learn from you about nutritional and flavourful aspects of food. I made use of this essential knowledge not only in the pre-2017 lunches but also in the post-2017 lunches. You and **Durgesh** made sure that there was more to lunch than just cold sandwiches.

Durgesh, it was a big relief to have someone to discuss polymer physics and rheology with. I believe that it takes only two to form a team, and the fact that a team was working with polymers gave me enough confidence on my approach and results. It is this confidence that makes all the difference and helps break the behaviour of doubt that is a very common side effect of doing a PhD. I would also like to thank you for spending those long and tedious hours in the clean room with me for making my wafers, and for ever being ready to do so. I really appreciate it.

Aswin, you were my first student but for a greater part, someone who sat next to me as a fellow PhD student. In either case, I believe I had much to learn from you than the other way around. I admired the way you helped me take decisions keeping the bigger picture in mind. As simple and obvious as this may sound, we often tend to forget the higher purpose of our actions and our inactions. Thank you for instilling its importance in me and for constantly reminding me about it. **Dominik**, you were the infectious positive energy in our office, the thread that bound all of us together and the best venting instrument a co-worker could ask for. You kept the spirit of the discussion, *any* discussion, alive and no matter what anyone says, you gave the most logical arguments to my profound lunch questions. Thank you for carrying and supporting me in the *both* the survival runs and for being my partner in crime to all the crazy experiments we did in the office.

Serhii, there were many ways in which you have helped me. When it was about micro-fabrication, you were the go-to person. When things didn't work out in the clean room, I always came to you for answers. When I had doubts about microscopy, you cleared them like an expert. When experiments didn't work out in micro-fluidics, you always had a sound explanation as to what went wrong. I believe that at one point, you

were assisting me in all aspects of my PhD, from my experiments, to the theory to even my writing. I know that at the end of my PhD, I used to claim that I was the senior most PhD in the group, but the truth is, that you were, in all ways possible, the *senior* most PhD. You not only helped me with genuine sincerity and dedication, but everyone who came knocking at your door for advice. Thank you for supporting all of us like a big brother.

Damiano, your characteristic wink whenever we bumped into each other in the corridor is too inviting to not mention. I am not sure if you do that to everyone, but I would like to believe that this gesture is reserved for me only ;) Even though there was nothing common in our research, there was much to learn from you about hard work, dedication and the resolute focus towards completing the Ph.D. There were many late nights and weekends that I have spent in the department, and as I walked the corridors for an occasional break, it was immensely comforting to see that the light was on in room E2.420 and through the hazed glass wall I could see the silhouette of your head focussed on your screen. It made me feel less crazy about spending so many late hours at the university.

Fabio, although there was a substantial overlap of our global Ph.D. time-lines, our local time-schedules didn't overlap as much. However, your wit and your brilliance never failed to amaze me. Talking to you inspired me to do research for all the right and relevant reasons and not merely for the buzz words and "hot" topics. It is highly re-assuring to know that people like you are in academia, who are well aware of what the system is and what it has become, and possess the capability of changing it for the better.

Samir, your positivity and enthusiasm was highly infectious. Whenever it got boring around middle of the day, your call for lunch was just the thing we all needed. Thanks for keeping the mood and the spirit always high and for always being up for a drink. **Fatemeh**, I hope I haven't annoyed you with my ridiculous facts concerning the most useless of the topics. At the same time thanks for being a sport and actively participating in this endeavour. I also thank you for introducing me to *decaf* coffee. Now I know that there will always be a way out from caffeine addiction. **Hao**, I do not know how it was possible to find you each and every time I entered the office, and there have been quite some bizarre times as well. It is better for my sanity to believe that it was pure coincidence, rather than believing that you practically lived in the office. Nevertheless, thanks to you the office was never lonely at any time of the day *or night*, and there was always a stack of munchies to snack on, such that the focus on work was never lost.

Erik, it was good to have another comrade join the microfluidics battle. Your presence gave us the confidence of having a strong hold on microfluidics and tilting the battle in our favour. Thanks for also being an effective voice to the students of PPE and ChemE at the Ph.D. council. **Melvin**, it was a pleasure initiating the pizza ordering regime after the lunch lectures with you. It has now become one of the most looked forward monthly traditions at PPE. **Josette**, we only interacted during group meetings, journal clubs and lunch lectures and it was inspiring to know the level of organization and planning with which you approached these meetings.

Georg, Isabell, Hamid, Afshin, Feilong and **Fuweng** you guys made PPE lively and vibrant during the last phase of my Ph.D. Lunch became more about the ridiculously useless discussions and less about the food we consumed. I hope you guys realised that my questions during lunch were never about the answers. It was always about getting

to know you more, and for some reason, the more I go to know, the more happy I was. It might sound irrational but I like to think that I am never at the right place at the right time. But with all of you, along with the other PPE-ers, I genuinely believed that I was at the right place at the right time, only now that the time was almost over. As happy as I am wrapping up my thesis, there is a big part of me that is terribly sad of not being able to spend enough time with you.

Moreover, with a new set of inmates; **Zaid**, **Ruben**, **Alvaro**, **Aptem** and **Saeed**, joining the gang, going away not only makes me sad but also miserable. I wish I got to *interrogate* all of you as well during the lunch. **Alessandro**, I will always remember you making us laugh in the office. What I will never know for sure is if that behaviour that led to the laughs was intentional and deliberate or if it was just your normal existence. But I guess that is the beauty of it and I would like to keep it that way.

During my Ph.D. I was also lucky to have worked with some of the most talented and dedicated M.Sc. and B.Sc. students to whom I owe my sincerest gratitude. **Robbert**, **Bouke**, **Hugo**, **Sara**, **Victor**, **Yasmine**, and **Dipendra**, if I could finish multiple projects, each involving different competencies, it is because of all of you.

Robbert, when you started your M.Sc. thesis I was distracted with a manuscript for another project and I could not devote as much time to your project as I would have liked to. However, your brilliance and dedication made sure that the quality of project was not compromised. This gave me enough freedom to set-up new projects and set up a solid foundation for my Ph.D. You yielded results that at one point seemed impossible in our lab. **Bouke** and **Hugo**, you soon took over the legacy that **Robbert** left behind. As challenging as a project can get with an extremely tedious chip manufacturing and equally nasty reagents flowing inside, within three months you culminated the projects with such immaculate detailing and precision that the entire road map became clear to me. **Victor**, then you stepped in and set up a whole new ecosystem for producing vesicles using microfluidics. You became so indispensable to the success of the project that we had to ask you to stay for a little longer post your successful graduation. I shall be forever grateful that you gladly obliged to this request. Your sincerity and dedication to your commitments has instilled a strong work ethic inside of me and I have learnt a lot from you in this regard.

Sara, we started on a project related to cells, and this domain was completely new to me. Dealing with cells required a brilliant plan and strict adherence to it. Your hard work, dedication and a penchant for planning made all of this possible and we not only managed to survive but also thrive. For once, after a long time, I could see the light at the end of the tunnel for a project. **Yasmine**, you took over from Sara and provided the final push that was needed. I thank you both for your sincerity in this endeavour and for seeing the project all the way through to a publication.

Dipendra, your raw and unfiltered expressions and interaction was like a breeze of fresh air. Thanks for not only being a sincere student with a slightly twisted sense of calendar, but also a friend who always had the anti-dote to the frequent stress bursts I experienced during the final year. You came in and revived the vesicles and DNA project. I had almost given up on the experiments but it was your dogged determination to see green inside of red that made sure that the project was finished with elegance resulting in a publication. I also thank you for pointing out to me that it was time that I needed to hit

the gym. As polite and as well-intended this advice was, I have taken it far too seriously. You have woken up the sleeping lion and I hope you are soon ready for the monster that you might have accidentally created.

Dorien, I was not your primary supervisor. **Ankit**, I was not even your supervisor. But I am glad I got to know both of you and interact with you as much as I did with **Dipendra** and **Yasmine**. The coffee breaks where I often consumed double dose of caffeine along with the banter of your hilarious anecdotes and expeditions was a much needed respite from the final year stress. **Ankit**, thanks for bringing a tiffin full of biryani for me for lunch. I will never forget this wonderful gesture. And thanks for inviting me to your house whenever you made plans to cook it. I can start eating rice again if I get it in the form of your biryani. Thanks for also inviting me to your wedding. I am terribly sorry that I couldn't make it due to unemployment and border control issues, but my best wishes are with you and your better half.

I also owe an immense gratitude to the permanent staff of PPE. **Wim** your help was extremely instrumental in getting my experiments up and ready. I wish to also thank you for the long hours you spent in the clean room for making my wafers and training me for the proficiencies. I realised that I took more time than needed to feel ready for the exam, but you were always patient with me and made sure I could handle the ever fuming concentrated nitric acid with enough confidence. **Stefan**, thanks for fabricating the microfluidic needles for me at such short notice. It elevated our experiments to a whole new level of simplicity and elegance. **Mojgan**, having you besides us to consult for the bigger questions concerning the lab was a big relief. We could (*almost*) manage the little things in the lab, but when it came to right code of conduct, good lab habits and big orders, we could easily depend on you. This not only saved us a lot of time but gave us immense confidence to manage the bio-labs. **Christiaan**, thanks for helping out with the pulse generator. We came knocking at your door knowing that we could get the best of the help over here. Thanks for making sure that the pulse generator, the heart of all our experiments, was working the way it was supposed to and thanks for also taking over the communication with the manufacturer when we had no idea how to go about it.

Ruud, PPE was always an eclectic group in terms of the research topics. Yet you made the group feel like less of an organizational division sharing a common name, and more like a family. Thanks for providing a stimulating atmosphere which not only challenged us intellectually but was also warm and welcoming. However this warm and welcoming feeling was perhaps only limited to the department premises, Christmas dinners and PPE days. At PPE outings during paint-ball, go-karting and egg-on-a-spoon race, your competitive streak was a pleasant surprise.

Volkert, I genuinely regret not being in a project where I could learn from you. However, with you being in proximity there was always substantial knowledge and wisdom trickling down that was up for grabs, and I made sure to never miss such golden opportunities. Your dedication and hard-work towards the causes that you believe in have inspired us all. In a world that demands us to be practical, constantly reminding us that nothing is perfect, you made us believe that there is nothing wrong in striving for perfection. Thanks for also taking out the time to discuss the breakup of droplets, and even vesicles, at T-junctions. I remember that there were some thought provoking and extremely fundamental questions that you asked during my M.Sc. thesis, which got me

thinking. Back then, I did not have an answer, but now after five years I do have some explanation for it and it has made me feel a lot better. I know that this is the time for acknowledgements so I would not go into the details of the question. The point I am trying to make here has nothing to with the question or the explanation, but to the fact that even small interactions with you have had a long lasting impact in me by keeping the scientific curiosity alive in the right spirit.

Gabrie, I have received the best career advice from you. However, the discussions about food and nutrition were eye opening as well. I will never look at milk powders and frozen pizzas the same way I used to. I can now only imagine what a discussion with you about a career in food and nutrition would be like. **Peter**, your lecture was our first introduction to the Department of Chemical Engineering when we started our M.Sc., and one could not have asked for a better introduction to one of the finest departments in the world. It made us believe that we were at the right place, and what a perfect place it has indeed been for us. **Henk**, I remember that during one of the PPE events we celebrated the completion of 1000! Although the meaning of 1000 was kept a secret till the very last minute, I did have a hunch of it being about the number of your bike rides. It has inspired me to keep a record of my long walks as well, and as far as 1000 seems, I am determined to keep walking.

Elly, thanks for helping me organize my life as a Ph.D. student. I often forgot and missed important deadlines but you always managed to bring me back on track and that gave me a lot of comfort. I will always remember the warmth and patience with which you addressed all my queries and concerns and helped me in the best way possible. If I have also managed to have three extremely smooth and successful extensions of my visa in a highly complex bureaucratic system, it is only because of you. **Astrid** you have been extremely contributory in the timely completion of my Ph.D. thesis. I came to you at very short notices and still you managed to organise meetings with Michiel and Pouyan, and that made all the difference. I owe you an immense amount of gratitude for not only organising these meetings, but also for organising them each and every time I needed them.

If PPE hardly had any borrels, it was due to TP. Friday drinks and borrels hosted by TP inherently implied that PPE was always welcome. This was a lovely gesture and a genuine thanks to **Siddhartha (Sid)**, **Manas**, **Manu**, **Luis**, **Elin** and other members of TP.

Sid, it has always been a pleasure talking to you about *anything and everything* since there is always something that I end up learning. I am amazed by the depth of your knowledge on a vast variety of topics. Equally, or probably far more, interesting to me is your spontaneity. How effortlessly you come up with the wittiest of the remarks makes me doubt the authenticity of the situation. It is so apt, it almost feels as if you orchestrated the whole thing just to use it. On a formal note, thanks for assisting me with the final formalities of the Ph.D. and also helping me approach it with the right attitude. Quite often I used to come knocking at your door with doubts and unnecessary worries about the formalities and associated bureaucracies, but ended up leaving calm, composed and confident. Thanks for being so patient with me.

Manas, if your name comes up in a conversation, or you just happen pass by my thoughts, it never fails to put a smile on my face. I have realised that while all of us operate on a single calendar, you on the other hand operate on multiple calendars. It is

refreshing and reassuring to see you that you are always busy with something and that you are always learning something. Thanks for being the jolly personality around. There is *never* a dull moment with you.

Dries, you have been one of my closest Dutch friends. When I got to know that you were Maulik's thesis supervisor I was a little bit jealous of not having a daily supervisor as nice and awesome as you. This was not only because of your academic brilliance but also because you were always immensely inclusive. Thanks for making us a part of all the activities. You gave me supervisor goals that I strived to achieve during my *reign* as well. I also owe my gratitude to you for being a big sport to my witless sarcasm and baseless jokes. The fact that you understood them as sarcasm (or atleast I hope that you did) and played along, gave me freedom to express myself freely which I guess only brought us closer. Our Spain trip was fun, however I apologise of not being at the best of my behaviour. The temperature fluctuations from Barcelona to Zaragoza to Valencia were too much for me to handle, but you made sure that I felt comfortable and also made sure that I still have a very nice time. I hope I can make up for it, and the best way to do so would be with you in India.

Cees, you were an equal culprit in giving me supervisor goals. You, along with **Conrad**, had the best of the "set-ups", both inside and outside of the labs, and were constantly redefining of what was possible in the old ChemE building. Your invitation to pre-2016-17 borrels on Thursdays in the E-cast usually meant the end of the week for me. Yet I fell for them each time. You also introduced me to the concept of a *meter*, and since then the least count of the number of beers I order has changed forever. When others invited me for a game of battleship, I happily volunteered not knowing what it entailed. The dedication and the level of detail with which you and **Conrad** built the *Battleship* never ceases to amaze me. With all that said, I also owe my sincerest gratitude to you for not only inducing me but also properly initiating me into the *NSS*.

Conrad, the craziest of the times during my M.Sc. were spent at our infamous office. Under your esteemed tutelage I did manage to end up on the wall of shame and nothing makes me more proud. Thanks for introducing me to Pierogis, but I guess the crown jewel has to be reserved for the ingenius sandwiches you made *outside* our office. **Conrad**, you made sure that our office never lacked any amenities and made my stay extremely comfortable in one of most stressful environments. I am glad that we are still in touch and would be even more delighted to continue this streak.

Chirag, I wish we could spend more time together. Even if the duration was less, I do believe that there wasn't any lack of intensity in our interaction. The comfortable home that was ready for me when I came from India after a short break post M.Sc., and the warm meal with which you greeted me, immediately made me realize that I was at a place which I can call another home. Thanks for giving me memories of the most amazing curries I made with you and the endless chicken nuggets we ate together. I also realised that you always had a crate of beer in your room and your were quite active in replenishing the stock when it was getting over. That is such a nice philosophy to abide by. After a stressful day of work, your divine words of bottle "*phodna*" is just what I needed. **Hrushi**, you were my go to man for all things related to transport phenomena. Although I miss not having you here, I wish to congratulate you on becoming a father.

Sahil, it took me some time to understand the philosophy you expounded concern-

ing the purpose of a job. Now that I understand it, I realise that there is immense wisdom in it. As I find myself at cross roads deciding a direction for my future, your advice has given me a much needed perspective. **Robert**, it was a pleasure bumping into you at the corridor and share occasional moments of big miseries and small victories. I hope my tendency to use self deprecation as a defence mechanism against the current state of affairs did not scare you too much. I thank you for also teaching me what is important in life; "*education is important, but biceps are importanter*". As true and sensible as it might be, I find it funny using it in the acknowledgements of my (educational) Ph.D. thesis.

Prachi, thanks for dragging me, **Maulik** and **Kartik** out of our lazy shoes and reminding us to enjoy life. It was only due to your efforts that festivities, birthdays and even random holidays were celebrated with enthusiasm. If we did not miss home and family during Diwali and Holi, it was only because of you. You also made us realise that not only big, but also small, victories should be a cause for celebration. All these efforts made sure that there was always something to look forward to, and life did not get too monotonous. Often, you were also the voice of reason, and handled my stupidity with a lot of practicality never giving up on me, even though I might have given you enough opportunities to do so. **Aparna**, **Aruna** and **Samiya** I also thank you all for being in touch and keeping the discussion in our group alive.

Sneha and **Abhay**, we started and finished our graduation and under-graduation together. Even though now each of us went ahead to do a Ph.D., this time we chose different places. I thank you for sharing this long educational adventure that soon turned into a strong friendship. Thanks for always being there during the tough times and for making me look at Ph.D. with the correct perspective. **Sneha**, you not only helped me during BITS, M.Sc. and my Ph.D., but you are also continuing to help me, as it completely inherent in your nature, post Ph.D. as well. I owe my sincerest thanks to you for it.

Turkuaz and **Alois**, thanks for always having me over at your house for celebrating sinterklaas. By constantly being a part of this tradition, it gave me a sense of belonging which is often hard to get by in a far away land. The warmth I received at your house not only during sinterklaas but also during board game nights and *just-casual-heavy* drinking sessions only added to this feeling of belonging. I think the interior design of your house changed quite frequently, but the warm welcoming feeling was always constant. I will always remember the infamous night at Doerak, but I would also not fail to acknowledge the irony of it, since I hardly remember anything of that night. How you guys managed to catch the flight the next morning is still incomprehensible. Thanks for allowing me to be a part of your happy celebrations, it made me happy as well. **Turkuaz**, thanks for designing the cover of this thesis as well. I hope the content inside of it can do justice to the beauty and elegance of the art on it.

Gijs and **Pieter**, you guys give me hope that there is good humour in the Netherlands. **Gijs**, as funny as your are, whether intentionally or un-intentionally, what I learnt the most from you is how to break down problems and frame them into questions. I know that this might not be the first thing that you would associate yourself with, or probably other people will associate you with, but this has often stood out for me. If a problem is properly framed into a question then more than half the work is already done, and a solution is not far away. **Pieter**,there will always be many questions that will

remain unanswered. But for questions concerning transport phenomena, I now have the good fortune of being able to ask the best person, and *I know* that my emails would be answered. Thanks for showing me how to approach and follow your passion, and for reminding me to follow the classics instead of pop culture literature, in order to build a sound base in your research topic. I still remember the stack of literature you gave me before I started my journey. It taught me how to approach new research topics.

Thomas, as funny and as humorous as you are, thanks for also being one of the most gentle, caring and understanding friends I have ever had. Your un-deterring commitment to help others has also helped me out on multiples occasions. When I lost my passport, you were there in an instant to help look for the lost document and also assist with the formalities. You have not only supported me in my crazy ideas concerning my career, and life in general, but have also encouraged me to pursue it. In this process I have learnt a lot from you about what is important in life and what is not. Your efforts to chose a sustainable lifestyle do not come from a point of view of fear or from recent fads, but from the strong morals inherent in you, and that is immensely inspiring. I try to follow your lead in this regard, but occasionally fail, probably due to lack of courage or conviction, which however is abundant in you. Thanks for not only being the best of the friends but also for being someone to look up to. Lastly, thanks for also introducing me to **Maja**. **Maja**, thanks for receiving me with utmost excitement and enthusiasm each time I come to meet you and also thanks for walking me through the dunes in The Hague.

Yadnyesh you were always up for ordering food with me, and an equal partner in crime for eating outside. This helped me unwind in the way I liked the most. **Nishchay** thanks for reminding me to chill out from time to time and for making me realise the true meaning of "*in bade bade deshon mein, yeh chhoti chhoti batein... you know what I mean...*". It is the philosophy to abide by when things go wrong. **Mogre**, you have been highly pro-active in keeping touch with all of us after our M.Sc. It takes efforts like these to keep the relations going. Thanks for making this effort even when I was significantly falling behind in this pursuit. Occasional dinners and drinks at your place, along with **Swej**, were highly refreshing and rejuvenating. Thanks to both of you for also inspiring me to lead a balanced life.

Nachi, **Sinha**, **Abhishek**, **Sapra**, **Ali**, **AB**, and **Nikunj**, in short **Bros!**, as bland and conventional as this name sounds, you guys are quite the opposite. Even though you weren't here physically, you all were a constant source of inspiration and have guided me in many ways for the better. Not only have you guys made me realise that there is humour in every situation, you have also taught me how to find it. It is exactly this philosophy which removes the toxic behaviour of categorising situations and times as either good or bad, and rise above these pointless classifications. If there are lessons on philosophy that I have learnt during my Ph.D. (Doctor of Philosophy), this is a substantial one, and I learnt it from you.

Saikat, whenever I had crazy ideas and whenever my mind wandered in obscure directions about who I am, what I want to be, and what the future holds for me, I had you, an old trusted friend, to fall back upon. The patience with which you listened to me and then gave me sound advice was a perfect blend of rooting me back to reality, and at the same time, allowing me to dream big. Thanks for always picking up the phone and

listening to me.

Anvit, Varun, Raghav, Deepanshu, Rohan, Yuvraj, Gaba, Uti and **Saurabh**, although we have been friends since school, I can say with full conviction that our conversations, from back then to the current times, have not evolved even a single bit. But by no means does this upset me. Rather it makes me happy to know that the innocence is still intact and our high-school spirits are still alive in the *graveyard*. Quite often, after stressful days when everything seemed hopeless, the conversations in the group never failed to make me smile and give the energy to carry on.

Samyak, it is funny how things work out. Who would have thought we would end up together in Netherlands? But I am not only glad that we did, I am also thankful to you for being there in the most soothing and understanding way possible, in one of my most difficult times. It also makes me immensely happy to know that you and **Vasundhara** always had the door to your house open for me, where I always felt wanted. I will never forget the warmth I received from both of you.

Pooja, I met you at the very last stage of my Ph.D. It is that stage when you constantly dislike your state and your work, and occasionally even detest it. These were probably not genuine feelings but I guess were a natural reaction to pressure. Talking to you made me realise that what I was doing mattered, was necessary and perhaps even noble. Thank you for not only tolerating my inquisitiveness towards the discipline of science, but also being enthusiastic and excited about it. This is what I loved, and I was losing it towards the end. You came in and helped me retain it, hold it tight and made me like it even more. It is highly unfortunate to stop believing in something that you love and I shall always be indebted to you for not letting that happen. I want to also thank you for teaching me how to care better. Even though I cared, I often got absorbed in my own troubles that I lost touch of showing the little signs of care and concern. It is these little things that hold biggest of the relationships together, and thanks for making me realise their importance. Above all, thanks for assuring me that I shall never walk alone.

Nirupama aunty and **Anju maasi**, for your concern, constant support and encouragement I will always be indebted. **Nirupama aunty** thanks for making me believe that while turbulent times do come, they are never permanent. It re-instilled hope in me at a time when there was a crisis of hope. **Anju maasi**, thank you for constantly checking up on me. Even when I couldn't keep in touch for an extended period of time, a message from your side made all the difference. It made me feel as if I had parents on either side of the world.

Rohan, some of my best memories in the Netherlands and a few other parts of Europe are when you were here. But I guess it was never about Europe. In fact, some of my best memories in the States and even in India were when you were in close proximity. So it has always been *you*. Whenever you are in proximity, both me and **Shaarang** end up having the best of the time. Thanks for always bringing things into perspective, and that too in the most comic and hilarious way possible. Your dialogue "*Biwi hai!*" is perhaps the dialogue of the century for me and **Shaarang**. **Rhea** and **Sonam didi** thanks for being the younger and the elder sister in my life. Thank you for allowing me to care for, and be cared by, you.

Mom, Dad, Shaarang, Meesha and **Karan** when it comes to acknowledging you for all that you have done for me, I see it as a completely pointless exercise. It is not because

I take all of you for granted but mainly because words will never do justice to it. I feel that by putting it into words, I am defining, and hence also confining, your contribution which is as limitless as your love. Your efforts and all that you have done for me cannot be reduced to a definition. At the same time, it also feels incorrect to close it off in this manner. As genuine as it may be, it gives off a sense of laziness and I can assure you that this is not the case. So going against my own explication, I want to say that none of this was possible without you. Not only have you given me complete freedom to pursue whatever I wanted to but also provided me with all the necessary means to achieve it. If I was limited, it was only because of my abilities. However, you also managed to breach that barrier, providing me with confidence by genuinely believing in me. So if none of this was possible without you, none of this is also worth it, if not for you. I wish to thank you for all that you have done for me and *thank you for all the good that is inside of me.*

CURRICULUM VITÆ

Shaurya SACHDEV

30-05-1991 **Born in New Delhi, India**

2009 - 2013 **B.E. (Hons.) Chemical Engineering**
BITS Pilani, Goa, India

Summer Internship: Chambal Fertilizers and Chemicals Limited, Rajasthan, India

Semester Internship: Credit Suisse, Pune, India

2013 - 2015 **M.Sc. Chemical Engineering**
Delft University of Technology, The Netherlands

Thesis: Breakup dynamics of non-Newtonian (polymer) droplets in microfluidic devices : from necking to rupture
Supervisor: Dr. P. E. Boukany

Research Internship: Molecular Dynamics at CNRS, University of Lorraine, France
Supervisor: Dr. M. Tarek

2015 - 2020 **Ph.D. Chemical Engineering**
Delft University of Technology, The Netherlands

Thesis: Response of DNA molecules to external fields: Electric and Hydrodynamic
Promotors: Prof. dr. ir. M. T. Kreutzer & Dr. P. E. Boukany

List of Publications

5. **Sachdev, S.**, Moreira, S. F., Keehnen, Y., Rems, L., Kreutzer, M. T., & Boukany, P. E. *DNA-membrane complex formation during electroporation is DNA size-dependent.* Biochimica et Biophysica Acta (BBA)-Biomembranes, 1862(2), 183089 (2020).

4. **Sachdev, S.**, Muralidharan, A., Choudhary, D. K., Perrier, D. L., Rems, L., Kreutzer, M. T., & Boukany, P. E. *DNA translocation to giant unilamellar vesicles during electroporation is independent of DNA size.* Soft matter, 15(45), 9187-9194, (2019).

3. Pesch, G. R., Lorenz, M., **Sachdev, S.**, Salameh, S., Du, F., Baune, M., Boukany, P. E. & Thöming, J. *Bridging the scales in high-throughput dielectrophoretic (bio-) particle separation in porous media.* Scientific reports, 8, 10480 (2018).

2. Kawale, D., Bouwman, G., **Sachdev, S.**, Zitha, P. L., Kreutzer, M. T., Rossen, W. R., & Boukany, P. E. *Polymer conformation during flow in porous media.* Soft matter, 13(46), 8745-8755, (2017).

1. **Sachdev, S.**, Muralidharan, A., & Boukany, P. E. (2016). *Molecular processes leading to "necking" in extensional flow of polymer solutions: Using microfluidics and single DNA imaging.* Macromolecules, 49(24), 9578-9585, (2016).